Development of New Ligand Scaffolds for the Preparation of Heterobimetallic Complexes

Alexander Richard Treleven
Marquette University

Development of New Ligand Scaffolds for the Preparation of Heterobimetallic Complexes

By

Alexander R. Treleven, B.Sc. (Hons)

A Thesis submitted to the Faculty of the Graduate School,
Marquette University,
in Partial Fulfillment of the Requirements for
the Degree of Master of Science

Milwaukee, Wisconsin

May 2016

ABSTRACT

DEVELOPMENT OF NEW LIGAND SCAFFOLDS FOR THE PREPARATION OF HETEROBIMETALLIC COMPLEXES

Alexander R. Treleven

Marquette University, 2016

There is currently much interest in the development of methods to harness sustainable, CO_2 neutral, non-fossil fuel based energy sources due to diminishing worldwide supply of fossil fuels and concerns over historically high levels of CO_2 in the atmosphere, which may have a devastating impact on the world's climate. One such avenue is through the conversion of atmospheric CO_2 into useful, high-energy density, organic fuel sources. Photosynthesis is the biological process by which plants convert sunlight, water, and CO_2 into the reduced organic materials that we extract from the earth and burn (completing the cycle back to CO_2) to release the energy stored in the bonds of the molecules. The development of synthetic methods to mimic the enzymatic processes of photosynthesis in order to utilize CO_2 as a carbon feedstock for organic fuels would be of tremendous benefit.

The one electron reduction of CO_2 to CO_2^- is a highly unfavorable process as evidenced by the relatively high reduction potential of -1.9V. The two electron reduction of CO_2 via proton assisted electron transfers is a more favorable process. Noble metals are known to undergo 2 electron processes though they are generally quite rare, expensive, and toxic to work with. Efforts have been made to use the more abundant first row transition metals (base metals) to mediate 2 electron processes with little success as they are more likely to undergo 1 electron redox processes. One such approach that has shown some success in achieving 2 electron processes with base metals is through the use

of bimetallic cooperativity where two separate metal centers, each involved in a 1 electron event, work in tandem to achieve a net 2 electron redox event.

This thesis describes investigations into metal complexes of new ligand designs involving a hard-soft approach to preferentially bind different metals in a site specific manner intended for the production of heterobimetallic complexes. Two classes of ligands are explored and described: (1) a series of P_2N_3 pincer type ligands and (2) a series of N-confused Trispyrazolylmethane (Nc-Tpm's) ligands.

ACKNOWLEDGEMENTS

Alexander R. Treleven

I would like to express my special appreciation and thanks to my advisor, Professor James R. Gardinier, for his tremendous guidance throughout my studies at Marquette University. I would like to thank him for encouraging my research and for allowing me to grow as a research scientist. I would also like to thank my committee members Professors Adam Fiedler and Jier Huang, for their encouragement, insightful comments, and support. I would like to thank my current and former group members, Kristin Meise and Dr. Jeewantha Hewage for their support and friendship throughout my time at Marquette.

I would like to thank the faculty members Dr. Sheng Cai (for help with NMR studies) and Dr. Sergey Lindeman (for providing single crystal diffraction analysis data). Finally, I would like to thank the Graduate School and all of the Marquette University administration.

TABLE OF CONTENTS

LIST OF TABLES

LIST OF FIGURES

LIST OF SCHEMES

Chapter 1

Introduction

There are two major energy related problems that are expected to impact the world over the next 50 years or so. The first problem is that sources of fossil fuels are expected to diminish so significantly that increased worldwide competition over control of these sources will lead to higher monetary and political costs.[1] The second problem is that the historically high levels of CO_2 currently in the atmosphere will continue to increase which is expected to have devastating impact on the world's climate. Also, because the ocean is a major sink for atmospheric CO_2, these projected impacts could also include ocean acidification.[2] Finding ways to harness sustainable, CO_2-neutral, non-fossil fuel based energy sources such as solar, wind, geothermal, and nuclear energy are of paramount importance to remedy these problems. Along with the challenges in generating sustainable energy are the challenges of transforming the energy produced by these sources into forms that can be safely transported, stored, and used on demand.[1]

The source of the carbon found in the fossil fuels and most synthetic organic chemicals that is used in our daily lives originates from atmospheric CO_2. Photosynthesis is the biological process used by plants to convert sunlight, water, and CO_2 into reduced

organic materials that we eventually extract from the earth and burn (completing the cycle back to CO_2) to release the energy stored in the bonds of the molecules.

Over billions of years of evolution, biological systems have developed diverse mechanisms for using sunlight to promote the fixation and transformation of CO_2 and of other small molecules. There are also multiple enzymes for the reduction of N_2 into ammonia, the production of H_2, and others to oxidize water and reduce oxygen. All of these enzymatic processes involve the storage and releasing of the energy in chemical bonds in a controlled and productive manner. If we are to overcome the looming energy challenges of the next few decades, then the development of the abilities to control these processes outside of the biological systems is of paramount importance. Thus by studying the metabolic processes observed in nature, we can gain insight into how to synthesize catalysts that will enable us to activate and transform CO_2 into useful, high energy density, organic fuel sources.

In order to be able to activate CO_2, one must first take a look at the general features and properties of the molecule in order to understand the best way to "attack" it. CO_2 is a linear molecule with relatively short bonds (1.16 Å) that is composed of polar C=O bonds though the overall molecule is non-polar due to the geometry of the dipole vectors. The Lewis structure of CO_2 is shown in Figure 1.1.

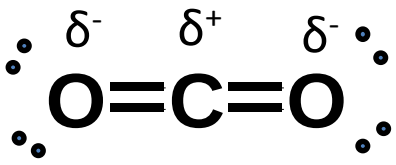

Figure 1.1. Depiction of the electronic distribution in CO_2 illustrating that the carbon atom is susceptible to nucleophilic attack while the oxygen atoms are susceptible to electrophilic attack. δ = partial informal charge.

In order to "activate" CO_2 by reduction, the bond order of the C-O bonds must be decreased and the molecule must be bent. The lowest unoccupied molecular orbital (LUMO) of normal CO_2 is centered on carbon, making it susceptible to nucleophilic attack and reduction. The highest occupied molecular orbital (HOMO) is mainly centered on the oxygen atoms, in accord with the expectations based on the Lewis structure. The frontier molecular orbitals of bent CO_2 shown in Figure 1.2 are similar, so will be involved in the interactions with nucleophiles and electrophiles.[1]

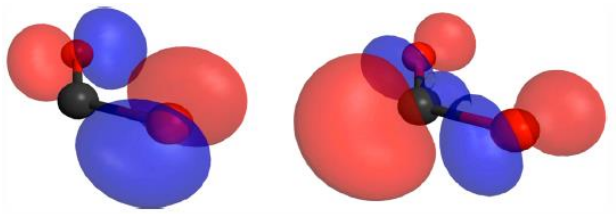

Figure 1.2. The wavefunction iso-probability contours for the HOMO (left) and LUMO (right) of bent CO_2 illustrating the strong charge localization. Illustration taken from reference 1.

As shown in the right side of Figure 1.2, the strongly localized wavefunction probabilities on the open side of carbon help to facilitate the transfer of electron density from an incoming nucleophile into the LUMO, enhancing the interaction with

nucleophiles. As shown in the left side of Figure 1.2, the localized electron density on oxygen of the HOMO (lone pairs) helps to facilitate interactions with electrophiles. When these two processes work in tandem, shown in Figure 1.3, the activation barrier to overcome the transformation is decreased, evident from the differences in the potentials of one-electron and two-electron reductions of CO_2, shown below in equations 1 – 6. The formation of new O-E and Nu-C bonds also plays a role.

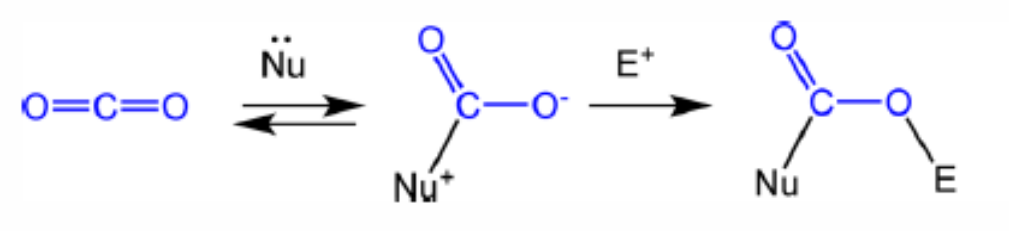

Figure 1.3. The combination of nucleophilic and electrophilic interactions affords a net two-electron reduction of CO_2.

As can be expected, the sensitivity of the energetic requirements of CO_2 reduction to pH and the number of electrons involved is very high. The reduction potentials for various half-reactions at pH 7 vs. NHE are shown in equations (1-6).

$CO_2\,(aq) + e^- \rightarrow CO_2^{-\bullet}\,(aq)$	$E^\circ = -1.9$ V	(1)
$CO_2\,(g) + 2H^+ + 2e^- \rightarrow CO\,(g) + H_2O$	$E^\circ = -0.52$ V	(2)
$CO_2\,(g) + H^+ + 2e^- \rightarrow HCO_2^-\,(aq)$	$E^\circ = -0.43$ V	(3)
$CO_2\,(g) + 4H^+ + 4e^- \rightarrow HCHO\,(aq) + H_2O$	$E^\circ = -0.51$ V	(4)
$CO_2\,(g) + 6H^+ + 6e^- \rightarrow CH_3OH\,(aq) + H_2O$	$E^\circ = -0.38$ V	(5)
$CO_2\,(g) + 4H^+ + 4e^- \rightarrow CH_4\,(aq) + 2\,H_2O$	$E^\circ = -0.24$ V	(6)

As shown in equation 1, the one-electron reduction of CO_2 is highly unfavorable with a large negative reduction potential of -1.9 V, due, in part, to the large amount of rearrangement energy required to bend the linear CO_2 molecule.[3] When the multielectron and multiproton reactions are coupled together, the overall transformation becomes much easier, as indicated by the milder reduction potentials (equations 2-6). As expected, these proton assisted electron transfers are more favorable under more acidic conditions (lower pH's)[4] and they are also solvent dependent.

Nature utilizes a variety of enzymes to activate small molecules. Gaining a better understanding of the reaction chemistry involved in the catalytically active sites in the enzymes could allow for experimenters to gain some insight into how these reactions are

performed in nature. This insight would in turn allow for rational and intelligent catalyst design for these CO_2 reduction reactions.

One class of enzymes that catalyzes the reduction of CO_2 in nature is the CO dehydrogenases. X-ray diffraction studies of these enzymes have been reported at sufficiently high enough resolution to gain some insight into the structure of the catalytically active sites. At the heart of one of the active sites is a Fe_3S_4 cluster that affixes terminal Ni and Fe centers in close proximity[5], as shown in Figure 1.4.

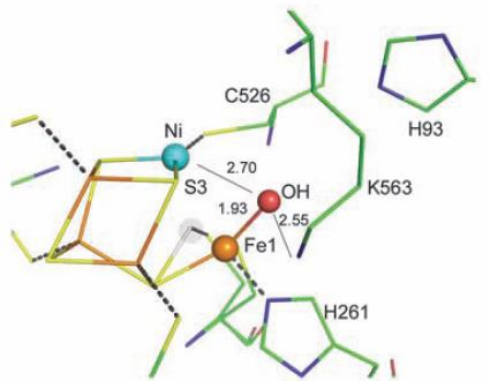

Figure 1.4. The catalytically active site of a CO dehydrogenase with a [FeNi] cluster active site. Illustration taken from reference 5. The close proximity of the Ni and Fe atoms (2.70 Å) allows for cooperation between both metals to activate the substrate.

In this site, the first coordination sphere of the terminal Fe^{II} atom consists of a cysteine, a histidine, a μ_3- sulfido ligand, and a fourth ligand of light atoms (likely H_2O or OH) while the first coordination sphere of the coordinatively unsaturated Ni^{II} atom consists of 3 S-

ligands in an unusual T-shaped geometry that may suggest the presence of a fourth hydride ligand.[6]

Based on the evidence gathered from single crystal X-ray diffraction, ^{13}C NMR experiments that independently provided evidence for the involvement of a CO_2 binding site and for an internal proton transfer network during catalysis by CO hydrogenase,[7] among other data, a mechanism for the reduction of CO_2 to CO by the enzyme was proposed (Figure 1.5).

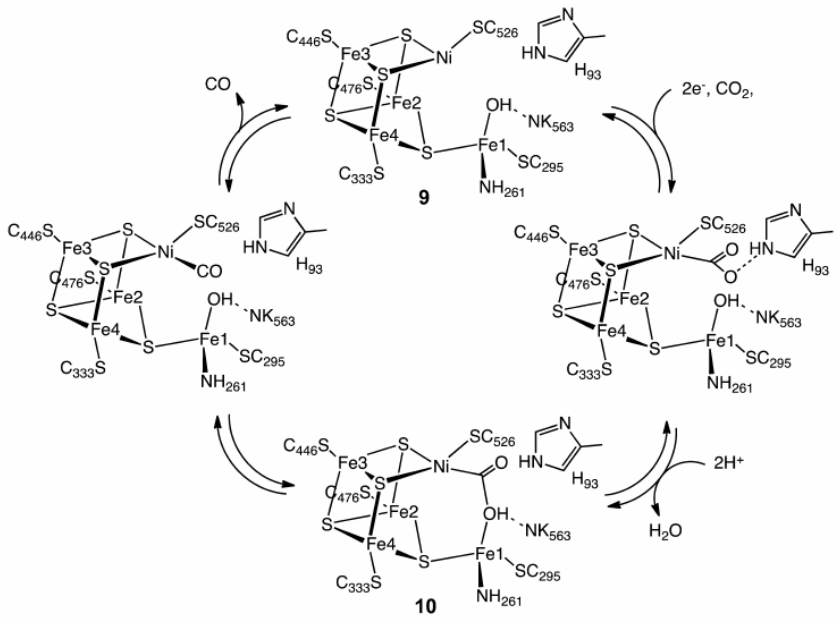

Figure 1.5. The proposed catalytic mechanism for the reduction of CO_2 to CO (and H_2O) by the [FeNi] based enzyme CO dehydrogenase. Illustration taken from reference 1.

Crystal structures were obtained for three different products of the reaction with CO_2. Treatment of crystals of the resting state of the enzyme with a reducing agent (Ti^{III} citrate) and bicarbonate ion showed the second stage of the catalytic cycle. This analysis showed CO_2 bridged across the Ni and Fe centers, as shown in Figure 1.6.

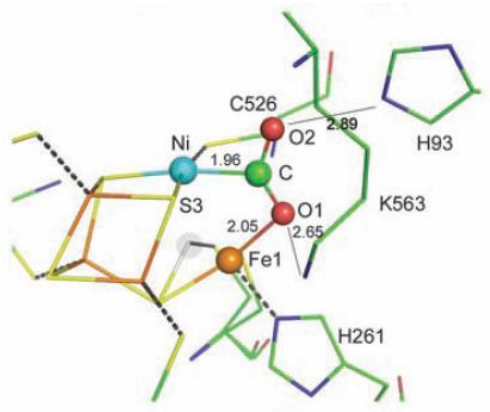

Figure 1.6. The second stage in the catalytic cycle of CO dehydrogenase. Illustration taken from reference 5. The bent CO_2 molecule is shown as a bridging ligand between the Ni and Fe sites demonstrating that both metal centers are involved in the mechanism of the reduction of CO_2 to CO.

The bridged CO_2 shown to be interacting with both metal centers simultaneously along with the observation that the Ni and Fe centers in the first stage of the cycle (Figure 1.4) were in close proximity to one another (2.70 Å) suggests the likelihood of cooperative interactions between the two metal centers during catalysis.

The cooperative behavior such as that found in the natural NiFe system has been mimicked in other purely synthetic, abiotic, systems whereby an electron rich center is positioned close to an electron poor center. These abiotic systems may be solid-state

compounds used in heterogenous catalysis or solution based compounds used for stoichiometric or catalytic transformations. Thus, there is extensive interest in CO_2 mineralization[8] using highly abundant geochemical systems such as in Equations 7-9:

$$CaO{\cdot}MgO \text{ (dolomitic lime)} + CaCl_2{\cdot}MgCl_2 \text{ (brine)} + CO_2 \rightarrow 2CaCO_3 + 2\ MgCl_2 \quad (7)$$

$$NaAlSi_3O_8 \text{ (alibite)} + CO_2 \rightarrow NaAl(CO_3)(OH)_2 \text{ (dawsonite)} + 3\ SiO_2 \quad (8)$$

$$H_2O + CO_2\ (g) + M_2CO_3\ (M = Ca, Mg, Fe) \rightarrow M(HCO_3)_2\ (s) \quad (9)$$

Similarly, other metal oxides are implicated as catalysts for methanol synthesis by hydrogenation of CO_2 (Equation 10).[9]

$$CO_2 + 3\ H_2 \rightarrow CH_3OH + H_2O \quad (10)$$

Here, active catalysts are Cu on MgO or Ni on ZnO. Most recently, it was found that Zn/ZnO was found to be an especially effective catalyst system for the reduction of $NaHCO_3$ (that can be generated from CO_2 and NaOH) to sodium formate, surpassing other metal supported systems with contributions from reactions (11 and 12).[10]

$$Zn + H_2O + NaHCO_3 \rightarrow ZnO + Na(HCO_2) + H_2O \quad (11)$$

$$ZnO + H_2 + NaHCO_3 \rightarrow ZnO + Na(HCO_2) + H_2O \quad (12)$$

In this system in-situ formed Zn-OH and Zn-H are proximal so as to act cooperatively to reduce the bicarbonate ion to formate.[10]

One class of soluble homogenous systems for CO_2 activation is "frustrated Lewis acid-base pairs" (FLP's).[11] FLP's operate on the concept where steric congestion prevents combinations of Lewis acids and bases from forming classical Lewis acid-base adducts but instead form close "encounter complexes" that set up a localized electric field gradient to help polarize incoming molecules.[12] These FLP's have been shown to produce some remarkable reactivity, including reversible activation of H_2[13], B-H activation[14], and N-H activation[15], among examples of many others. Ménard and Stephan[11] showed an example of an irreversible capture of CO_2 by $AlBr_3$ with $PMes_3$ (Mes = 2,4,6-$C_6H_2Me_3$) in an unusual acid-base ratio of 2:1, as shown in Figure 1.7.

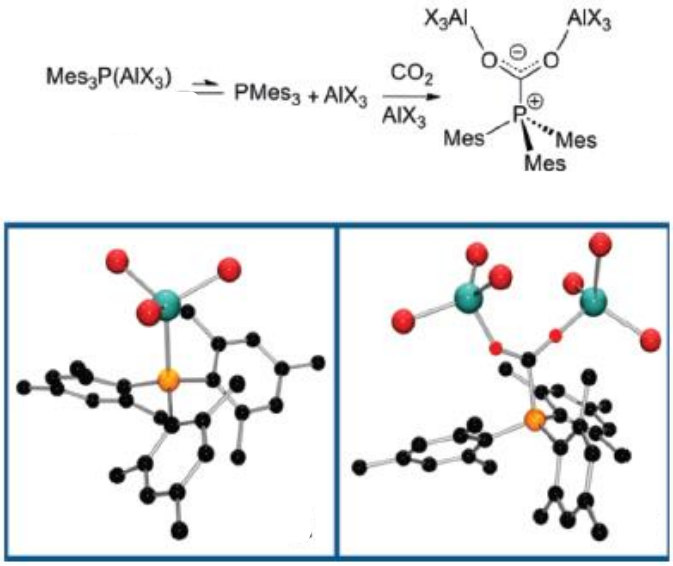

Figure 1.7. Demonstration of CO_2 capture by FLP's utilizing $AlBr_3$ and $PMes_3$ (Mes = 2,4,6-$C_6H_2Me_3$) in a 2:1 acid-base ratio. X = Br. Illustration taken from reference 11.

This activated CO_2 species reacted with excess ammonia borane (NH_3BH_3, a hydrogen source) at room temperature to give methanol upon quenching with water.[11]

There are a few other types of systems that exploit chemical cooperativity to activate small molecules. One type utilizes metal-ligand cooperativity that features a compound with a coordinatively unsaturated metal bound to an electron rich ligand site, as shown in Figure 1.8.

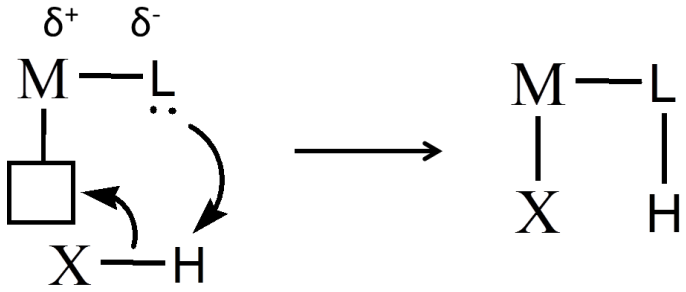

Figure 1.8. Metal ligand cooperativity where a coordinatively unsaturated metal bound to an electron rich ligand work together to activate a small molecule H-X breaking the H-X bond and forming two new bonds.

For example, Gusev and coworkers[16] showed that an NNP pincer ligand bound to a coordinatively unsaturated ruthenium site could activate H_2 by utilizing metal ligand cooperativity between a vacant ruthenium site and an amido lone pair, as shown in Figure 1.9.

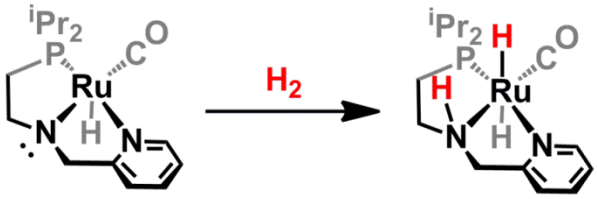

Figure 1.9 Metal ligand cooperativity being utilized to activate H_2. Illustration taken from reference 16. The Ruthenium metal center is coordinatively unsaturated, meaning it has an open coordination site available to bind and incoming substrate. The electron rich anionic amine serves as the electron rich ligand bound to the metal center.

Grützmacher and associates[17] showed the activation of N-H bonds with their amine based diene ligand bound to a coordinatively unsaturated Rhodium center along with a triphenyl phosphine ligand, as shown in Figure 1.10.

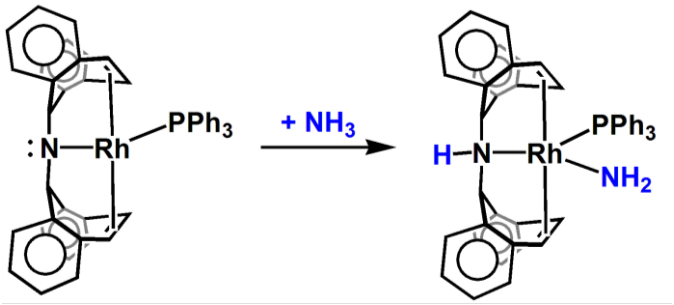

Figure 1.10. Metal ligand cooperativity in the activation of the N-H bonds of ammonia forming two new bonds. Illustration taken from reference 17. It is noted that the oxidation number of the metal does not change in these types of reactions.

Another similar approach toward the activation of small molecules through cooperative effects is through the use of metal-metal cooperativity, as shown in Figure 1.11.

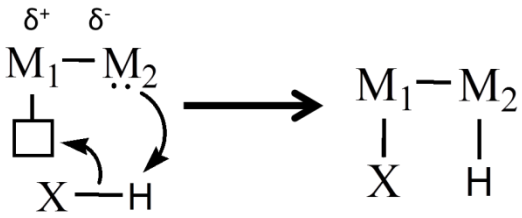

Figure 1.11. Metal-metal cooperativity utilizes two different metal sites with differing electronegativities to activate polar bonds.

Metal-metal cooperativity takes advantage of the polar nature of heterometallic bonds (owing to the different electronegativities of the metals). A complication arises in these

compounds because both metals need to be coordinatively unsaturated with one of the metals being more electron deficient than the other, inviting coordination by Lewis bases. As discussed previously, this motif may be useful toward the activation of small molecules with polar bonds (CO_2) because electron density can be removed from one atom of the molecule (the more electron rich atom in the bond) while donating electron density to the more electron deficient atom, reactivity can be increased, as illustrated in Figure 1.12.

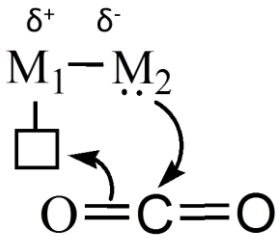

Figure 1.12 The idealized mechanism for the activation of CO_2 utilizing metal-metal cooperativity.

Among the examples in the literature of the utilization of metal-metal cooperativity to activate small molecule substrates, there are generally two types: those supported by a bridging ligand and those without a bridging ligand (unsupported), as shown in Figure 1.13.

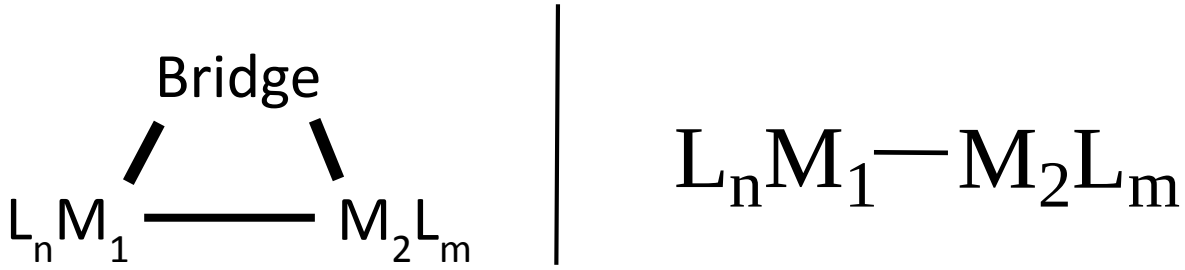

Figure 1.13 Supported vs. unsupported heterobimetallic complexes.

The supported complexes (Fig. 1.13, left) features some type of bridging ligand (usually an organic linker) to help hold the metals together to facilitate metal-metal bonding. The unsupported variety (Fig. 1.13, right) is held together by the interactions between the metal d orbitals of the two metals in the bond exclusively. The ligand scaffold is only there to stabilize the individual metal sites, not to help hold them in close proximity to one another. One of the first examples of a supported heterobimetallic complex that showed some activity toward CO_2 was developed by Bergman and associates.[18] They made use of a tert-butyl amido linker to help facilitate bonding between IrCp* and $ZrCp_2$ fragments in their heterobimetallic complex. They demonstrated some remarkable reactivity with their complex by showing that it could activate a variety of small molecule substrates, including the activation of N-H, H-H, O-H, and C=O bonds, as shown in Figure 1.14.

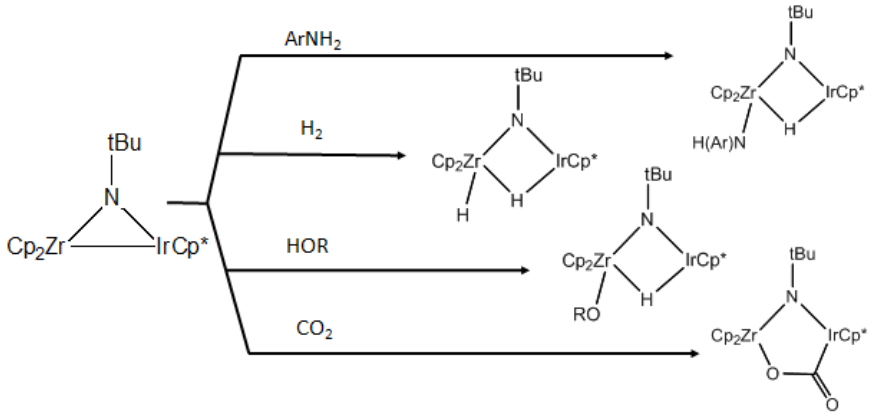

Figure 1.14. Substrates and products seen in reactivity studies of the supported heterobimetallic Zr/Ir complex including activation of N-H, H-H, O-H, and C=O bonds.

Though this complex showed some remarkable activity and demonstrated the utility of this approach, it is far from ideal. The major disadvantage of this complex is that it incorporates Iridium as one of the metals in the complex. Although it is observed in the literature that noble metals are some of the most efficient and useful catalysts, they are also relatively scarce and expensive. Noble metals such as Iridium are also generally quite toxic and difficult to work with safely so efforts toward replacing noble metals as the active sites in homogeneous catalysts to first row transition metals (less expensive, more abundant, less toxic) have been explored.

Another problem to this type of complex is that the synthesis was not trivial. Another approach to binding two metals with varying degrees of electron density is to make use of a hard-soft concept to bind specific metals to specific sites. The idea is that the ligand design will incorporate two different ligand binding sites (a hard and soft site)

to preferentially and selectively bind harder or softer metals. In general, hard metals tend to be small, electron deficient cations with large positive charges (e.g. Zr^{4+}, Mg^{2+}) whereas softer metals tend to be more electron rich, large polarizable cations (e.g. Ag^{+}). Hard ligand donors tend to be nitrogen or oxygen while softer donors tend to be phosphorus or sulfur.

This hard-soft concept has been utilized by Christine Thomas and coworkers[19] in their studies of CO_2 reduction using the phosphinoamide ligands, shown in Figure 1.15.

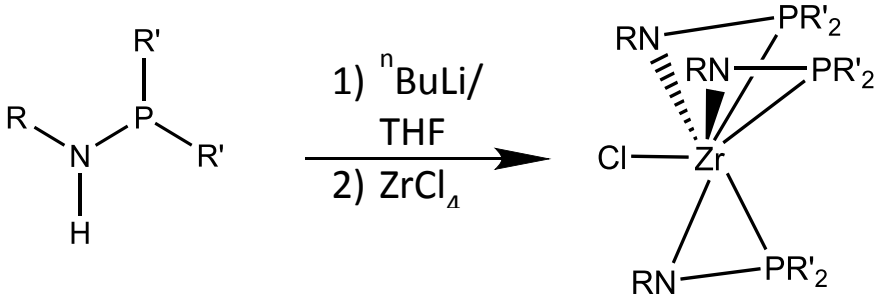

Figure 1.15. Phosphinoamide ligands (L) used by Thomas[19] with hard and soft donor sites. R = 2,4,6-trimethylaniline, ^{i}Pr. R' = iPr, Ph.

Through deprotonation of the amine using ^{n}butyl lithium in THF followed by addition of $ZrCl_4$ allowed for the isolation of the $ZrCl(L)_3$ metalloligand shown above in Figure 1.15. Subsequent treatment of the metalloligand with 1 eq of CoI_2 in THF allowed for the isolation of the heterobimetallic complex (1) shown in Figure 1.16. Complex (1) was reduced using a 0.5% Na/Hg amalgam in THF to yield the diamagnetic (d^{10}) complex that upon exposure to CO_2, showed the ability to add CO_2 across the metal-metal bond,

breaking one of the C=O bonds, which resulted in a terminal CO and a bridging O between the two metal centers, shown in Figure 1.17.

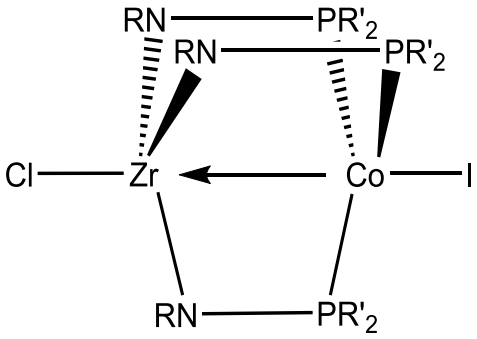

Figure 1.16 Heterobimetallic complex developed by Thomas that demonstrates the hard/soft binding concept. The hard ligand donor atoms (N's) preferentially bind the hard metal (Zr^{4+}) while the softer ligand donor atoms (P's) preferentially bind the softer metal center (Co^{+}). R = 2,4,6-trimethylaniline, ^{i}Pr. R' = iPr, Ph.

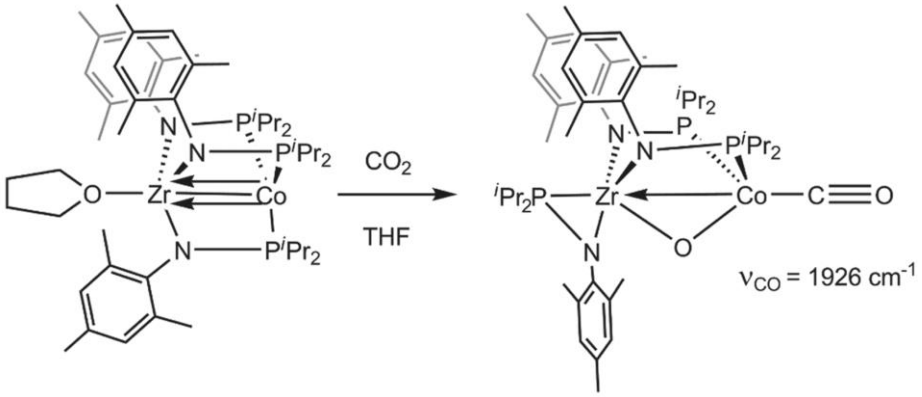

Figure 1.17 Activation of CO_2 by a heterobimetallic Zr/Co complex resulting in a terminal CO along with a bridged oxo species from reference 19.

The oxo bridged species was characterized in a number of ways including x-ray crystallography, infrared absorption spectroscopy (ν_{CO} = 1926 cm^{-1}), and magnetic studies (S = 1). All characterization data was consistent with the structure shown in the right of Figure 1.17.

The authors went on to show that the activated CO_2 could be converted to carbon monoxide (CO) and methanol through three additional stoichiometric reactions, shown in Figure 1.18. Addition of methyl triflate (MeOTf) to the anionic oxo species resulted in formation of corresponding methoxide species (1). Addition of 1 eq of HCl to the methoxide species afforded complex (2). Complex (2) was photolyzed in the presence of I_2 to regenerate complex (3). The authors showed through the stoichiometric reactions that the process is feasible to return the catalyst to a reactive species, though catalytic turnover has not yet been achieved.

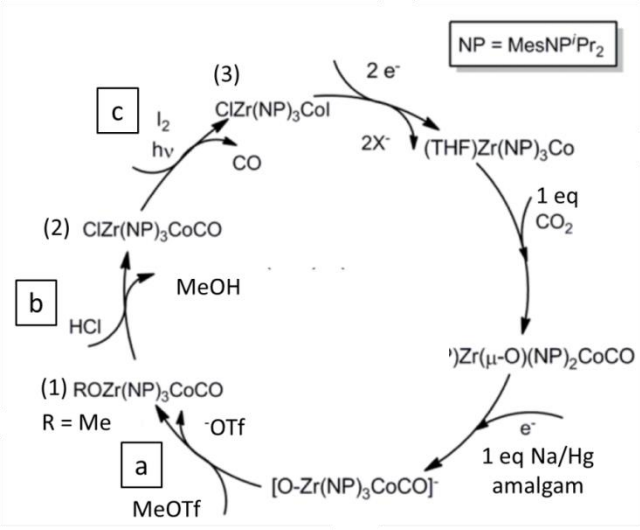

Figure 1.18. The stoichiometric conversion of CO_2 to carbon monoxide (CO) and methanol (MeOH) using Thomas's bimetallic catalyst. Illustration taken from reference 19.

Another type of ligand design for the development of supported bimetallic complexes is the pyrazole derived compartmental ligand, as was demonstrated by Meyer and associates[20], shown in Figure 1.19.

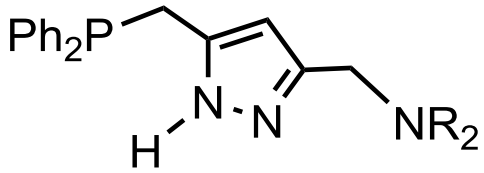

Figure 1.19. Compartmental ligand with hard and soft binding sites. R = CH_2CH_2SEt.

The compartmental ligand with different chelating arms in the 3- and 5- positions of pyrazole has been shown to be an effective ligand scaffold for the preparation of heterobimetallic complexes containing Pd(II) in the soft site (P-N) and Ni(I) in the harder site (N_2S_2). Treatment of the deprotonated ligand with 1 eq $PdCl_2$ followed by 1 eq $NiCl{\cdot}6H_2O$ in sequential order led to isolation of the heterobimetallic complex only, without any evidence of the formation of its homobimetallic analogues[20], demonstrating that the complexation reaction is highly selective.

Another approach toward the activation of small molecules utilizing metal-metal cooperativity is to use unsupported metal complexes, as was previously shown in Figure 1.13. Unsupported metal complexes have been known for some time. Doyle and associates[21] made some unsupported Fe – Cu metal cluster complexes that contained two distinct metals in close proximity to one another (bound together in this case), as shown in Figure 1.20.

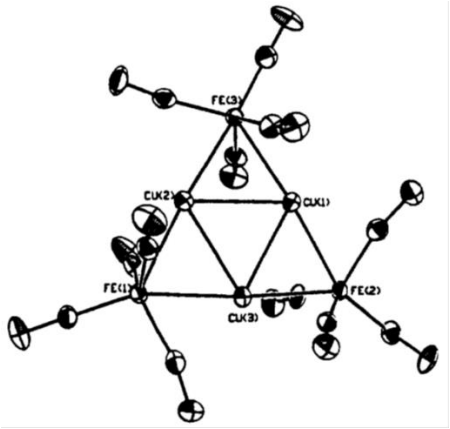

Figure 1.20 An ORTEP diagram of the structure of the $Cu_3Fe_3(CO)_{12}^{3-}$ anion with unsupported metal-metal bonds. View is perpendicular to the plane containing the six metal atoms and only the metal atoms have been labeled for clarity. Illustration taken from reference 21.

A number of other types of unsupported mixed metal clusters are known though their reaction chemistry was largely unexplored.[21]

More recently, the Mankad group[22] has taken a different approach toward making unsupported bimetallic systems. They have made use of bulky nitrogen containing heterocyclic carbenes (NHC's) to stabilize a Cu metal center and have reacted this copper

chloride metalloligand precursor with a variety of anionic metal fragments, whose relative nucleophilicities have been measured and tabulated.[23] The general scheme toward the synthesis of these complexes is shown in Scheme 1.1.

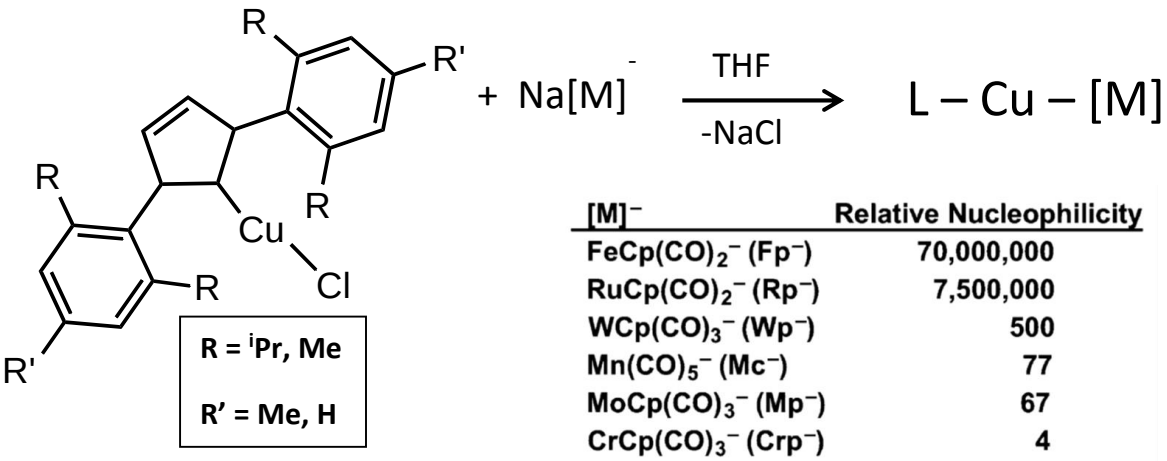

[M]⁻	Relative Nucleophilicity
$FeCp(CO)_2^-$ (Fp^-)	70,000,000
$RuCp(CO)_2^-$ (Rp^-)	7,500,000
$WCp(CO)_3^-$ (Wp^-)	500
$Mn(CO)_5^-$ (Mc^-)	77
$MoCp(CO)_3^-$ (Mp^-)	67
$CrCp(CO)_3^-$ (Crp^-)	4
$Co(CO)_4^-$ (Cc^-)	1

Scheme 1.1. The general strategy employed by the Mankad group to synthesize a series of unsupported bimetallic complexes. Illustrations taken from references 22 and 23.

Unsupported metal complexes have some unique challenges associated with them if the ligands stabilizing the metal centers are not sufficiently bulky enough to prevent ligand redistribution to form an ionic pair of dimers, as shown in Figure 1.21.

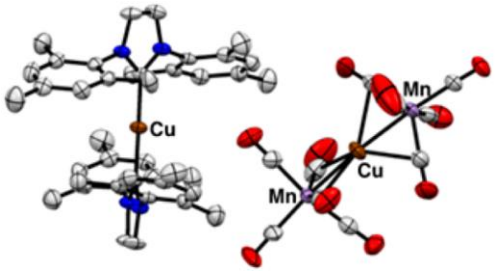

Figure 1.21. Structure of the ion pair of dimers obtained from equilmolar mixtures of (NHC)CuCl and $Na[Mn(CO)_5]$. Bulkier NHC ligands are required to prevent this isomerization. Illustration taken from reference 22.

The authors found that when isopropyl groups are used as the R groups shown in Scheme 1.1, that the metal complexes do not form the ion pair of dimers.

They then sought out to explore the reactivity of these mixed-metal complexes by attempting the C-H borylation of D_6-benzene. The general method of this study is shown below in Scheme 1.2.

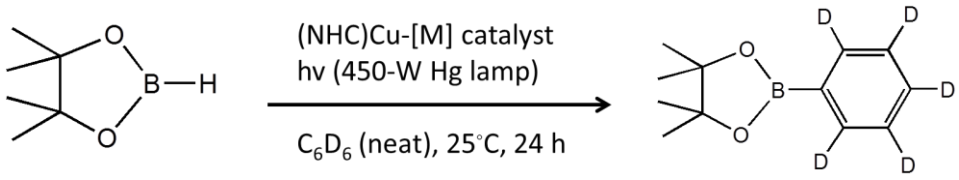

Scheme 1.2 The general reaction method performed on a series of unsupported metal complexes.

The reactions were performed under an N_2 atmosphere with 5 mg of catalyst and 1 mL of D_6-benzene. Ten equivalents of pinacol borane were then added and the reaction vessel was irradiated with UV light for 24 hours. An internal standard (either mesitylene or 1,3,5-trimethoxy benzene) was added and the products of 3 repeated reactions were determined by ^{1}H and ^{11}B NMR spectroscopy. The experimenters performed the previous reaction on the series of metal complexes, as summarized in Table 1.1.

Entry	Catalyst	Loading	[B]–H	NMR Yield
1	(BDI)Zn–Fp	10 mol%	HBpin	37%
2	(IPr)(Cl)Zn–Fp	10 mol%	HBpin	0%
3	(IPr)Cu–Fp	10 mol%	HBpin	71%
4	(IPr)Cu–Fp	5 mol%	HBpin	71%
5	(IPr)Cu–Fp	2.5 mol%	HBpin	26%
	(IPr)Cu–Fp*	10 mol%	HBpin	24%
6	(IMes)Cu–Fp	10 mol%	HBpin	33%
7	(SIMes)Cu–Fp	10 mol%	HBpin	0%
8	Fp_2	10 mol%	HBpin	<5%
9	KFp	10 mol%	HBpin	0%
10	FpBpin	10 mol%	HBpin	8%
11	(IPr)Cu–Cl	10 mol%	HBpin	0%
12	(IPr)Cu–Fp	10 mol%	HBcat	24%
13	(IPr)Cu–Fp	10 mol%	B_2pin_2	61%

Table 1.1. A summary of the results of the reactions shown in Scheme 1.2. Table taken from reference 22. BDI stands for β-diketoiminate (not discussed). IPr stands for the isopropyl version of the NHC ligand in Scheme 1 where R = iPr. IMes stands for the mesitylene version of the NHC ligand in Scheme 1 where R = Me.

Through this study, the authors were able to make some conclusions about the catalytic activity of their unsupported bimetallic catalysts. They found that the bulky isopropyl NHC's performed the best under these conditions and that increased catalyst loading did not improve the yield, as shown by entries 3 and 4. They also found that the optimal catalyst reacted with a variety of other substrates as well, including catechol borane (HBcat) and a pinacol borane dimer (B_2Pin_2). Most importantly, the authors found that the monometallic analogues, shown in Figure 1.22, did not achieve catalytic turnover, at best only observing stoichiometric conversion of substrate to product.

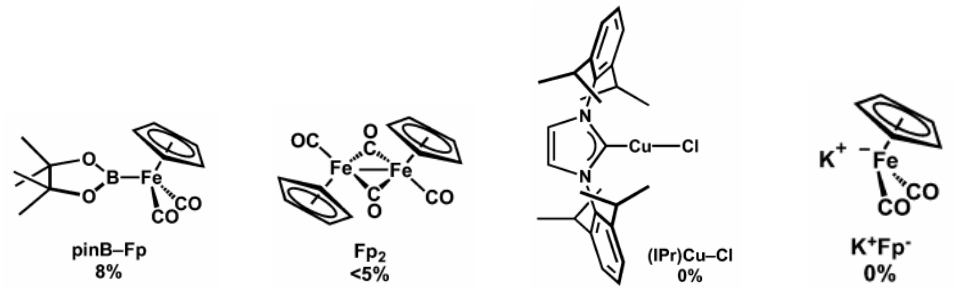

Figure 1.22. Monometallic analogues of bimetallic catalysts for Scheme 1.2. Illustrations taken from reference 22.

The above observations demonstrate that both metal centers are required to achieve catalytic turnover in this reaction as the addition of either of the monometallic analogues did not. From these data the authors were able to propose a catalytic mechanism consistent with their observations, shown in Figure 1.23.

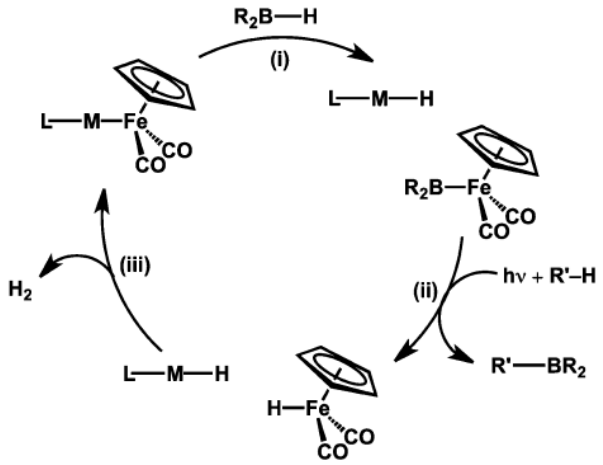

Figure 1.23. The proposed catalytic mechanism of the C-H borylation reaction by the heterobimetallic catalyst (NHC)Cu-FeCp(CO)$_2$. Illustration taken from reference 22.

As seen in Figure 1.23, the mechanism features three critical steps to achieve catalytic turnover: i) bimetallic oxidative addition with metal-metal bond cleavage, ii) photochemical C-H borylation by the resulting boryl-iron intermediate, and iii) H-H bimetallic reductive elimination with metal-metal bond reformation. The authors believe that bimetallic oxidative addition of HBpin by (NHC)Cu-$FeCp(CO)_2$ is an equilibrium process that lies toward the (NHC)Cu-$FeCp(CO)_2$ side and that small concentrations of (NHC)Cu-H and $FeCp(CO)_2$-Bpin account for the observed reactivity.[22]

This study was the first example of the use of 1st row transition metals to catalyze a C-H borylation reaction, reactivity previously only observed with the use of noble metals such as Rhodium[24], as shown in Figure 1.24.

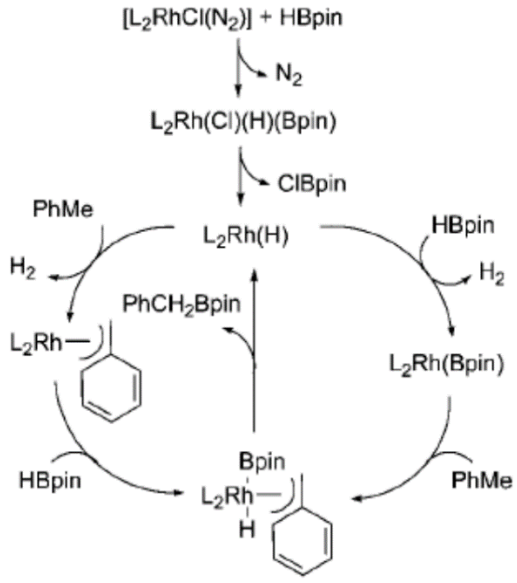

Figure 1.24. The catalytic reaction mechanism of the C-H borylation of toluene by a noble metal catalyst (Rh in this case). L = P^iPr_3. Illustration taken from reference 24.

Noble metals are known to undergo 2 e^- redox processes, as was shown in Figure 1.23. This can be a challenge for first row transition metals as they tend to undergo 1 e^- redox processes. Utilization of the concept of bimetallic cooperativity allows for these first row transition metal to work together to net a 2 e^- redox event, though each individual metal center only undergoes a 1 e^- event[22], as shown in Figure 1.25.

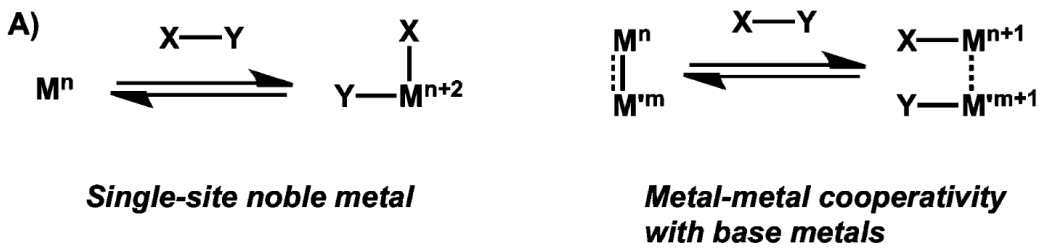

Figure 1.25. Oxidative addition by a single-site noble metal (left) and by metal-metal cooperativity with base metals (right). Illustration taken from reference 22.

From these experiments, the authors were able to make some general conclusions. Bulky heterocyclic carbenes are particularly well suited to stabilize a wide range of unsupported Cu-M bonding as well as prevent isomerization through ligand redistribution. Cu-M bond distance in unsupported bimetallic complexes tends to decrease with increasing nucleophilicity of the anionic metal fragments bound to them. Bimetallic versions of classical oxidative addition and reductive elimination steps have been demonstrated with 1st row metals. Catalytic C-H borylation reactions have been demonstrated using 1st row metals by utilizing metal-metal cooperativity, reactivity that previously required the use of noble metals.

1.1 Goal of research

The overall purpose of this work was to explore the possibility of preparing hetero-bimetallic complexes utilizing a hard-soft approach to preferentially bind different metals in a site specific manner and to examine the properties of these metal complexes toward the activation of small molecules, mainly CO_2. With these concepts in mind, a number of target ligand scaffolds were envisioned that might be able to bind two or more different metals in close proximity to one another. The first type is of a series of pincer-type ligands shown in Chart 1.1.

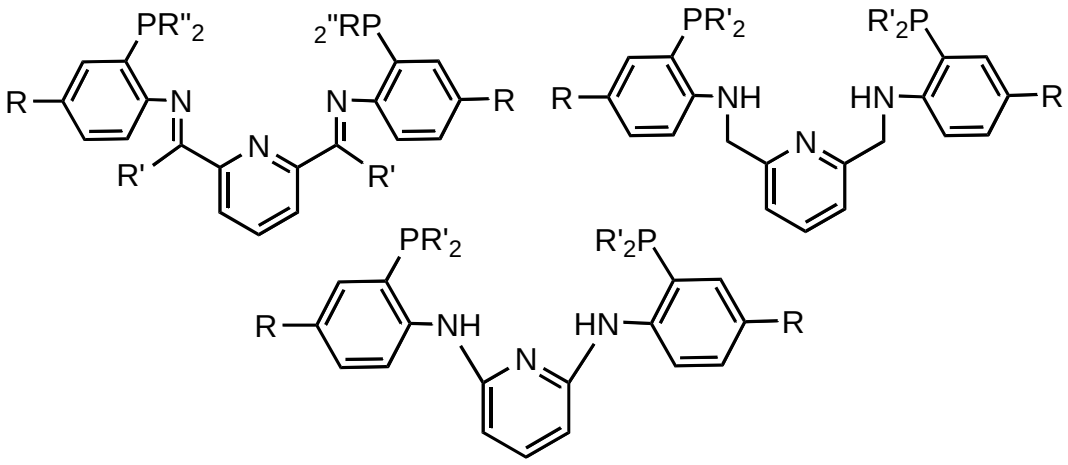

Chart 1.1. Pincer-type target ligand scaffolds with separate hard and soft binding sites.

The next type is another pincer-type ligand that is asymmetrical and contains N-P bonds, shown in Chart 1.2.

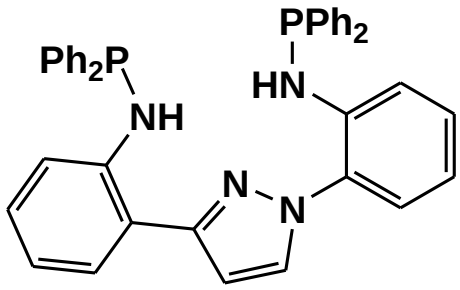

Chart 1.2. Pincer-type target ligand scaffold with separate hard and soft binding sites.

With these ligands one can envision that the harder metal will chelate to the N3 portion of the molecule while a softer metal (or two) can bind to the phosphorus atom. In each case, changing substituents near the metal center may provide steric shielding necessary to prevent dimer formation, but still allow access to small molecules. Another series of target scaffolds potentially capable of binding two different metals are nitrogen-confused scorpionate (NC-scorpionate) ligands, shown in Chart 1.3.

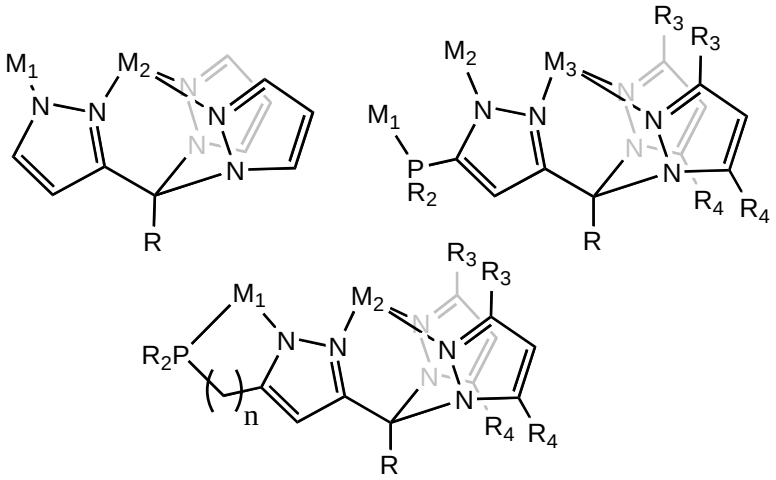

Chart 1.3 N-confused scorpionate target ligand scaffolds. R = H, Me, Et. R_2 = Ph, ^{i}Pr. R_3 = R_4 = H, Me.

The NC-scorpionate ligands are named due to the apparent "confused" positioning of one of the pyrazole heterocycles compared to traditional tris(pyrazolyl)methane (Tpm) scorpionates, where by the C and N atoms of the ring are interchanged, as shown in Figure 1.26.

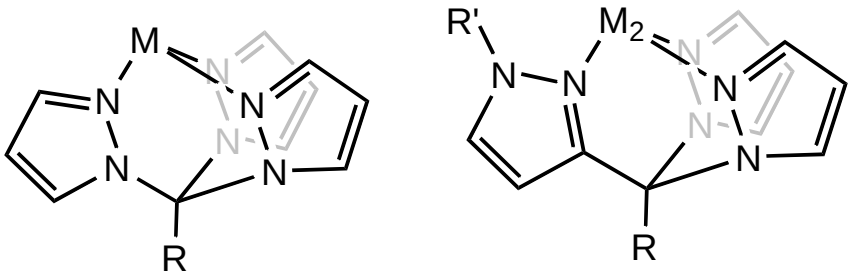

Figure 1.26. Traditional tris(pyrazolyl) methane (Figure 1.26, left) and N-confused tris(pyrazolyl) methane (Figure 1.26, right).

This nomenclature was clearly inspired by the complimentary NC-porphyrins[25], shown in Figure 1.27.

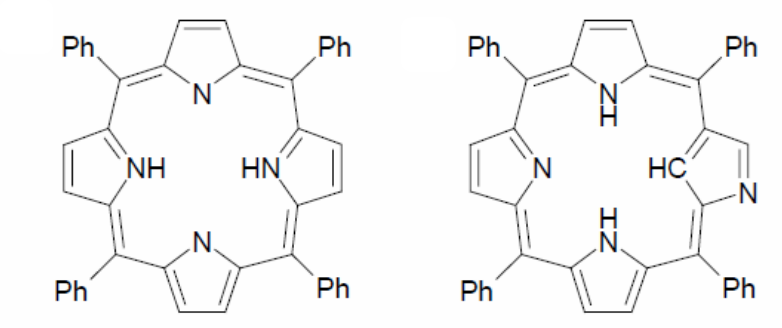

Figure 1.27. The structures of freebase tetraphenylporphyrin (left) and the internally protonated freebase N-confused tetraphenylporphyrin. Illustration taken from reference 25.

None of these ligands have been prepared before. So the challenge is many-fold. First, the preparation of the ligands is required. Second, the reactivity toward metals needs to be investigated with an aim to prepare mono- and bimetallic derivatives with low coordination numbers to ensure reactivity with incoming molecules. Third, we will explore the possibility of forming metal-metal bonded species. Lastly, the reactivity with small molecules H_2 and CO_2 with highly reactive variants will be pursued.

Chapter 2

PREPARATION OF NEW P_2N_3 PINCER-TYPE LIGANDS AND THEIR METAL COMPLEXES.

2.1 INTRODUCTION

The overall purpose of this work was to explore the possibility of preparing heterobimetallic complexes utilizing a hard-soft approach to ligand design intended for the preferential, site-specific binding of different metals. The properties of these metal complexes toward the activation of small molecules, mainly CO_2, will be explored.

N3-pincer scaffolds such as shown in Figure 2.1 have been shown to support highly reactive metal complexes that are capable of mediating small molecule activation reactions and catalytic transformations. The Chirik group made use of iron complexes of a redox-active

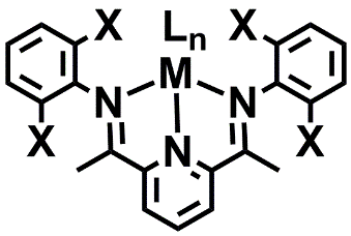

Figure 2.1. Generic depiction of a metal complex of a redox-active pyridine(diimine), (PDI), N3- pincer ligand.

pyridine(diimine) ligand (PDI) as catalysts for the intermolecular [2+2] cycloaddition of unactivated alkenes and cross cycloaddition of alkenes and dienes as regio- and stereoselective routes to cyclobutanes.[26] Brookhart et al [27] also utilized similar Fe(PDI) catalysts that showed excellent selectivity and reactivity for the oligomerization of ethylene. Recently, Bart and coworkers have shown that triply reduced PDI ligands help support unusual oxidative addition type chemistry at a uranium IV center, Figure 2.2.[28]

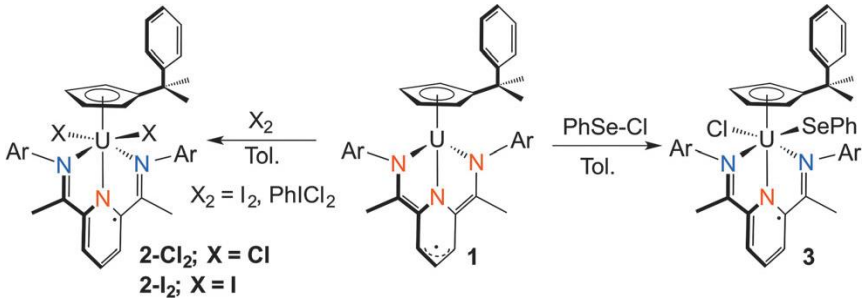

Figure 2.2. Small molecule activation reactions promoted by uranium complexes of triply reduced PDI ligands from reference 29.

In most of the cited work with PDI ligands, bulky aryl groups, such as 2,6-xylyl, 2,6-diisopropylphenyl, or mesityl are bound to nitrogen to provided steric protection and low coordinate metal centers. We envisioned that replacing these aryls with phosphinoaryls would maintain steric bulk but would add the capacity for forming heterometallic complexes as in Scheme 2.1. Unfortunately, ligands such as those in Scheme 2.1 are not found in the literature so the initial challenge was to prepare the

ligands. Then, if successful, prepare and study the reaction chemistry of their metal complexes.

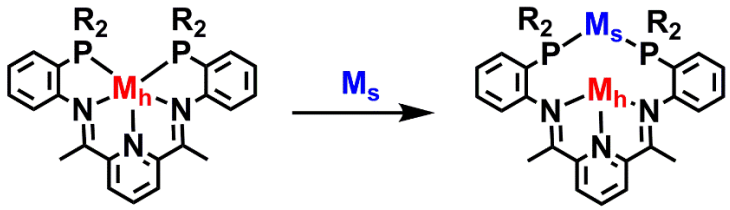

Scheme 2.1. Hypothetical Mono- and heterobimetallic complexes of P_2N_3-pincer ligands (M_s = soft metal; M_h = hard metal).

2.2 RESULTS AND DISCUSSION.

A. P_2N_3-PDI Type Ligand.

A number of methods were explored in an attempt to make a ligand such as that in Scheme 2.1 but most were unsuccessful, as outlined later. The most promising route to a **(PDI-P_2N_3)** ligand scaffold is shown in Scheme 2.2.

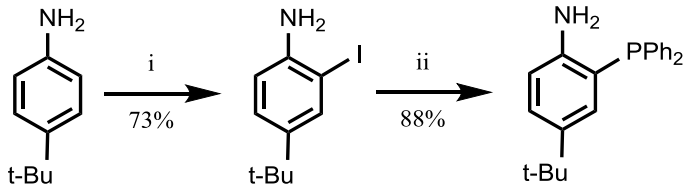

1A **1B**

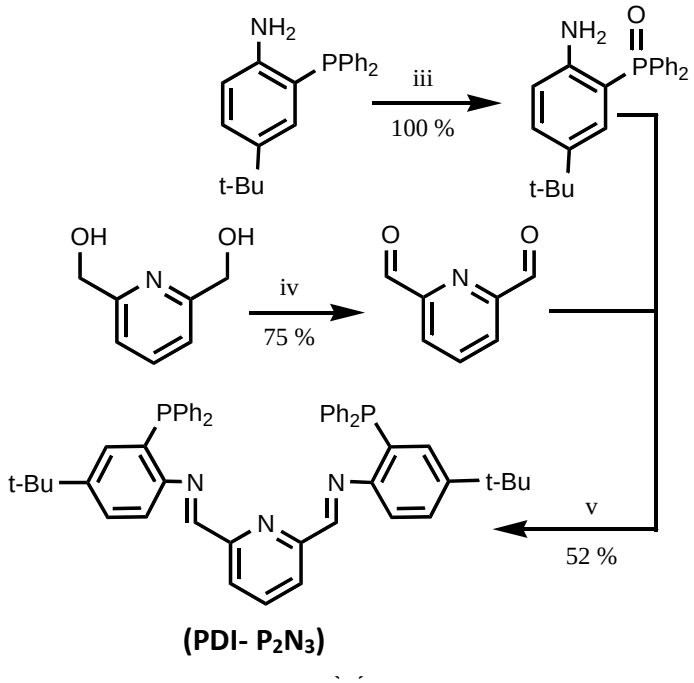

Scheme 2.2. The synthetic route toward the preparation of the **(PDI- P_2N_3)** ligand. Key: i) 0.55 eq Ag_2SO_4, 1.05 eq I_2, EtOH, 4 hrs; ii) 1.1 eq $HPPh_2$, 2 eq Cs_2CO_3, 35 mol% DMED, 0.5 mol% $Pd(PPh_3)_4$, toluene, Δ 15 hrs; (b) Key: iii) 30% w/w H_2O_2 in water, DCM, 5 minutes; iv) 2 eq SeO_2, dioxane, Δ 4 hrs; 3 eq aniline, 10 mol% p-toluenesulfonic acid monohydrate, toluene, Dean-Stark conditions, Δ 16 hrs; v) 10 mol % p-toluenesulfonic acid monohydrate, toluene, Dean-Stark conditions.

Commercially available 4-*tert*-butylaniline was iodinated at the 2 position to afford the iodo aniline precursor (**1A**) in modest yield that was used as the intermediate in the next step. A palladium(0) catalyzed reaction between $HPPh_2$ and **1A** led to the isolation of a diphenylphosphino aniline precursor (**1B**) in good yield. Oxidation of the precursor was found necessary to give a condensation reaction with the known diformylpyridine.[30] Attempts to directly condense the diphenylphosphino-tert-butyl aniline precursor (**1B**), as well as the iodo aniline precursor (**1A**), directly onto 2,6-diformyl or 2,6-diacetylpyridine were unsuccessful. A summary of the attempted reactions of this type are shown in Figure 2.3.

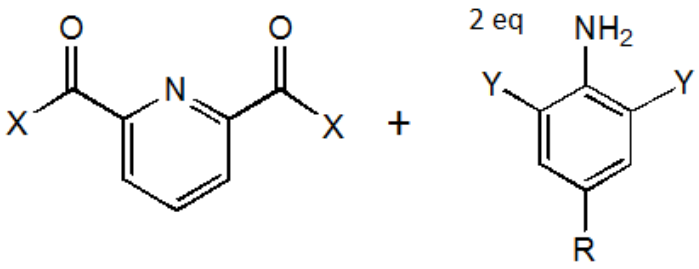

X	Y	R	Conditions	Success
H	H	Me	MeOH (RT)	Y
H	H	Me	Tol (Dean-Stark)	Y
H	I	Me	MeOH (RT)	N
H	I	t-Bu	Tol (Dean-Stark)	N
H	I	Me	EtOH (reflux)	N
H	PPh_2	t-Bu	Benz (Dean-Stark)	N
H	PPh_2	t-Bu	EtOH (reflux)	N
Me	H	Me	MeOH (reflux)	Y/N
Me	PPh_2	Me	EtOH (reflux)	N

Figure 2.3. Summary of results from condensation reactions between diformyl- or diacetyl-pyridine and various anilines.

The condensation of anilines onto the diformyl and diacetyl pyridine derivatives proved to be largely successful. Incorporation of either an iodine or diphenylphosphino substituent at the 2 position of the aniline prior to condensation led to re-isolation of starting materials. Condensation of the phosphine oxide version of **1B** onto 2,6-diformylpyridine was met with limited success. The reported 52% yield was achieved once; the product is easily identified by its ^{1}H NMR spectrum by the presence of a resonance at 8.3 ppm for the imine proton. Unfortunately, the synthesis was not reproducible, for reasons that are not clear. Preliminary work aimed at removing the oxygen atom from phosphine by various reductive pathways was unsuccessful, as either the imine portion of the ligand was also reduced ($LiAlH_4$), or only one oxygen atoms was removed, or no reaction occurred. Future work should be devoted to attempting to

reproduce the successful result as well as finding a way to reduce the oxidized phosphine. A promising strategy was found on a model system to prepare the phosphorus sulfide analogue and deprotect with diisobutylaluminum hydride (DIBAL-H) showing approximately 30 % conversion to the desired product.

B. H_2(Fl-P_2N_3) Type Ligand.

Owing to synthetic difficulties described above and the result of over-reduction, we turned our attention on preparing a pincer with saturated organoamine arms or to explore other scaffolds altogether. Thus, for the former, the new ligand **H_2(Fl-P_2N_3)** was prepared as outlined in Scheme 2.3.

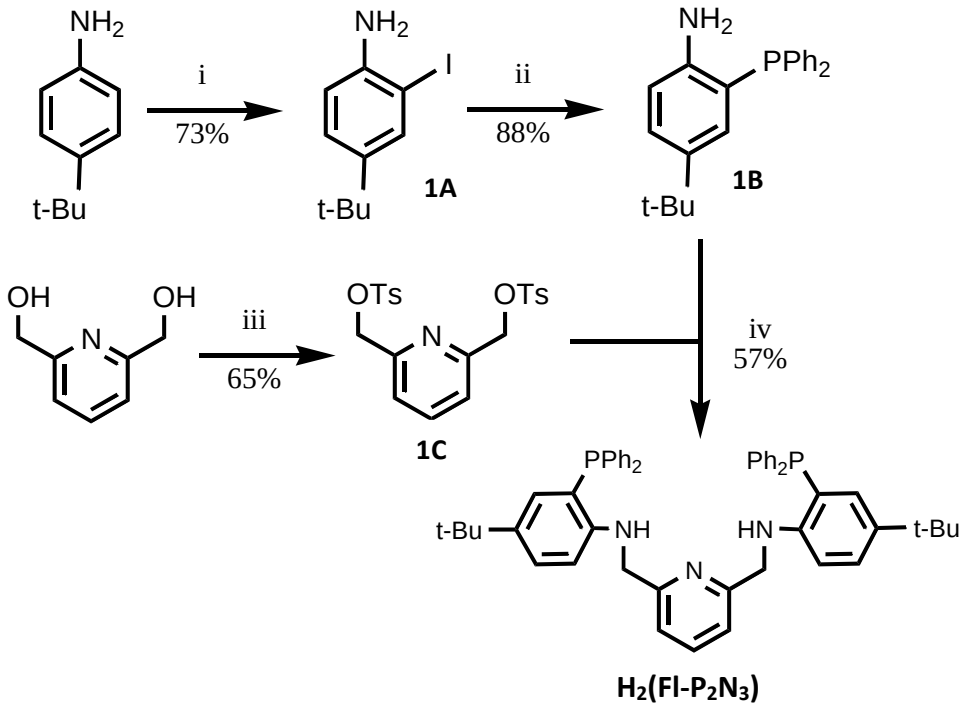

Scheme 2.3. The synthetic route toward the development of **H_2(Fl-P_2N_3)**. Key: i) 0.55 eq Ag_2SO_4, 1.05 eq I_2, EtOH, 4 hrs; ii) 1.1 eq $HPPh_2$, 2 eq Cs_2CO_3, 35 mol% DMED, 0.5 mol% $Pd(PPh_3)_4$, toluene, Δ 15 hrs; iii) 40 wt% KOH (aq), 2 eq p-toluenesulfonyl chloride, CH_2Cl_2, 0°C → room temp. 15 hrs; iv) 2.2 ^{n}BuLi, THF, 0°C → room temp. 16 hrs.

Commercial pyridinedimethanol was converted to the ditosylate precursor (**1C**) in modest yield by a literature method.[31] Deprotonation of the diphenylphosphino aniline precursor (**1B**) with ^{n}BuLi followed by introduction of the electrophile **1C** gave the desired target ligand **H_2(Fl-P_2N_3)** in modest yield after purification via column chromatography. The necessity of column chromatography to purify **1A**, **1B**, and **H_2(Fl-P_2N_3)** makes their isolation fairly time consuming; alternate purification methods would be beneficial and are being explored.

A monometallic Pt(II) complex of **H_2(Fl-P_2N_3)** has been successfully prepared and characterized. That is, reaction of **H_2(Fl-P_2N_3)** with $Pt(EtCN)_2Cl_2$ in CH_2Cl_2 led to

isolation of [(Cl)Pt(H_2{Fl-P_2N_3})]Cl·H_2O·CH_2Cl_2, **2.1**·H_2O·CH_2Cl_2, as a pale yellow solid. Complex **2.1**·H_2O·CH_2Cl_2 appears to be hygroscopic but otherwise air-stable in the solid state as well as in solution and no special precautions were used for its handling. X-ray quality single crystals of **2.1** were grown by slow evaporation of a concentrated CH_2Cl_2 solution. A view of the structure of **2.1** is shown in Figure 2.4. Here the ligand is bound to platinum(II) through two phosphorus and one amino nitrogen atom. Platinum has a square planar geometry (sum of angles about Pt = 359.8°) where the fourth site is occupied by a chloride. The second chloride is a counter ion

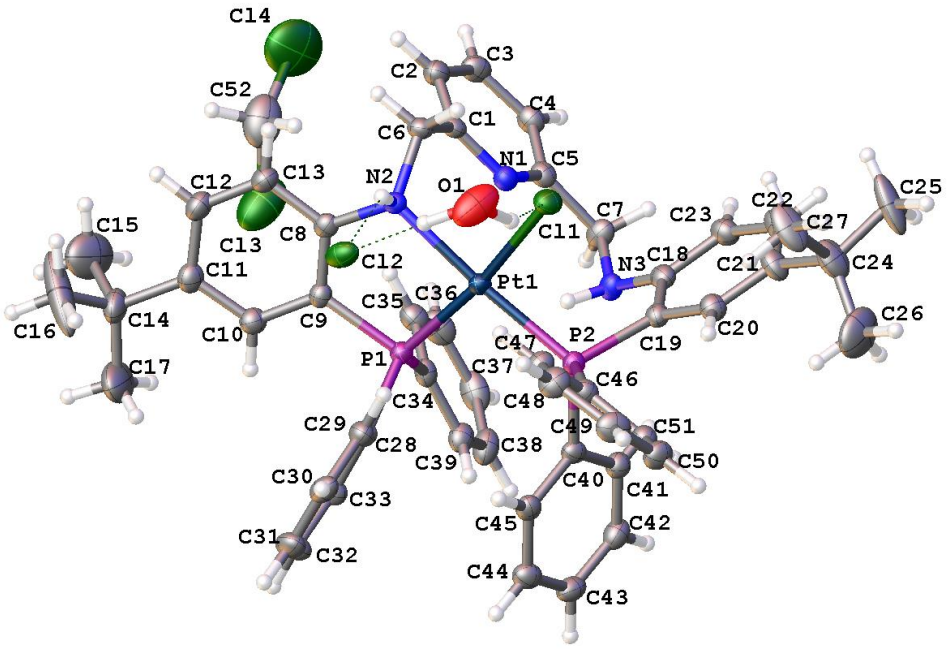

Figure 2.4. The crystal structure of {[H_2(κ^2*P*, κ *N*-fl-P_2N_3)]PtCl}Cl·H_2O·CH_2Cl_2, **2.1**. Selected Bond distances (Å): Pt1-P1 2.2138(8), Pt1-P2 2.2505(8), Pt1-N2 2.142(2), Pt1-Cl1 2.3772(8). Selected bond Angles (°): P1-Pt1-P2 100.88(3), P1-Pt1-N2 84.72(7), N2-Pt1-Cl1 87.79(7), Cl1-Pt1-P2 86.44(3).

and is hydrogen-bonded to a hydrogen on the same amine that is bound to the metal and to a water molecule, presumably adventitious from the air or solvent. There appears to be a vacant "pocket" near the two unbound N donors of the ligand that might be accessible to another small, hard metal ion.

The solution characterization seems to parallel expectations based on the solid state structure. The ^{1}H NMR spectrum shows resonances in the normal range between 0 and 9 ppm indicating that the Pt(II) d^8 complex is diamagnetic, as expected. The number of resonances is consistent with an asymmetric solution structure; there are more unique signals than would be expected for a symmetrically bound ligand. In agreement with ^{1}H NMR data, the ^{31}P NMR spectrum of **2.1** shows two unique sets of doublet resonances ($J_{P\text{-}P}$ = 15.6 Hz) for the phosphorus atoms, observed at δ_P = 25.0 (P_1) and -0.3 (P_2) ppm respectively that have satellite resonances caused by coupling between the ^{195}Pt and ^{31}P nuclei with $J_{P\text{-}Pt}$ values of 1927 (P_1) and 1647 Hz (P_2). The large difference in the chemical shifts of the phosphorus resonances ($\Delta \approx 25$ ppm) suggests that the P atoms are in vastly different chemical environments. The P-P coupling constant of 15.6 Hz is consistent with both P atoms being bound to the Pt center in a cis configuration, as seen for a similar Pt complex prepared by Tasker et al [32] with asymmetric *cis*- bound phosphorus atoms in a square planar geometry.

Future directions would involve inserting an additional hard metal into the vacant site of the platinum complex. Future attempts to put Ti and Zr(IV) complexes as hard centers, followed by the formation of heterometallic complexes by binding Pt(II) or Ni(0) to the softer portion of the ligand would be useful.

C. H_2(R-P_2N_3) Type Ligand

Finally, a different rigid, potentially dianionic P_2N_3 ligand **H_2(R-P_2N_3)** was prepared (Scheme 2.4) in order to examine its ability to support heterometallic complexes.

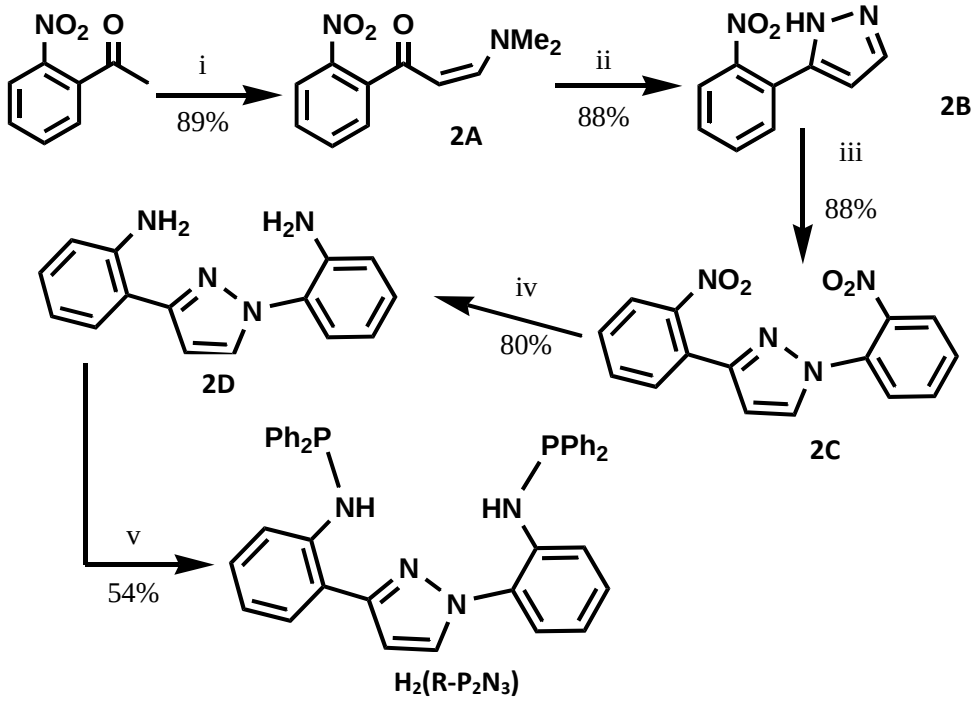

Scheme 2.4. The synthetic route toward the preparation of the **H_2(R-P_2N_3)** ligand scaffold. Key: i) 1 eq N,N'-dimethylformamide dimethyl acetal, DMF, Δ 3 hrs; ii) 1.1 eq $H_2NNH_2 \cdot H_2O$, EtOH, Δ 2 hrs; iii) 1 eq NaH, 1.8 eq 1-fluoro-2-nitrobenzene, DMF, Δ 24 hrs; iv) 12 eq NH_4Cl, 6 eq Fe, EtOH, H_2O, Δ 16 hrs; v) 2.2 eq ^{n}BuLi, 2 eq $ClPPh_2$,THF, -78˚C → room temp. 16 hours.

The reaction of commercially available 2-nitroacetophenone and N,N'-dimethylformamide dimethylacetal in DMF led to the clean formation of **2A** in good yield. Heating a solution of **2A** and hydrazine monohydrate in EtOH led to a good yield of the N heterocyclic product **2B** after purification via column chromatography. Deprotonation of **2A** with NaH followed by heating with 1-fluoro-2-nitrobenzene in DMF for 24 hours gave **2C** in good yield. Conversion of the nitro groups of **2C** to amino groups by treatment with NH_4Cl and Fe powder led to isolation of **2D** in 80% yield. Deprotonation of the amine protons with ^{n}BuLi followed by addition of chlorodiphenyl phosphine gave the desired ligand **H_2(R-P_2N_3)** in modest yield after trituration in Et_2O and subsequent filtration. The overall yield was 30% over five steps (with the last step being the most problematic) and one purification by column chromatography. Ideally, for widespread use in the inorganic community, one would like to decrease the number of steps, increase the yield, and eliminate purification by column chromatography altogether, which are areas of pursuit in future optimizations.

Several monometallic (Zr, Pt, and Ag) complexes of **H_2(R-P_2N_3)** have been prepared and partially characterized. Treatment of **H_2(R-P_2N_3)** with 1 eq of $Pt(EtCN)_2Cl_2$ in CH_2Cl_2 gave [{H_2(R-P_2N_3)}PtCl]Cl·$2CH_2Cl_2$, **2.2**·$2CH_2Cl_2$ as a precipitate. Long colorless X-ray quality needle crystals were grown by mixing CH_2Cl_2 solutions of reagents in a vial and leaving the resulting solution undisturbed for 2 days. The structure of **2.2**·$2CH_2Cl_2$ is shown in Figure 2.5.

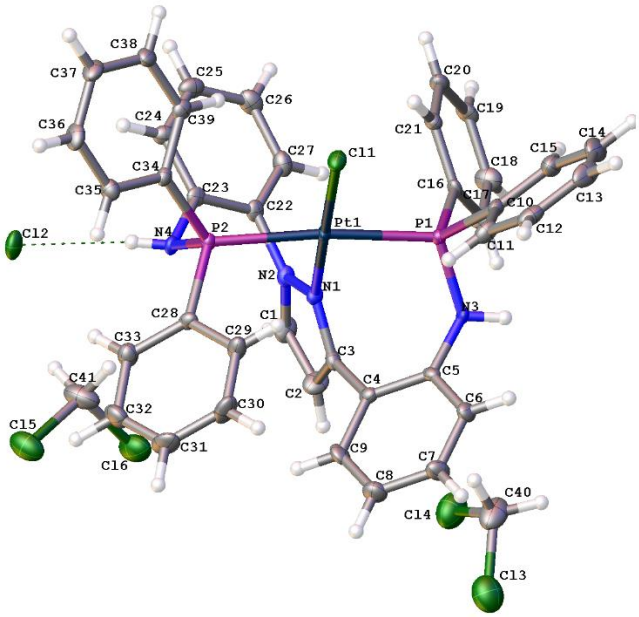

Figure 2.5. The crystal structure of complex **2.2**·$2CH_2Cl_2$. Selected Bond distances (Å): Pt1-P1 2.2991(8), Pt1-P2 2.3143(8), Pt1-N1 2.019(2), Pt1-Cl1 2.2862(8),. Selected bond Angles (°): P1-Pt1-P2 172.93(3), P1-Pt1-N1 86.02(8), N1-Pt1-Cl1 178.12(8), Cl1-Pt1-P2 93.80(3).

The Pt(II) ion has a square-planar coordination and forms a complex cation by binding to the ligand through two trans-spanning phosphorus atoms and the central pyrazolyl nitrogen that is trans- to the chloride ligand. The Pt-P, Pt-N, and Pt-Cl bond lengths are in accord with expectations. The terdentate $\kappa^2P,\kappa N$ binding mode gives a chiral helicoid conformation via folding of the two seven-membered chelate rings. In actuality, the structure is disordered in a 2:1 ratio such as to interchange the C3 and N2 atoms (only the major component of the disorder is shown in Figure 2.5) giving a pseudo local 2-fold axis along the Pt-Cl bond. Hydrogen bonding between the N4-H to the chloride anion leads to polymer chains in the crystal packing. In this complex, there does not appear to be a secondary binding pocket for an additional metal.

The solution characterization data also seems to agree with expectations based on the solid state structure. The ^{1}H NMR spectrum shows resonances in the normal range between 6 and 8 ppm indicating that the Pt(II) d^8 complex is diamagnetic, as expected. In agreement with ^{1}H NMR data, the ^{31}P NMR spectrum of **2.2**·2CH_2Cl_2 shows two unique sets of doublet resonances ($J_{P\text{-}P}$ = 16.9 Hz) for the phosphorus atoms, observed at δ_P = 32.6 (P_1) and 27.3 (P_2) ppm respectively that have satellite resonances caused by coupling between the ^{195}Pt and ^{31}P nuclei with $J_{P\text{-}Pt}$ values of 1936 (P_1) and 1965 Hz (P_2).

A silver(I) complex of **H_2(R-P_2N_3)** was prepared because it was envisioned that such complexes may be useful reagents for other metal derivatives. Thus, the reaction of Ag(OTf) and 2 eq of **H_2(R-P_2N_3)** in THF led to the isolation of **[Ag{H_2(R-P_2N_3)}$_2$](OTf)**, **2.3**. X-ray quality crystals were grown by slow vapor diffusion of Et_2O onto a concentrated dichloroethane solution and the structure of **2.3** is shown in Figure 2.6.

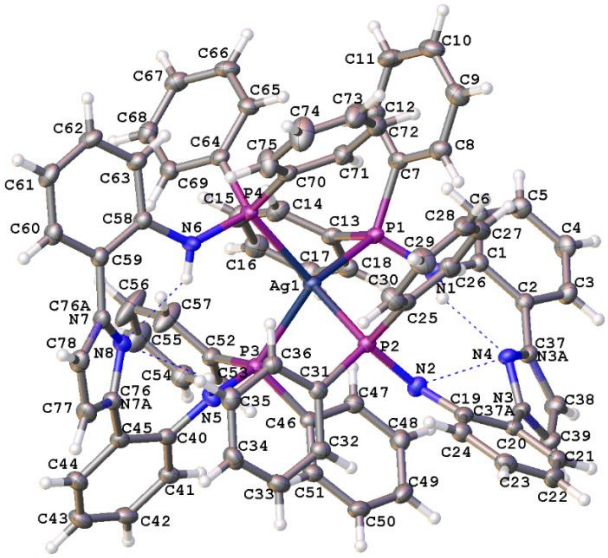

Figure 2.6. The crystal structure of [Ag{H_2(R-P_2N_3)}$_2$](OTf), **2.3**. Selected Bond distances (Å): Ag1-P1 2.5166(6), Ag1-P2 2.5170(6), Ag1-P3 2.5525(6), Ag1-P4 2.4909(6) etc. Selected bond Angles (^{o}): P1-Ag1-P2 113.52(2), P1-Ag1-P3 110.30(2), P2-Ag1-P3 96.60(2), P4-Ag1-P1 110.75(2), P4-Ag1-P2 111.84(2), P4-Ag1-P3 113.18(2).

The Ag(I) ion has a tetrahedral AgP4 coordination geometry as a result pf the chelating κ^2 P-coordination mode of each ligand. The Ag-P distances are in line with those of [Ag(P(p-tolyl)$_3$)$_2$(salH)] (salH = deprotonated salicyclic acid).[33] There are four intra-molecular H-bonds N-H···N although not all of them are equivalent (acceptor atoms N4 and N2 form one longer and one shorter H-bond each). Thus, there appears to be binding pockets for the insertion of two hard metal ions into the N_3 donor positions. Future work should be devoted to attempting to bind additional metal ions into these sites. Moreover, the complete characterization of this complex and of the mono-ligated derivative, [Ag{H_2(R-P_2N_3)}](OTf), if it can be prepared, should be obtained.

Finally, **Zr(NMe$_2$)$_2$(κ^5-R-P_2N_3)**, **2.4**, was prepared by the combination of Zr(NMe$_2$)$_4$ and **H_2(R-P_2N_3)** in a 1:1 ratio in deuterated benzene under an inert atmosphere. The yield has not yet been quantified because the air-sensitivity of the complex complicated an initial attempt (see below). Nonetheless, X-ray quality crystals of **2.4** (the structure is shown in Figure 2.7) precipitated out of an undisturbed reaction mixture (over 24 hours).

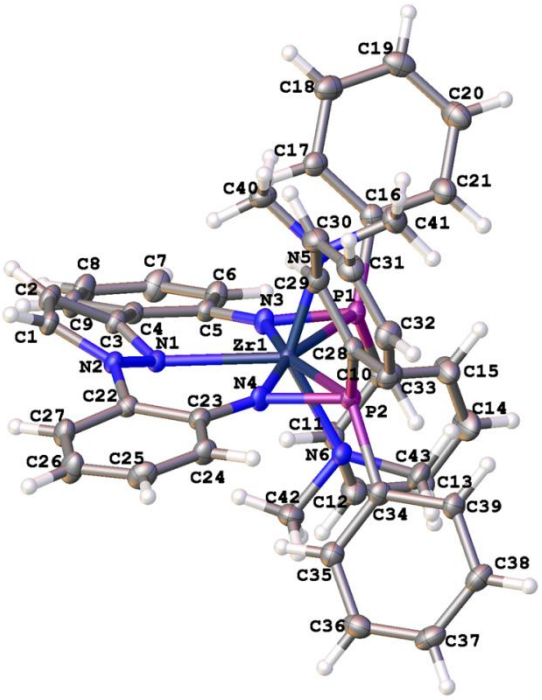

Figure 2.7. The crystal structure of **Zr(NMe$_2$)$_2$(R-P$_2$N$_3$)**, **2.4**. Selected Bond distances (Å): Zr1-P1 2.7387(7), Zr1-P2 2.7638(7), Zr1-N1 2.358(2), Zr1-N3 2.172(2), Zr1-N4 2.173(2), Zr1-N5 2.073(2), Zr1-N6 2.063(2). Selected bond Angles (^{o}): P1-Zr1-P2 129.45(2), N1-Zr1-P1 114.96(6), N1-Zr1-P2 115.59(6), N3-Zr1-P1 37.89(6), N3-Zr1-P2 167.34(6), N3-Zr1-N1 77.07(8).

In this complex, all potential donor atoms are bound to zirconium. The metal has a very distorted pentagonal-bipyramidal ZrN_5P_2 coordination environment. The equatorial pentagonal ZrN_3P_2 is practically planar (sum of angles = 360.05 ^{o}) but the axial N5-Zr-N6 unit is bent (135.22 ^{o}) where the dimethylimino ligands are inclined toward the biggest opening (two *cis*- P atoms) in the equatorial plane. The pyrazolyl ring is rotated by ~30° out of the plane relative to its neighboring benzene (and the pentagonal ZrN_3P_2 plane). At first glance, this structure suggests that the P donor atoms might not be available to bind another metal because they are bound to Zr. However, Nagashima and

co-workers showed through x-ray crystallography and ^{1}H NMR spectroscopy that the phosphines in a similar complex, $(Ph_2PN^iPr)_3ZrCl$, dissociate from the metal center at room temperature.[34] Treatment of the $(Ph_2PN^iPr)_3ZrCl$ complex with CoI_2 led to isolation of the bimetallic complex shown previously (Chapter 1, Figure 1.16). These findings give promise that complex **2.4** may serve as a viable metalloligand precursor for the assembly of bimetallic complexes.

The free ligand shows chemical shifts for the P atoms at δ_P = 31.1 and 29.2 ppm in benzene-d_6. These resonances disappear entirely and are replaced by a new set of resonances found at δ_P = 34.7 and 4.8 ppm respectively upon the addition of 1 eq of $Zr(NMe_2)_4$. The large difference in the observed chemical shifts suggests that the P atoms are in vastly different chemical environments. It is likely that only one of the P atoms is bound to Zr in solution. As indicated earlier, attempts to isolate this product outside of the glovebox without an inert atmosphere led to decomposition as determined by the ^{31}P NMR spectrum that was different than the in-situ prepared sample and by the presence of an insoluble solid. Thus despite having such a high coordination number, the complex is quite reactive, another observation that provides hope that the ligand arms are available for further reaction. Future work should be devoted to trying to isolate and fully characterize the zirconium precursors, this new complex, other heterobimetallics outlined in chapter 4, and to explore their reactivity with CO_2 and H_2.

2.3 CONCLUSIONS

A number of novel P_2N_3 pincer type ligands have been successfully prepared and characterized including the H_2(Fl-P_2N_3) and the H_2(R-P_2N_3) ligands. The necessity for column chromatography limits the scale that these ligands can be prepared on. That fact, along with the observation that these ligands are sensitive to phosphine oxidation makes this class of ligands difficult to work with.

A number of monometallic complexes with the P_2N_3 ligands have been successfully prepared and partially characterized. The metal complexes [(Cl)Pt(H_2{Fl-P_2N_3})]Cl·H_2O·CH_2Cl_2, [Ag{H_2(R-P_2N_3)}$_2$](OTf), and Zr(NMe_2)$_2$(κ^5-R-P_2N_3) all appear to have additional vacant sites available to bind a 2nd metal and therefore may show promise as metalloligand precursors toward heterobimetallic complexes. Initial attempts to prepare bimetallic complexes from these precursors have all been unsuccessful as these complexes appear to be quite reactive and sensitive to decomposition. Great care would need to be taken to ensure inert atmosphere conditions throughout the syntheses of these complexes in future experiments.

Chapter 3

IRON(II) COMPLEXES OF *N*-CONFUSED TRIS(PYRAZOLYL)METHANE, *NC*-TPM, LIGANDS

3.1 INTRODUCTION

As stated in Chapter 1 we identified N-confused tris(pyrazolyl)methanes, *nc*-Tpms, as candidates for the development of heterobimetallic complexes. Specifically, since iron complexes have shown promise for the activation of CO_2 or H_2 in both synthetic and biological systems, an investigation into iron complexes of *nc*-Tpms Chart 3.1 (A and B) was initiated. Here the

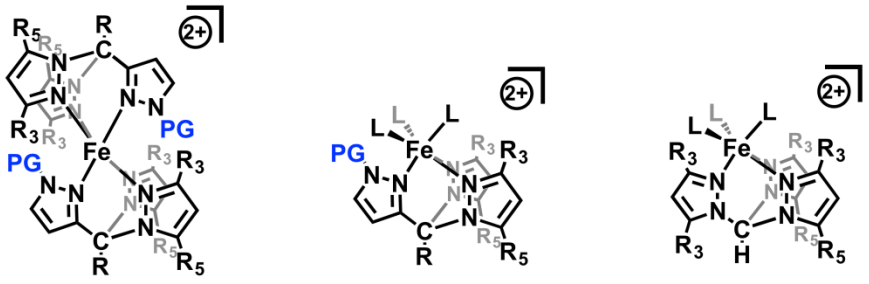

Chart 3.1. (A) Homoleptic and (B) heteroleptic iron(II) complexes of N-confused tris(pyrazolyl)methanes, *nc*-Tpm's (PG = Protecting group) and comparison of the latter with (C) traditional tris(3,5-diorganopyrazol-1-yl)methanes, TPMs.

protecting groups (PG) may be removed before or after iron complexation, as needed, to give a second site for metal binding. Ideally, heteroleptic iron(II) complexes would serve as starting materials for heterobimetallics. However, heteroleptic iron scorpionates (Tpm or Tp) can only be isolated if sufficiently bulky groups are located at the R_3 position of the pyrazolyls. Otherwise, homoleptic complexes are unwittingly obtained regardless of the ratio of reagents. Of importance, both $[Fe(Tpm^*)_2]^{2+}$ [35] (Tpm* = tris(3,5-dimethylpyrazol-1-ylmethane) and $[Fe(Tpm^*)(H_2O)_3]^{2+}$ [35] have been isolated but Fe(Tp* = tris(3,5-dimethylpyrazol-1-ylborate)$(H_2O)_3]^+$ is unknown because preparative reactions only give $Fe(Tp^*)_2$.[36] The *nc*-TPMs have never been prepared before so it is unknown what steric threshold will need to be crossed before heteroleptic derivatives can be obtained. Thus, the first goal of this work was to prepare examples of nc-Tpm's and determine their coordination chemistry with iron(II). The characterization of homoleptic iron(II) complexes will facilitate their identification in reactions designed to prepare heteroleptic derivatives. Secondly, the homoleptic derivatives may also be important for advancing the understanding of ligand design on spin-crossover (SCO) behavior, common to other scorpionates.[35]

Spin crossover (SCO) complexes have received much interest in recent years due to their potential applications as molecular switches.[37] Useful molecular switches require a change in the electronic properties of a material in response to an external perturbation

of some kind (thermal, light, pressure, etc…). Spin-crossover complexes are one such example of molecules that exhibit this unique behavior. SCO behavior may sometimes be observed in octahedral transition metal complexes with d^4-d^7 electron counts (though d^6 seems to be the most widely studied) if the ligand has an intermediate ligand field strength (Δ_o), comparable to the pairing energy, or the energy penalty of having two electrons paired up in the same orbital. The relatively large number of d^6 SCO systems versus other electron counts is due in part to the stability of the low spin (LS) form of complexes and the maximum change in magnetic moment on transition to the high spin (HS) state that gives rise to a large increase in entropy, as shown in Figure 3.1. The difference in magnetic moment between the two states allows for easy

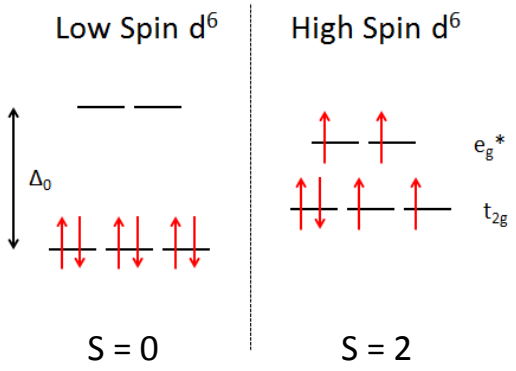

Figure 3.1. For octahedral Fe(II), the low spin (LS) configuration is diamagnetic, or has no unpaired electrons while the high spin (HS) configuration has 4 unpaired electrons. SCO occurs when an external perturbation causes a switch in the spin state from LS to HS or vice versa. Δ_0 = the ligand field strength.

detection of SCO events using a number of methods including the Evans NMR method [38] or simply using a magnetometer. Along with a change in the magnetic moment are a number of other pronounced differences between the properties of complexes found in each state.

Comparison of the x-ray crystallographic data of HS and LS complexes shows that the Fe-N bonds in LS Fe(II) complexes are about 10% shorter (1.8 to 2.0 Å) than those observed in HS systems (2.0 to 2.2 Å). This can be explained by the fact that in the high spin state, electrons are populating the e_g* antibonding orbitals which decreases the overall bond order and leads to longer bond lengths.[37] The Mössbauer spectra of each state are very different as well due to the differences in the electron density of the nuclei of the HS and LS states. These differences lead to measurable changes in isomer shift and quadrupole splitting.[39] Infrared (IR) or Raman spectroscopy can also be used to observe the differences of the bond vibrations of the two states.[40] Electronic spectroscopy can be used to distinguish spin states of iron(II) complexes.[41] If there are no charge transfer bands, then LS complexes have two higher energy d-d bands that gives rise to purple or dark red coloration whereas HS complexes have a single low energy d-d band in the NIR region rendering the complex colorless or pale blue. Finally, the differences in spin states can also be measured with Differential Scanning Calorimetry (DSC). Heat is taken up upon SCO from the LS to HS state and evolved when returning to the LS state.[42] DSC can be used to determine the ΔH and ΔS of the SCO event.[40]

A wide range of perturbations can induce spin crossover including light irradiation or changes in pressure (increasing pressure favoring the smaller LS state). The most common perturbation studied is the effect of inducing a spin transition by a

change in temperature. The low spin state is favored enthalpically due to better bonding and higher crystal field stabilization energy so it is more stable at lower temperatures.[37] The high spin state is favored entropically due to greater electronic and vibrational contributions so it is more stable at higher temperatures.[37]

As shown in the previous paragraphs, there are many ways to measure the spin state of a SCO complex. For temperature induced spin state transitions, the temperature can be followed plotted against the magnetic moment in order to determine the temperature of the SCO event, called the $T_{1/2}$. The $T_{1/2}$ is defined as the temperature at which the ratio of HS to LS states is 1:1 (or 50/50), shown in Figure 3.2.

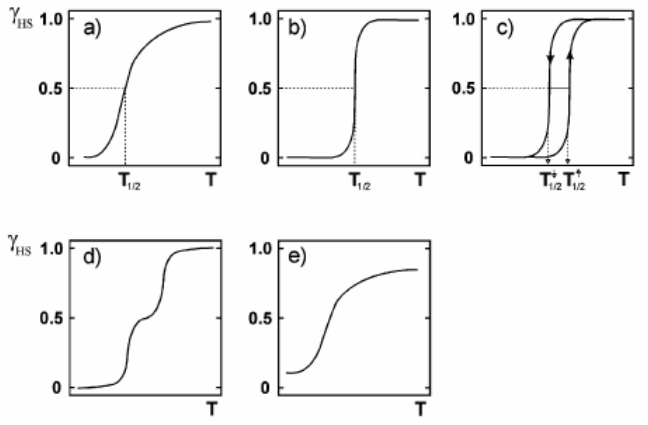

Figure 3.2. Schematic illustrations of the 5 main types of SCO events: a) gradual but complete b) abrupt c) abrupt with thermal hysteresis d) two-step e) gradual but incomplete. The x axis is temperature and the y axis is the HS fraction (Υ_{HS}). $T_{1/2}$ is the temperature at which the ratio of HS to LS states is (1:1). Illustrations are taken from reference 37.

SCO complexes exhibit a variety of SCO profiles as shown in Figure 3.2. The control of temperature profiles of the SCO event is currently a hot research topic, including what parameters influence the position of $T_{1/2}$ or the presence and width of a hysteresis loop.[43] It is important to note that SCO behavior can be observed either in the solution (usually gradual) or the solid state. In the solid, different solvents or crystal packing (dictated by ion shape, charge, guest molecules, or simply noncovalent interactions in different polymorphs) can substantially impact SCO behavior.[43]

Iron(II) scorpionate complexes with Tpm ligands have been shown to exhibit SCO behavior. Reger and associates synthesized the complexes {Fe[HC(3,5-$Me_2pz)_3]_2$}$(BF_4)_2$ (**1**) and {Fe$[HC(pz)_3]_2$}$(BF_4)_2$ **(2).**[35] It was found that **(1)** is HS in both the solid state and in solution at 298 K but rapidly changes over to a 50:50 mixture of HS and LS states below 206 K.[35] It was noted that the mixture does not continue to change its composition as the temperature is lowered below 200 K and no hysteresis was observed upon cooling and heating.[35] In contrast, **(2)** was found to be LS at 298 K in the solid state and gradually changed over to the HS state upon heating and was found to be completely HS at approximately 470 K. In solution, both HS and LS forms were observed between the temperature range of 223-303 K, with the percentage of HS forms increasing with the temperature.[35] With this in mind, the preparation of nc-Tpms and their iron complexes was initiated.

3.2. Results and Discussion.

A. Bn-nc-Tpm Type Ligand.

The synthetic route to the new nc-Tpm ligands is shown in Scheme 3.1. The neat

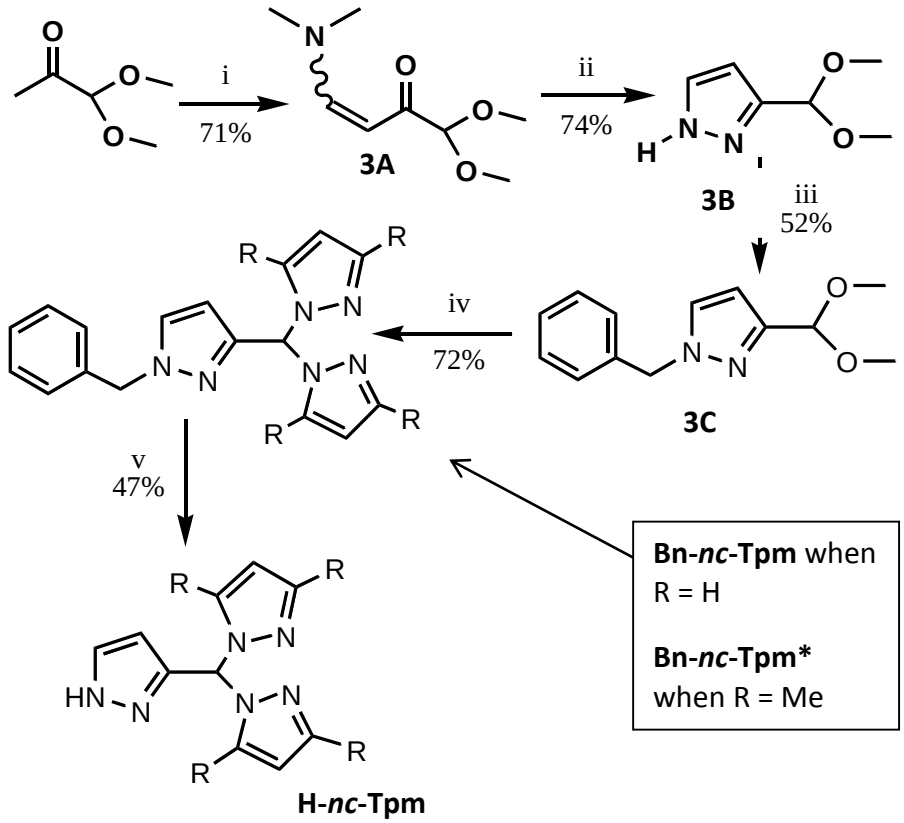

Scheme 3.1. Synthetic route toward the preparation of the new nc-Tpm ligands. Key: i) N,N'-dimethylformamide dimethylacetal, neat, Δ at 66°C, 16 hours; ii) $H_2NNH_2 \cdot HCl$, 10% (w/w) NaOH (aq), 4 hrs; iii) 1.1 eq NaH, 1.1 eq benzyl bromide, THF, 16 hrs; iv) 3 eq H-Pz (or 3,5-dimethyl-1H-pyrazole), 5 mol % p-toluene sulfonic acid monohydrate, toluene, distillation of by product (MeOH), 30 minutes; v) DMSO, KO^tBu, O_2 (g), quenched with HCl and K_2CO_3, THF, 20 minutes. R = H, Me.

reaction of commercially available methylglyoxal-1,1-dimethylacetal with N,N'-dimethylformamide dimethylacetal gave the pure acrolein intermediate (**3A**) after distillation in fairly good yield. This reaction suffered no setback in yield even when scaled up to a 200 mmol scale. A fair yield of pure pyrazole **3B** was formed in accord with the literature[44] by reacting **3A** with hydrazine hydrochloride in a 10 % (w/w) aqueous NaOH solution for 4 hours. This product could also be synthesized very easily on a large scale (200 mmol) as the only purification necessary is by standard workup procedures, extracting with Et_2O to give the pure product. N-protection by deprotonation of the pyrazole **3B** with NaH in THF followed by reaction with benzyl bromide gives impure **3C** (after removing solvent and passing through a plug of silica to remove salts) that can be used successfully in the next step of the reaction. If desired, **3C** can be isolated in modest yield after purification by column chromatography. Active distillation of solvent and methanol from a mixture of **3C**, catalytic pTsOH·H_2O and either pyrazole (H-Pz) or 3,5-dimethyl-1H-pyrazole (H-Pz*) over the course of 30 minutes gave the ligands **(Bn-*nc*-Tpm)** and **(Bn-*nc*-Tpm*)** in good (72 %) to excellent (94 %) yields respectively. Unfortunately, the use of column chromatography was required to purify these ligands on this step.

N-benzyl deprotection to give H-*nc*-Tpm, has proven more difficult than was anticipated. Deprotection by bubbling O_2 through a solution of **(Bn-*nc*-Tpm)** in DMSO, THF, and KO^{t}Bu led to the isolation of H-nc-Tpm in poor yield. Unfortunately, the yield is not high. Since the starting material seems to be consumed (TLC monitoring), issues other than incomplete reaction are responsible for the lower yield of this step. One possible origin of the modest yield arises from the product having partially soluble in

water, making it difficult to separate the product from DMSO; much of the product appears to be in the water layer. The method of quenching with HCl, then K_2CO_3, and removal of H_2O by vacuum distillation followed by extraction with acetone (to separate from KCl) and recrystallization from Et_2O (to separate from DMSO) has given the highest yield so far. A few attempts at benzyl-deprotection by using Pd^0 catalyzed hydrogenation in mixtures of MeOH and HCl (aq) only gave back unaffected starting materials.

B. Tos-nc-Tpm Type Ligand.

Due to synthetic difficulties with the deprotection of the benzyl group from the Bn-nc-Tpm ligand, another approach toward the isolation of the deprotected H-nc-Tpm ligand was initiated. The use of another protecting group, a tosyl group, was investigated, as shown in Scheme 3.2.

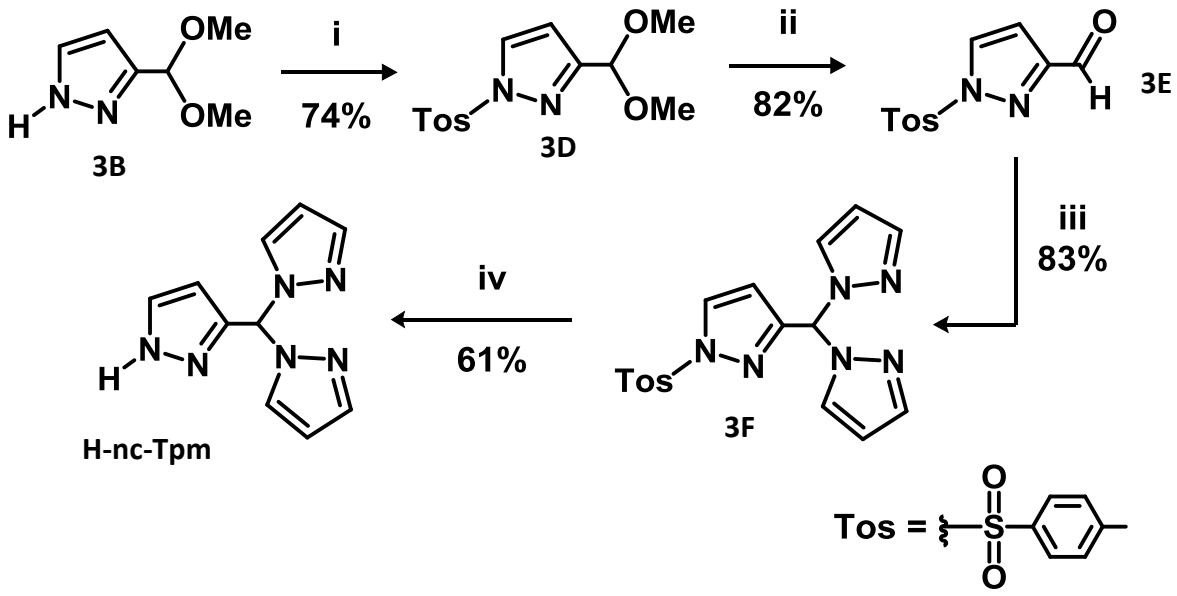

Scheme 3.2. Alternative route to H-nc-Tpm ligand. Key: i) 3 eq NaOH, 1 eq TosCl, DCM, 16 hrs; ii) 5 mol% trifluoroacetic acid, THF, H_2O, 16 hrs; iii) 3 eq. NaH, 3 eq. H-Pz, 1.5 eq. $SOCl_2$, 5 mol% $CoCl_2$, THF, 16 hrs; iv) 5M NaOH (aq), THF, 10 min.

The previously described pyrazole precursor **3B** was deprotonated by NaOH and reacted with p-toluenesulfonyl chloride (TosCl) to give the tosyl protected product **3D** in fair yield. The use of column chromotagraphy to purify the product can be avoided by triturating with diethyl ether and subsequent filtration, allowing for large scale quantities to be produced, albeit in lower yield (51%). Unfortunately, when the tosyl protected pyrazole derivative was subjected to the same conditions used to form the Bn-nc-Tpm derivatives described in Scheme 3.1, a mixture of unwanted side products was observed, including TsPzCH(Pz)(OMe) and oligo- and polymeric species from the self-condensation of $HPzCH(OMe)_2$. To circumvent this problem, the compound **3D** was treated with trifluoroacetic acid and water in refluxing THF in an acid catalyzed

condensation reaction, eliminating methanol and forming the aldehyde precursor **3E** in good yield and with minimal purification needed (recrystallization from boiling heptane).

The tosyl protected nc-Tpm derivative can then be prepared by treatment of **3E** with $SOPz_2$ formed in situ by the reaction of H-pyrazole and sodium hydride followed by addition of thionyl chloride ($SOCl_2$) to give compound **3F** is good yield and with minimal purification needed (recrystallization from boiling heptane). Tosyl deprotection was achieved more readily than was the case with the benzyl group by reacting compound **3F** with aqueous NaOH in THF to give the target ligand **H-nc-Tpm** in modest yield.

C. Fe(II) Complexes of Nc-Tpm Ligands.

Homoleptic iron(II) complexes of the various *nc*-Tpm's have been prepared by mixing THF solutions of a ligand (2 eq) with that containing an iron (II) salt (1 eq) followed by recrystallizing the precipitate by vapor diffusion of Et_2O into CH_3CN solutions of the complex. Scheme 3.3 summarizes the results of the various reactions. The reaction between (**Bn-*nc*-Tpm)** with either $[Fe(H_2O)_6](BF_4)_2$ or $Fe(OTf)_2$ gave

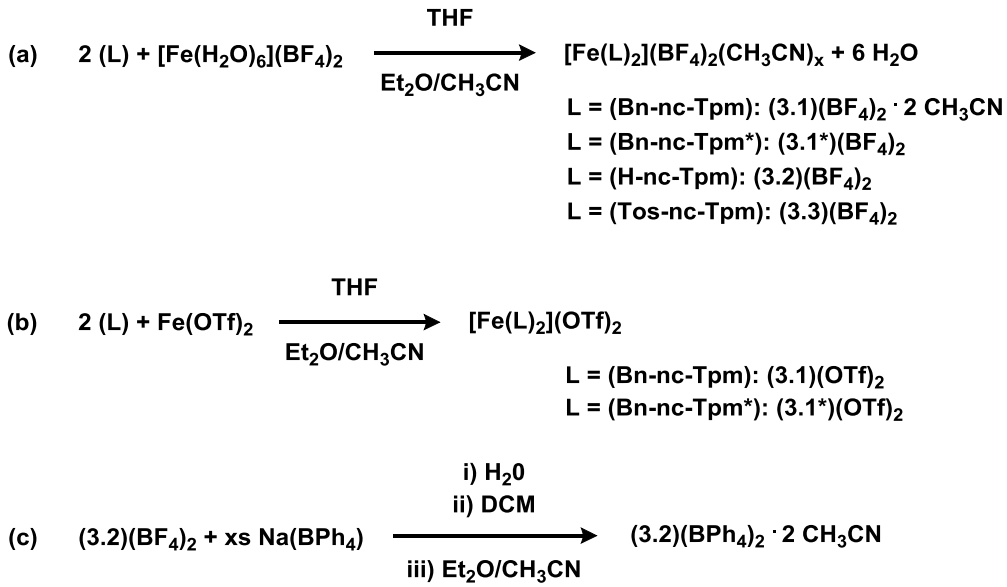

Scheme 3.3. Preparation of various iron(II) complexes of *Nc*-Tpm ligands. The solvent system for L = H-nc-Tpm in (a) is different, as explained in the main text.

[Fe(Bn-*nc*-Tpm)$_2$](X)$_2$, (3.1)(X = BF_4 or OTf)$_2$, as appropriate. Similarly, the use of 3,5-dimethylpyrazolyl variants instead of unsubstituted pyrazolyls gave [Fe(Bn-*nc*-Tpm*)$_2$](X)$_2$, (3.1*)(X = BF_4 or OTf)$_2$. The reaction between Tos-nc-Tpm with [Fe(H_2O)$_6$](BF_4)$_2$ gave [Fe(Tos-nc-Tpm)$_2$](BF_4)$_2$. Each of the five above complexes is a colorless paramagnetic solid at room temperature. In contrast, the crystalline complexes [Fe(H-*nc*-Tpm)$_2$](X)$_2$·CH_3CN (3.2)(X = BF_4 or BPh_4)·CH_3CN are pink diamagnetic solids at room temperature.

The SCO behavior of the compounds changes with the groups bound to the "confused" pyrazolyl, by the substituents on the other pyrazolyls, and with the anion type. For example, the complex [Fe(Bn-*nc*-Tpm)$_2$](BF_4)$_2$·2CH_3CN is colorless at room temperature but becomes dark pink upon cooling to 77 K. In contrast, the complex

[Fe(Tos-nc-Tpm)$_2$](BF$_4$)$_2$, **(3.3)(BF$_4$)$_2$** remains colorless at all temperatures. The average Fe-N bond distance recorded at 100 K is 2.215 Å, consistent with a high spin iron(II) center.

The solid state structure of [Fe(Bn-*nc*-Tpm)$_2$](BF$_4$)$_2$·2CH$_3$CN was determined at high and low temperature (Figure 3.3) which verified spin crossover behavior. The 100 K structure displayed average Fe-N bond

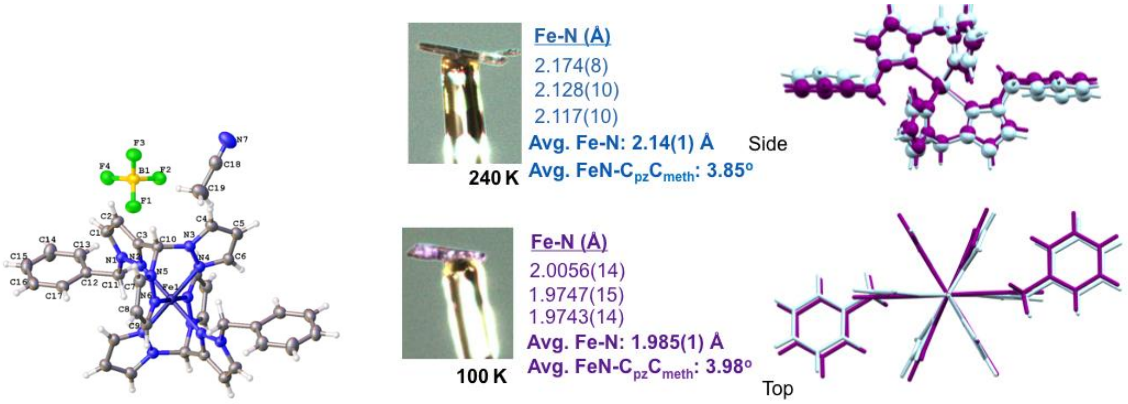

Figure 3.3. Left: View of the structure of (3.1)(BF$_4$)$_2$·2CH$_3$CN at 100 K. Center: Photographs of crystals at 240 K and 100 K and list of bond distances and angles. Right: Overlays of dications at high temperature (purple) and low temperature (pale blue).

distances of 1.984(1) Å, consistent with low-spin iron(II). For instance, the LS complex {Fe[HC(pz)$_3$]$_2$}(BF$_4$)$_2$ prepared by Reger et al [35], has an average Fe-N bond length of 1.972 Å. The 240 K structure of (3.1)(BF$_4$)$_2$·2CH$_3$CN had substantially longer Fe-N bonds (2.14(1) Å) and slightly more twisted pyrazolyl rings (FeN-C$_{pz}$C$_{meth}$ torsion angle 3.98°) than the LS structure (3.85°), in line with expectations of a high spin iron(II)

center. For example, the $\{Fe[HC(pz^*)_3]_2\}(BF_4)_2$ complex (pz* = 3,5-dimethylpyrazole), also prepared by Reger [35], has an average Fe-N bond length of 2.170 Å at room temperature.

Of further note, the dication is positioned on a crystallographic inversion center so that the benzyl groups are oriented outwards in a *trans*- geometry. There appeared to be two crystal types in the bulk sample, the needles used for X-ray diffraction and thin square plates (about 50%) that were too thin for single crystal X-ray diffraction; the plates are likely the *cis*- isomer. The crystal structure also has channels along the *z*- axis that are filled with the acetonitrile solvate molecules. The relative stability of the crystal solvate may be attributed to C-H…F interactions found within the channels though it is important to note that elemental analysis confirms that the solvent molecules are removed under vacuum.

Analysis of the ^{1}H NMR spectrum of **(3.1)$(BF_4)_2$** at room temperature shows that the complex is paramagnetic (HS) since broad resonances were observed over a large chemical shift range from 50.1 to -41.8 ppm, consistent with other paramagnetic HS Fe(II) complexes.[35] The solution magnetic moment (μ_{eff}) $\mu_{eff} = 7.07\ \mu_B$ measured by the Evans method [38] is significantly higher than the expected values (in the 4.9-5.5 μ_B range) for HS species with orbital contribution to magnetic moment.

In contrast to the above**,** $[Fe(Bn\text{-}nc\text{-}Tpm)_2](OTf)_2$, **(3.1)$(OTf)_2$,** does not change color on cooling to 77 K, it remains colorless (or pale yellow). Single crystal x-ray diffraction of **(3.1)$(OTf)_2$** at 100 K shows an average Fe-N bond distance of 2.184 Å, consistent with HS Fe(II). This is an interesting result considering that

(3.1)$(BF_4)_2$·2CH_3CN was low spin (Fe-N avg. 1.984 Å) at 100 K. These data show that the identity of the counterion and/or the solvate molecules can have dramatic effects on the SCO properties of the complexes.

Complexes with bulkier ligands, **[Fe(Bn-*nc*-Tpm*)$_2$](X = BF_4 or OTf)$_2$, (3.1*)(OTf)$_2$,** crystallized as paramagnetic, colorless solids without solvate molecules. Single-crystal x-ray diffraction data at 100 K show that these complexes are HS regardless of temperature with average Fe-N bond distances of 2.171 (X = BF_4) and 2.175 Å (X = OTf). It is noteworthy that the complex {Fe[HC(3,5-Me_2pz)$_3$]$_2$}(BF_4)$_2$ was HS at 298 K by magnetic, ^{1}H NMR and crystallographic (2.170 Å) studies but gave 50% SCO (with half of the metal sites converting to the LS state at low temperature) as a result of a phase transition at 206 K.[35] As above, there were two types of crystals in each sample, one type suitable for single crystal diffraction (which was solved) and one that was unsuitable. As shown in Figure 3.4, the structurally- determined sample had *cis*-**[Fe(Bn-*nc*-Tpm*)$_2$]$^{2+}$** dications. Presumably, the other half of the crystals contain *trans*-isomers.

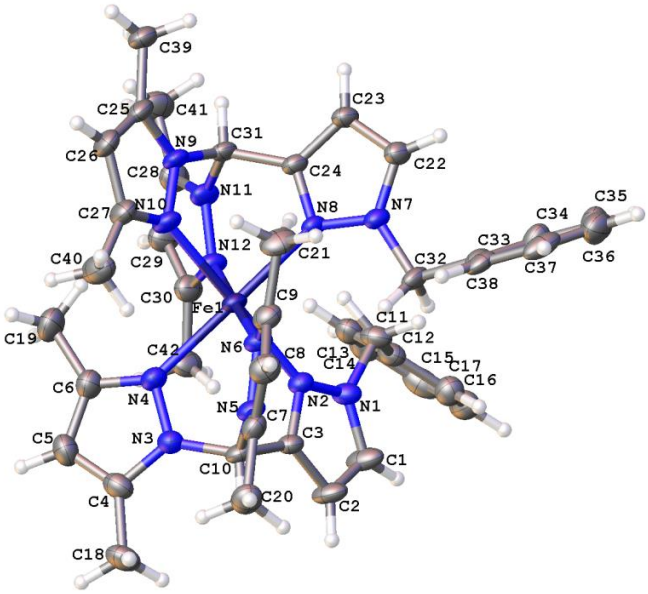

Figure 3.4. The structure of a *cis*-**[Fe(Bn-*nc*-Tpm*)$_2$]$^{2+}$** dication.

The solvent for the syntheses of iron(II) complexes of **(H-*nc*-Tpm)** was slightly different than the above four "protected" N-confused scorpionates. The complex **[Fe(H-*nc*-Tpm)$_2$](BF$_4$)$_2$** , (3.2)(BF$_4$)$_2$, was prepared by dissolving **(H-*nc*-Tpm)** in acetone and cannula transferring the contents to an acetone solution of half an equivalent of [Fe(H$_2$O)$_6$](BF$_4$)$_2$. Upon the addition of [Fe(H$_2$O)$_6$](BF$_4$)$_2$ a pink solution instantly formed. After some time, the solvent was removed by vacuum distillation and rinsed with acetone to give a pink solid in modest yield. Exhaustive attempts to grow single x-ray quality crystals using a variety of solvent systems were unsuccessful, as extremely small, twinned, crystals were obtained in all cases. These crystals turned colorless at about 370 K (and back to pink on cooling, similar to the temperature reported for FeTp$_2$ [35] or [Fe(Tpm)$_2$](BF$_4$)$_2$.[35] In order to gain structural information, the tetrafluoroborate

counter ion (BF_4) was interchanged with the tetraphenylborate (BPh_4) anion by reaction of **(3.2)$(BF_4)_2$** with excess $NaBPh_4$ in water followed by removal of solvent and crystallization from Et_2O/CH_3CN, as above. In this way, $[Fe(H\text{-}nc\text{-}Tpm)_2](BPh_4)_2$**,** **(3.2)$(BPh_4)_2$**, was isolated in low yield as a colorless solid powder that turned pink on cooling to 77 K. However, after recrystallization from CH_3CN (Et_2O vapor diffusion) x-ray quality deep pink crystals of **(3.2)**$(BPh_4)_2 \cdot 2CH_3CN$ were obtained. A portion of the 100 K crystal structure of **(3.2)**$(BPh_4)_2 \cdot 2CH_3CN$ is shown in Figure 3.5. Here, the average Fe-N bond distances are found to be 1.962 Å for LS iron(II).

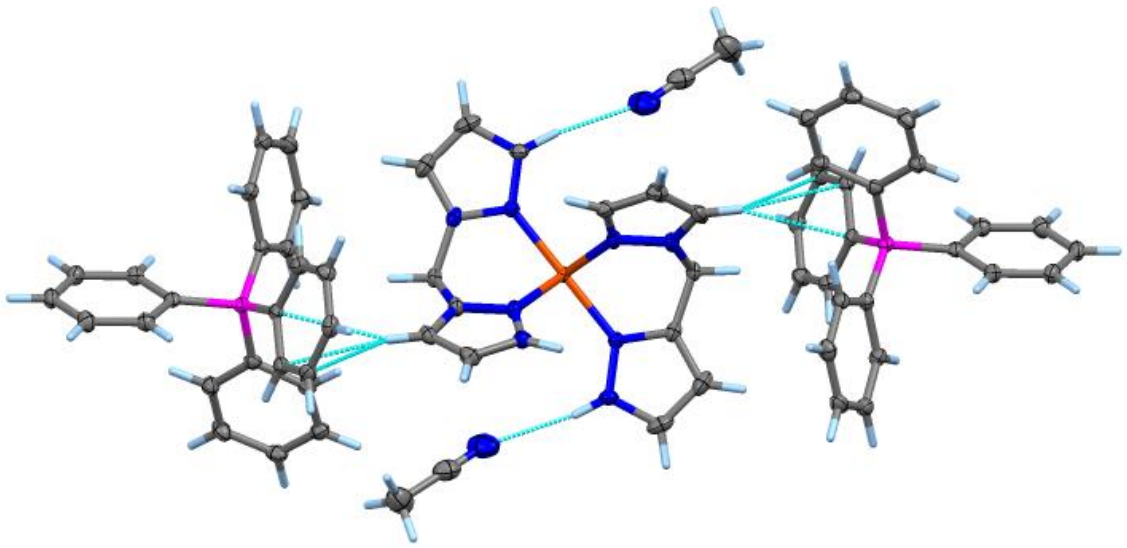

Figure 3.5. A portion of the 100 K structure of **(3.2)$(BPh_4)_2 \cdot 2CH_3CN$** showing disorder of one of the *nc*-Tpm units (left).

These distances are slightly shorter but comparable to Reger's [35] LS tris(pyrazolyl)methane complex (1.972 Å). In **(3.2)**$(BPh_4)_2 \cdot 2CH_3CN$ one of the nc-Tpm units is disordered over three positions such as to give a statistical mixture of cis- and trans- isomers in the solid state. Interestingly, the weakly hydrogen bound CH_3CN molecule is fully occupied, giving an indication of the weakness of the CN···H interactions. The thermal behavior of these crystals has not yet been investigated but is clearly different than the isolated powder presumably due the solvate molecules in the latter. More investigation into this system is warranted. In CD_3CN, the ^1H NMR spectrum of **(3.2)**$(BPh_4)_2 \cdot 2CH_3CN$ gives all resonances in the normal region of the spectrum (7.3 – 6.7 ppm) verifying that the complex is diamagnetic (LS) at room temperature in solution.

To gain more information about the magnetic behavior of the Fe(II) Nc-scorpionate complexes, samples were sent out to be interrogated by SQUID magnetometry. A plot of the variable temperature magnetic behavior of $(3.2)(BF_4)_2$ is shown below in Figure 3.6.

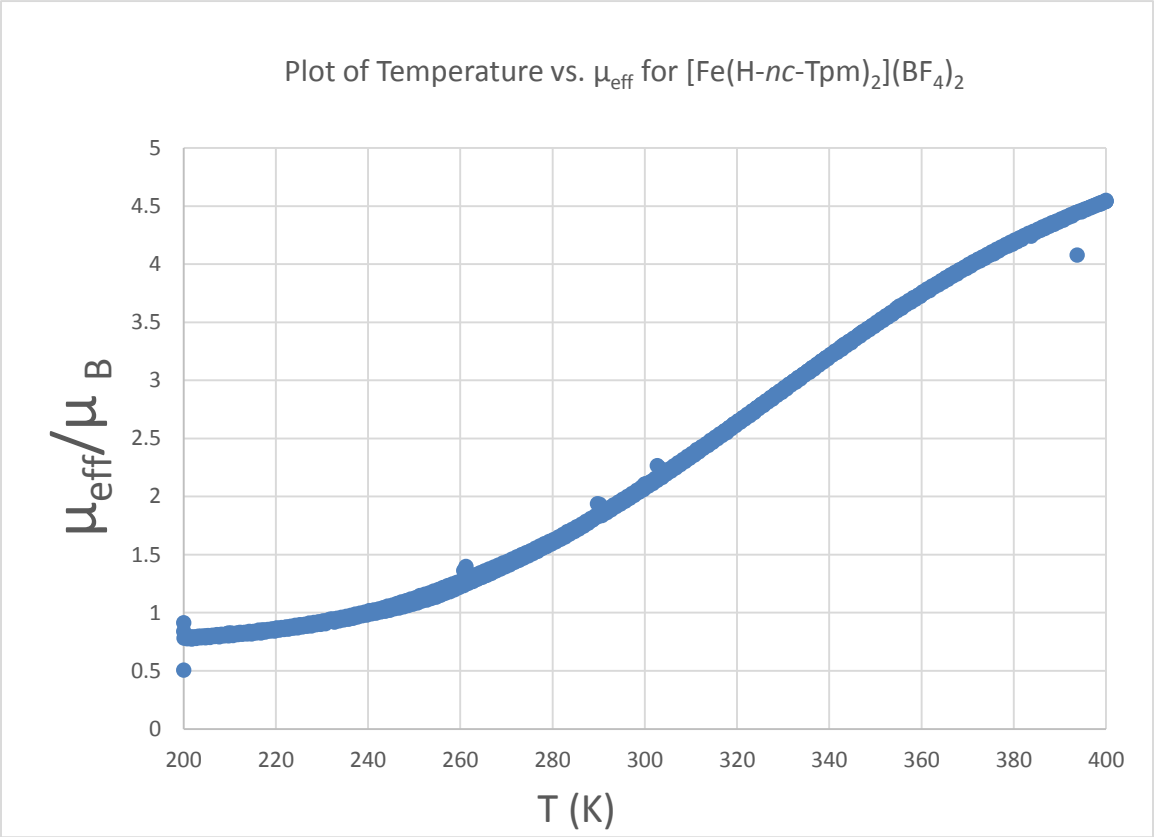

Figure 3.6: Variable temperature magnetic moment for $[Fe(H\text{-}nc\text{-}Tpm)_2](BF_4)_2$ from SQUID magnetometry measurements.

The plot shows that $(3.2)(BF_4)_2$ is completely low spin Fe(II) at 200 K (0.7 μ_B) and gradually begins SCO at higher temperatures. The sample is nearly fully high spin at 400 K (high T limit of the instrument) and has an estimated $T_{1/2}$ (with 50% high spin) at about 330 K. The value of $T_{1/2}$ = 330 K is somewhat lower than that of Reger's $[Fe(Tpm)_2](BF_4)_2$ [35] with a $T_{1/2}$ = 380 K.

For comparison, $[Fe(Tos\text{-}nc\text{-}Tpm)_2](BF_4)_2$ is high spin at all temperatures so there are no SCO events between 0 and 300 K, as shown by the magnetic data of this complex, shown in Figure 3.7.

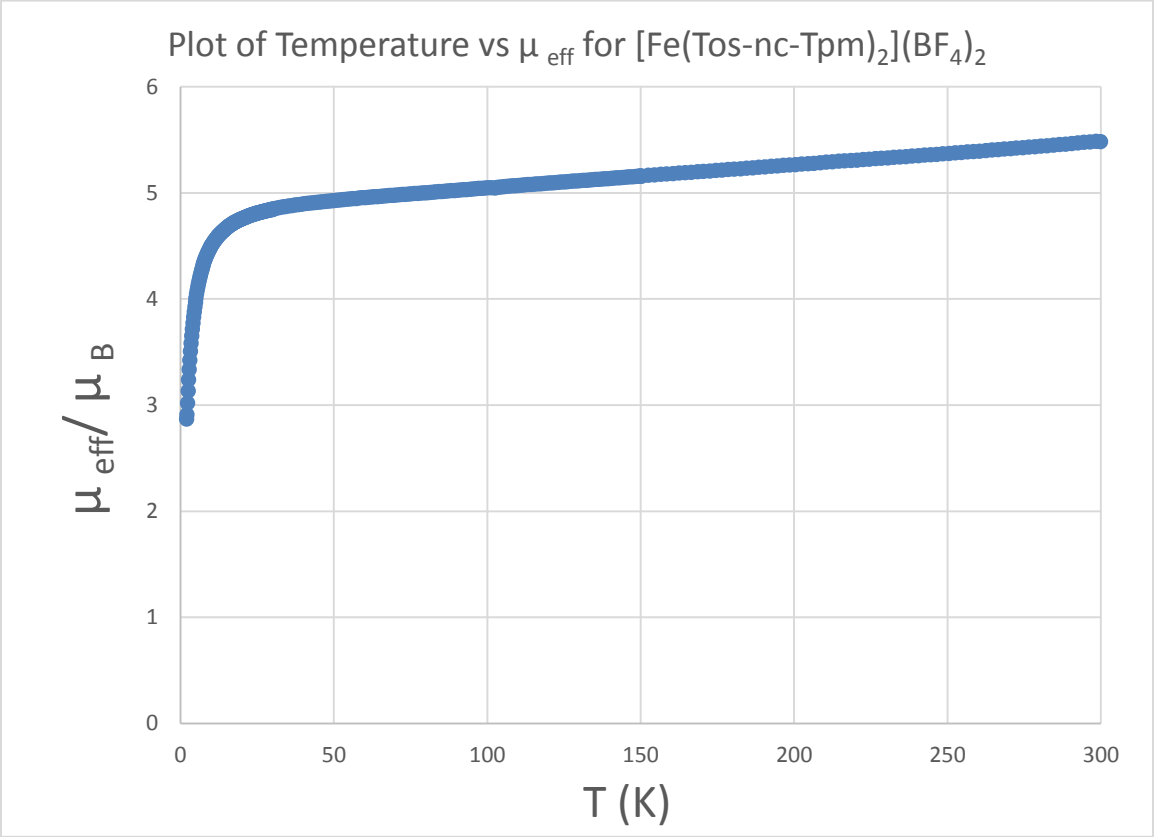

Figure 3.7: Variable temperature magnetic data for $[Fe(Tos\text{-}nc\text{-}Tpm)_2](BF_4)_2$.

A plot of the spin crossover behavior of a solid sample of $(3.1)(BF_4)_2 \cdot 2\ CH_3CN$ (that was crystallized, decanted, and dried under a stream of N_2 to prevent solvent loss) over the temperature range of 2 to 300 K is shown in Figure 3.8.

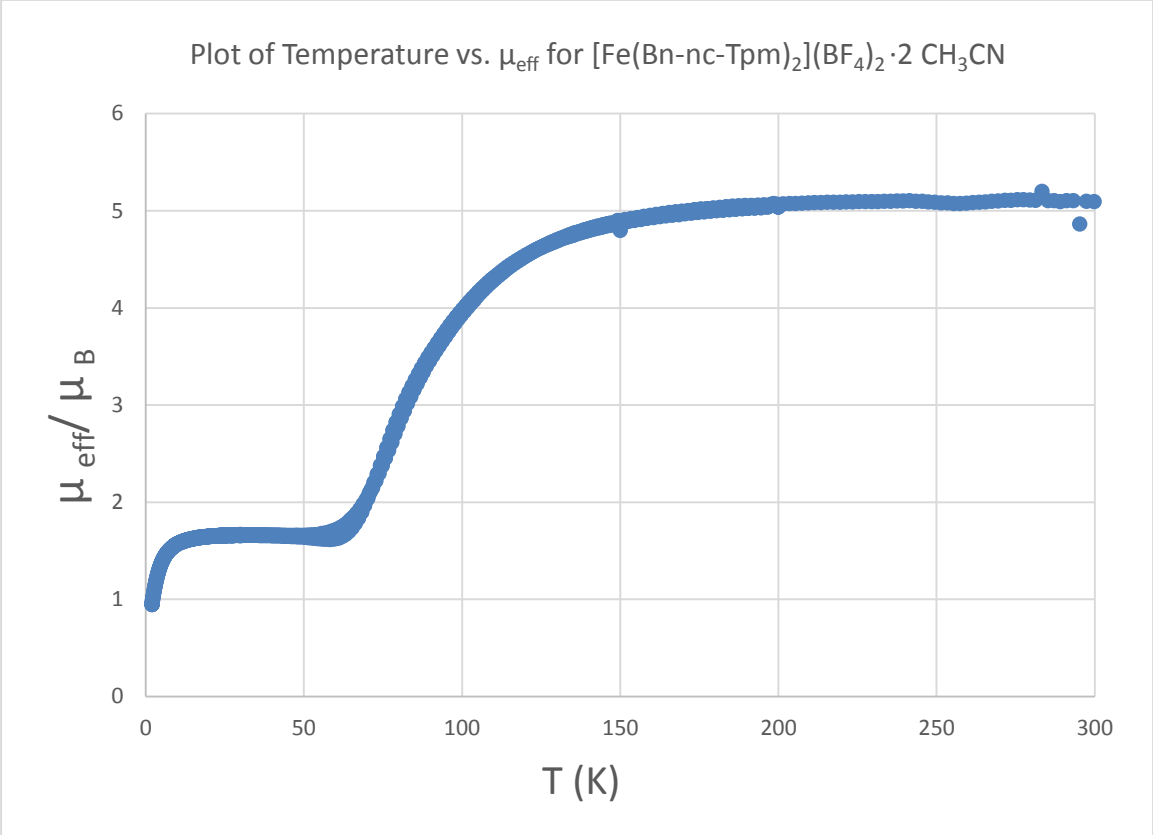

Figure 3.8: Variable temperature magnetic data for $[Fe(Bn\text{-}nc\text{-}Tpm)_2](BF_4)_2 \cdot 2\ CH_3CN$.

The plot shows that $(3.1)(BF_4)_2 \cdot 2\ CH_3CN$ is high spin between the temperature ranges of about 175 and 300 K with $\mu_{eff} = 5.1\ \mu_B$. The sample undergoes a gradual spin state change below 175 K and reaches a minimum effective moment of $\mu_{eff} = 1.67\ \mu_B$ at 60 K. The plot clearly demonstrates the SCO behavior, in agreement with the previous crystallographic and visual data discussed.

D. Future work.

As mentioned earlier, $[Fe(Tpm^*)(H_2O)_3\}(BF_4)_2$ has been prepared by Reger [35], initially observed as a side product in the development of $[Fe(Tpm^*)_2](BF_4)_2$ complexes (where they noted that this result was promoted when the $Fe(BF_4)\cdot 6H_2O$ reagent had been exposed to air prior to use). Reger complexes also showed the heteroleptic complex could be fully converted to the homoleptic complex by treating the former with additional ligand.[35] This observation led the Murray group to make extensive use of the tris(aqua)iron(II) Tpm* complex as a starting material for large numbers of mixed scorpionate systems.[45] The reactions of equimolar ratios of nc-Tpm's with iron salts will be pursued in attempts to make heteroleptic species. Clearly increasing the steric bulk around the pyrazole periphery to ^{i}Pr, Ph, ^{t}Bu, or Mes would help this line of investigation in determining what level of steric hindrance would be required to prevent to formation of the homoleptic complexes.

3.3 CONCLUSIONS

Two successful routes toward the preparation of the novel H-nc-Tpm ligand have been developed. The first route (Scheme 3.1) utilizes an N-benzyl protecting group that

has been found to be difficult to remove under mild conditions. Harsher conditions were required to remove the benzyl group and the product was difficult to separate from the reagents needed, leading to low yield of the ligand. These complications, along with the need for column chromatography throughout the synthesis makes this route less than ideal for widespread use in the inorganic community.

The second route (Scheme 3.2) utilizes a tosyl protecting group that has been found (as expected) to be considerably easier to remove under milder conditions. The synthesis of H-nc-Tpm through this route avoids the use of column chromatography altogether, allowing for large scale preparation of this ligand with relative ease. The intermediates along the path appear to be air and moisture stable as no special precautions were taken while handling them without any signs of decomposition.

A number of homoleptic Fe(II) Nc-Tpm metal complexes have been successfully prepared and characterized. The complex $[Fe(H\text{-}\textit{nc}\text{-}Tpm)_2](BF_4)_2$ was shown by various methods to have a LS Fe(II) center at low temperatures with gradual but incomplete SCO behavior upon warming to 400 K. In contrast, the complex $[Fe(Tos\text{-}nc\text{-}Tpm)_2](BF_4)_2$ was shown to be HS Fe(II) regardless of temperature, highlighting that even the addition of a single bulky substituent to the Tpm scaffold has a pronounced effect on the SCO behavior observed.

The complex $[Fe(Bn\text{-}nc\text{-}Tpm)_2](BF_4)_2 \cdot 2\ CH_3CN$ was shown to undergo SCO behavior upon cooling to 77 K by a number of methods. A search of the literature reveals that throughout numerous studies on Fe(II) scorpionates, those with substituents larger than methyls have never shown SCO behavior which has recently been summarized

nicely "… any substituents in the 3-position that are much larger than a methyl destroy any hope of observing spin state crossover behavior and essentially lock the complex into the HS form".[46] As far as we know, this is the first example of SCO behavior in a scorpionate that has a pyrazolyl substituent larger than a methyl proximal to the metal center. This ligand design may open the door synthetically to a wealth of nitrogen protection/deprotection reactions that should alter the electronic and steric properties about the metals first and second coordination sphere.

Chapter 4

FUTURE WORK

4.1 Future Work

Some target ligand scaffolds containing both hard and soft ligand donor sites for the preparation of bimetallic complexes have been prepared and characterized **H_2[Fl-P_2N_3]** and **H_2[R-P_2N_3]**). Monometallic complexes demonstrating the binding modes of both of the sites have been prepared and partially characterized. A short-term goal would be to prepare bimetallic complexes by reacting $Zr(NMe_2)_4$ with **{[H_2(κ^2*P*, κ *N*-Fl-P_2N_3)]PtCl}Cl**·H_2O·CH_2Cl_2, **(2.1)**.

For other systems, one can envision four different approaches to make heterometallic derivatives. The first is to bind a hard metal to the hard N3 donor site and isolate the complex before attempting to bind a soft metal to the soft P2 donor site. The second approach is to reverse the order and bind the soft metal before the hard one. Another approach would be to attempt the self-assembly of the metals to their respective sites. In other words, both metal reagents would be added to the same pot along with the ligand. A fourth strategy would be to bind the same metal in both sites and then attempt

trans-metalation to interchange one of them. All of these approaches will need to be explored.

The idea behind the ligand scaffold containing hard and soft donors is to bind hard and soft metals respectively. Ideally, these metals would be 1st row transition metals as they are cheaper, more abundant, and safer to handle than their 2nd and 3rd row counterparts. Sadighi and coworkers [47] showed that bulky N-heterocyclic carbene supported Cu(I) boryl complexes have been known to perform the catalytic reduction of CO_2 to CO with the addition of stoichiometric quantities of an oxygen acceptor [$(Bpin)_2$]. As discussed previously in chapter 1, nature is believed to utilize low valent Fe and Ni metal ions to facilitate CO_2 reduction through bimetallic cooperativity.[5] A combined theoretical and experimental study performed by Nakamura and associates [48] implicated that a Zn hydride intermediate may be responsible for CO_2 reduction to formic acid (under hydro thermal conditions). Thomas and coworkers [19] demonstrated the utility of a bimetallic Zr/Co catalyst for the reduction of CO_2 to MeOH, as was previously discussed in chapter 1. Thus, a good starting point for the formation of bimetallic complexes would be with combinations of these metals.

This next goal would be to prepare metal complexes of the NC-scorpionates with metal salts or halides to form MLX complexes where X = counter anion. Tris(pyrazolyl)borate complexes are known to form sandwich complexes (ML_2, L = polypyrazolylborate) which may not be very useful for small molecule activation chemistry. The MLX compounds can be unstable toward ligand redistribution reactions to form ML_2 and MX_2 compounds if steric bulk is insufficient.[49] Thompson and coworkers [50] studied a series of $[H_nB(3\text{-}Rpz)_{n-1}]^-$ metal complexes (R = Ph, ^{t}Bu) and

found that it did not appear to be possible to make ML_2 sandwich complexes with 1st row transition metals when ^{t}Bu or Ph groups were located at the 3 position of the pyrazoly rings.[50] The addition of potassium salts of the tris(pyrazolyl)borate ligands with tBu or Ph groups at the 3-positions to metal dihalides (MX_2, M = Co, Ni, Zn) yielded simple MLX compounds without any evidence of the formation of the sandwich complexes.[50]

NC-scorpionate ligands with varying degrees of steric bulk at the 3-position would need to be prepared to determine if the same behavior is observed in these complexes. This could be accomplished simply by the reaction of the appropriate pyrazole derivative (3,5-di-phenyl-1H-pyrazole, 3,5-di-isopropyl-1H-pyrazole, or 3,5-di-tert-butyl-1H-pyrazole, all commercially available) onto either the N-benzyl protected precursor (**3C**) or the N-tosyl protected precursor (**3E**), as shown in Schemes 4.1 and 4.2. Our lab has diisopropylpyrazole in stock, so this would be a good place to start. If the ^{i}Pr derivatives prove to be successful at preventing the formation of the sandwich complexes, then the other derivatives (Ph, tBu) may not need to be attempted.

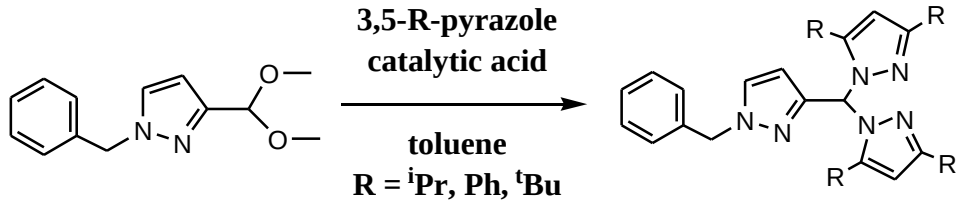

Scheme 4.1. Proposed synthetic route toward the preparation of bulky Bn-NC-scorpionates.

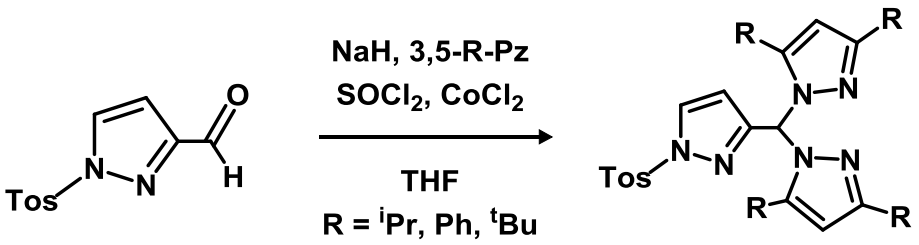

Scheme 4.2. Proposed synthetic route toward the preparation of bulky Tos-NC-scorpionates.

The next step then would be to combine the ligands and metals in 2:1 and 1:1 ratios to determine if: i) the ligands will bind the metals and ii) whether they will bind as sandwich complexes (ML_2) or as simple MLX complexes.

The next step then would be to attempt to bind an additional metal directly to the ligand scaffold through deprotection/deprotonation of the nitrogen of the N-confused pyrazole ring followed by addition of the appropriate metal reagent. A few strategies for accomplishing this can be envisioned. The first is to prepare the monometallic complex by binding a metal through the tridentate N-donors of the pyrazoles and then attempt to deprotect/deprotonate the nitrogen of the N-confused pyrazole followed by addition of the 2nd metal. The second strategy is to deprotect/deprotonate the ligand first, and then bind both metals simultaneously or in different sequential orders. Both of these strategies could be attempted.

Another goal of this research is to continue to develop the utility of the NC-scorpionate ligand scaffold by appending a soft donor site (P donor) to the periphery of the ligand scaffold to see if it will promote the binding of additional metals. Two

strategies for the syntheses of the new ligands are envisioned. One strategy is to use the tetrahydropyran (THP) protecting group on the nitrogen atom of the NC-scorpionate. The THP protecting group has been shown to promote deprotonation/lithiation at the pyrazolyl carbon nearest to which it is bound.[51] Deprotonation at the 5 position would be useful for the attachment of phosphorus donor groups directly (by reaction with commercial R_2PCl, R = iPr, tBu, Ph) or indirectly via incorporation of methylene spacers described in Chapter 1 (Chart 1.3). Two proposed synthetic routes toward the preparation of these ligands are shown in Scheme 4.3.

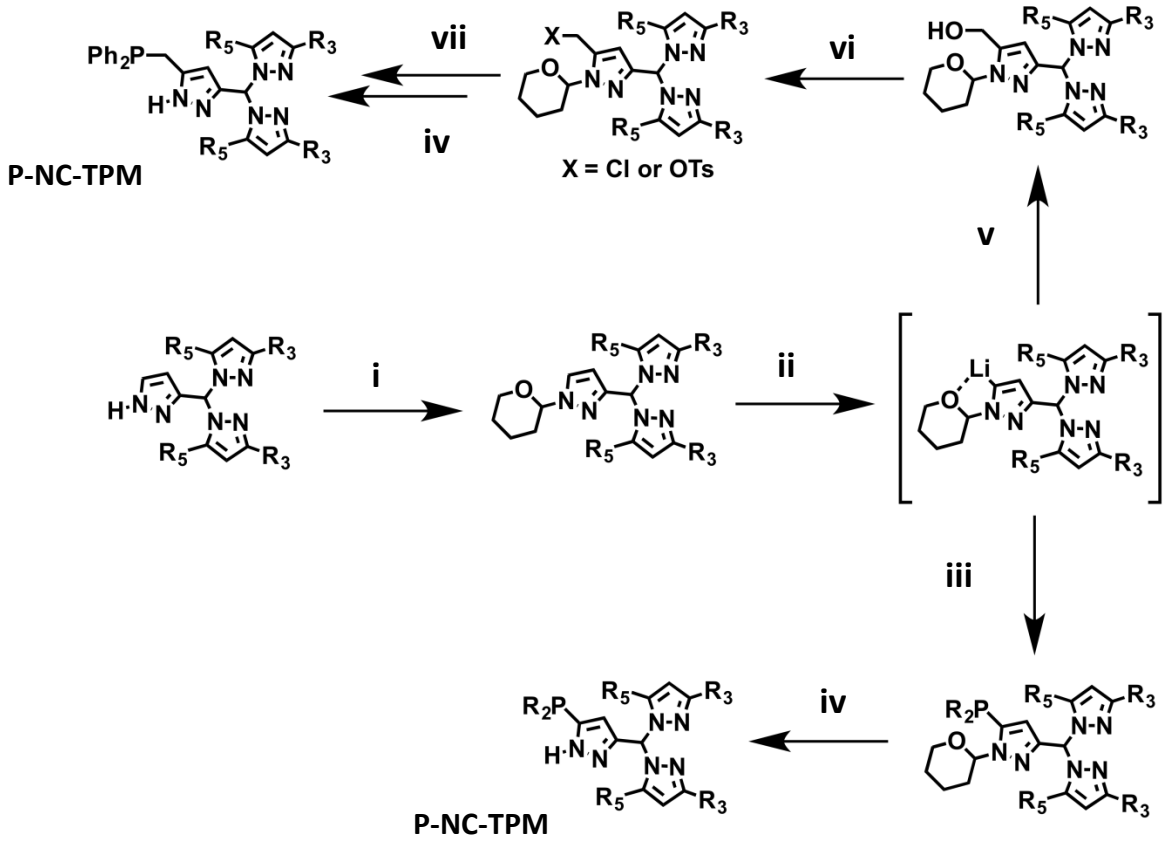

Scheme 4.3. The proposed synthetic route toward the preparation of P donor containing NC-scorpionates. Key: i) 3,4-dihydropyran, CF_3CO_2H, NaOH; ii) ^nBuLi ; iii) R_2PCl, R

= iPr, tBu, Ph; iv) HCl, H_2O; v) H_2CO, H_2O; vi) $SOCl_2$ (X = Cl) or KOH + TsCl (X = OTs); vii) Ph_2PH, ^nBuLi.

A potential pitfall of Scheme 4.3 is that similar conditions (^nBuLi followed by addition of electrophile) are employed for the functionalization of the apical carbon position of other known tris(pyrazolyl)methane ligands, as was demonstrated by Breher et al.[52] Such chemistry is not available for derivatives with bulky groups that "block" the methine hydrogen. Nevertheless, it might be necessary to attach an alkyl substituent of some kind (Me, Et, etc…) to the apical carbon position prior to this step to prevent a potential side reaction. Deprotection of the THP protecting group under acidic conditions will give the target ligand scaffold shown in Chapter 1 (Chart 1.3).

The next step then would be to attempt to prepare bimetallic complexes with these P-NC-TPM ligands using the previously mentioned metals. The metals could be introduced to the ligands in different sequential orders to determine whether the order of addition plays a role in binding, as previously described.

The final goal of this project would be to explore the reactivity of the bimetallic complexes toward the activation of small molecules, mainly CO_2. There are a number of known methods for the detection of the products of CO_2 reduction (CO, HCO_2H, CH_3OH, CH_4). The presence of formic acid (HCO_2H) or methanol can easily be detected and quantified by ^1H NMR. A simple method that can be used to detect carbon monoxide (CO) or methane is by GC-MS analysis of the reaction headspace. Another method for the detection of CO is the method of CO trapping that was recently used by Cummins.[53] In this method, the volatile materials are transported to a solution of

$Cp^*RuCl(PCy_3)$. The presence of CO is then indicated by a dramatic change in color from blue to yellow. Along with the color change, there is a change in the observed ^{31}P NMR chemical shift. The chemical shift for $Cp^*RuCl(PCy_3)$ is found at $\delta_P = 40.61$ ppm and for the CO bound complex $Cp^*RuCl(CO)(PCy_3)$ is found at $\delta_P = 51.74$ ppm. Integration of these peaks allows for determination of the ratios present.

Chapter 5

EXPERIMENTAL SECTION

5.1 General Considerations:

The compounds I_2, $AgSO_4$, 4-tert-butylaniline, Cs_2CO_3, diphenylphosphine, N,N'-dimethylethylenediamine (DMED), pyridine dimethanol, KOH, p-toluenesulfonyl chloride, ^{n}BuLi (1.6 M solution in hexanes), 2-nitroacetophenone, *N*,*N*-dimethylformamide dimethyl acetal (DMF-DMA), N,N'-dimethylformamide (DMF), hydrazine monohydrate, NaH, 1-fluoro-2-nitrobenzene, NH_4Cl, Fe powder, EtOH, chlorodiphenylphoshine, methylglyoxal-1,1-dimethylacetal, NaOH, $H_2NNH_2 \cdot HCl$, benzyl bromide, 1-bromo-2-fluorobenzene, phenyl boronic acid, Na_2CO_3, H-pyrazole, p-toluene sulfonic acid monohydrate, 3,5-dimethylpyrazole, dimethylsulfoxide (DMSO), potassium tertiary butoxide ($KO^{t}Bu$), HCl, K_2CO_3 were purchased commercially and used as received. The compound $Pd(PPh_3)_4$[54] was prepared according to a literature procedure. THF and Et_2O were dried over sodium/benzophenone ketyl. Toluene, CH_2Cl_2, and CH_3CN were dried over CaH_2. Solvents used in reactions were distilled under argon prior to use. Any water that was used was deionized.

5.2 Physical Measurements:

Midwest MicroLab, LLC, Indianapolis, Indiana 45250, performed all elemental analyses. Melting point determinations were made on samples contained in glass capillaries using an Electrothermal 9100 apparatus and are uncorrected. ^{1}H, ^{13}C, and ^{31}P NMR spectra were recorded on a Varian 400 MHz spectrometer. Chemical shifts are given in parts per million (ppm) and were referenced to solvent resonances at δ_H 7.26 and δ_C 77.16 for $CDCl_3$, δ_H 2.05 and δ_C 29.84 for D_6-acetone, and δ_H 1.94 and δ_C 118.26 for CD_3CN. Abbreviations for NMR: br (broad), m (multiplet), s (singlet), d (doublet), t (triplet), q (quartet). Electronic absorption (UV-Vis/ NIR) measurements were made on a Cary 5000 instrument. Magnetic susceptibility data were collected on a Quantum Design MPMS3 SQUID magnetometer.

5.3 Ligand Syntheses.

A. Toward H_2(Fl-P_2N_3) (1)

1A.

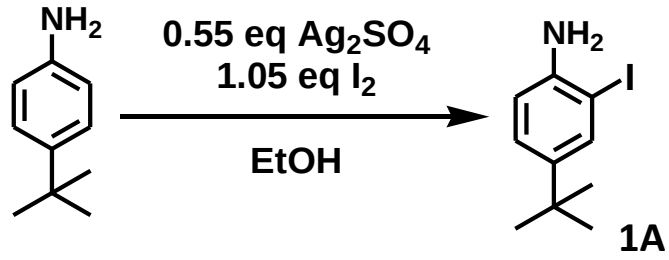

To a 250 mL Schlenk flask charged with I_2 (5.33 g, 21 mmol), Ag_2SO_4 (3.429 g, 11 mmol), and 100 mL of ethanol, was added 4-tert-butylaniline (3.185 mL, 20 mmol) all in one portion, upon which time a white solid (AgI) began to precipitate. The suspension was stirred at room temperature for 4 hours before being filtered through Celite. After removing solvents, the remaining reddish oil was partitioned between 50 mL water and 50 mL ethyl acetate in a separatory funnel. The aqueous phase was extracted with two more 50 mL portions of ethyl acetate. The combined organic layers were dried over $MgSO_4$, filtered, and solvent was removed *in vacuo*. The remaining red oil is purified on a column of silica gel by eluting with hexane/dichoromethane (1:1 v/v). The first fraction contains 2,6-diiodo-4-tert-butylaniline as a side product (R_f = 0.73, m = 0.53 g, yield = 7%). The second fraction contains the desired product, after concentration of eluent, as a red oil (R_f = 0.43, m = 4.02 g, yield = 73%). ^{1}H NMR ($CDCl_3$) δ_H: 7.62 (d, J = 2.2 Hz, 1H, Ar-H), 7.17 (dd, J = 8.4, 2.3 Hz, 1H, Ar-H), 6.71 (d, J = 8.3 Hz, 1H, Ar-H), 4.07 (br s, 2H, NH_2) 1.26 (s, 9H, CH_3) ppm. ^{13}C NMR ($CDCl_3$) δ_C: 144.3, 143.5, 135.8, 126.37, 114.7, 84.7, 33.9, 31.5 ppm.

1B.

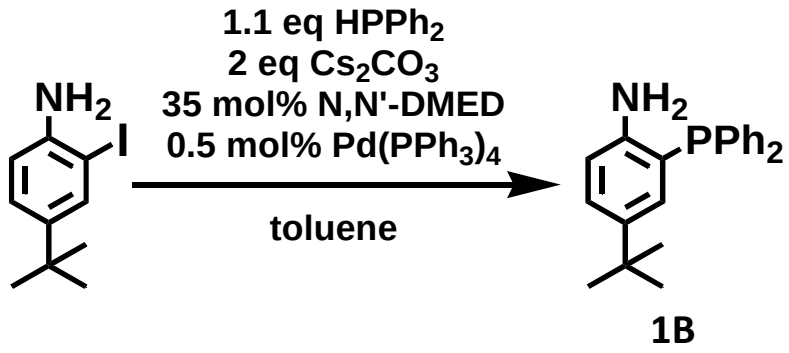

1B

A 100 mL Schlenk flask was charged with Cs_2CO_3 (4.74 g, 14.54 mmol) and a stirbar before being evacuated and taken into the glove box. Diphenylphosphine (1.39 mL, 8.00 mmol) and $Pd(PPh_3)_4$ (0.042 g, 0.036 mmol) were added to the flask and removed from the glove box. Meanwhile, argon gas was bubbled through another Schlenk flask containing **1A** (2.00 g, 7.27 mmol), DMED (0.26 mL, 2.54 mmol), and 45 mL toluene. The toluene solution was then canula transferred into the flask containing the Cs_2CO_3 and the former flask was rinsed two times (5 mL each). The contents of the flask were then heated at reflux for 15 hours, during which time a white precipitate formed. The mixture was brought to room temperature, filtered through Celite, and the solvent was removed under reduced pressure. The remaining brownish solid was partitioned between 50 mL water and 50 mL ethyl acetate in a separatory funnel. The aqueous phase was extracted with two more 50 mL portions of ethyl acetate. The combined organic layers were dried over $MgSO_4$, filtered, and solvent was removed *in vacuo*. The remaining yellowish solid is purified on a column of silica gel eluting with hexane/dichloromethane (2:1 v/v) to remove the impurities with higher R_f values before switching to pure CH_2Cl_2 to elute the desired product as a pale yellow solid after solvent was removed (R_f = 0.26, m = 2.13 g, yield = 88%). ^{1}H NMR ($CDCl_3$) δ_H: 7.34 (m, 10H,

PPh), 7.20 (dd, J = 8.3, 2.3 Hz, 1H, Ar-H), 6.79 (dd, J = 6.5, 2.3 Hz, 1H, Ar-H), 6.67 (dd, J = 8.3, 5.5 Hz, 1H, Ar-H), 3.25 (br s, 2H, NH_2), 1.10 (s, 9H, CH_3). ^{13}C NMR ($CDCl_3$) δ_C: 147.4 (d, J = 19.1 Hz), 141.4 (d, J = 2.4 Hz), 135.8 (d, J = 8.2 Hz), 133.8 (d, J = 18.7 Hz), 131.5 (d, J = 4.5 Hz), 128.9, 128.7 (d, J = 7.1 Hz), 127.5, 119.0 (d, J = 8.3 Hz), 115.4 (d, J = 3.0 Hz), 34.1, 31.4 ppm. ^{31}P NMR ($CDCl_3$) δ_P: -19.0 ppm.

1C. [31]

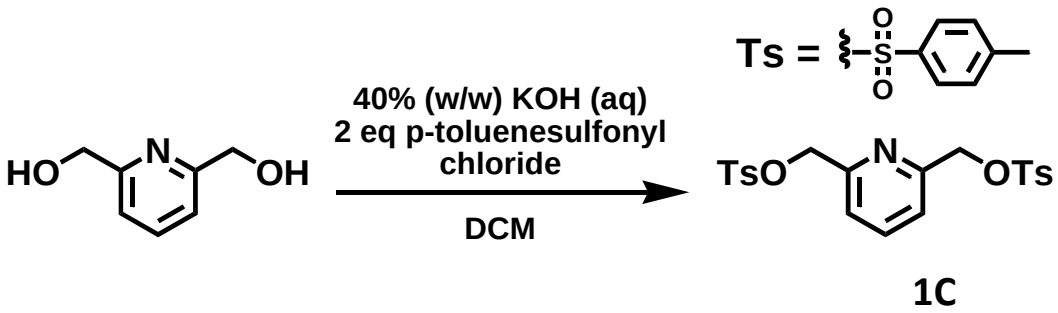

1C

Pyridine dimethanol (m = 2.122 g, 15.25 mmol) was dissolved in 40 mL CH_2Cl_2 and poured into a 250 mL round bottom flask containing a KOH solution (40 wt%, 20 g, 50 mL). The reaction vessel was cooled to 0°C and stirred for 30 minutes. P-toluenesulfonyl chloride was dissolved in 5 mL CH_2Cl_2 and added to the KOH solution all in one portion. The contents of the flask were stirred at 0°C for 1 hour and then at room temperature for 15 hours. A yellow precipitate formed during this time. An additional 50 mL each of CH_2Cl_2 and water were added to the flask and the contents were transferred to a separatory funnel. The water was extracted with 3 more 50 mL portions of CH_2Cl_2 and the combined organic layers were dried over $MgSO_4$, filtered, and solvent was removed *in vacuo*. The remaining yellow solid was triturated with methanol, filtered

with a Buchner funnel, and dried for 20 minutes on the funnel to afford the desired compound as a white solid (4.44 g, yield = 65%). ^{1}H NMR ($CDCl_3$) δ_H: 7.80 (m, 4H, tosyl H), 7.69 (t, J = 7.8 Hz, 1H, pyridine H), 7.33 (m, 6H), 5.05 (s, 4H, CH_2), 2.44 (s, 6H, CH_3). ^{1}H NMR data matches literature values.[31]

1D. [55]

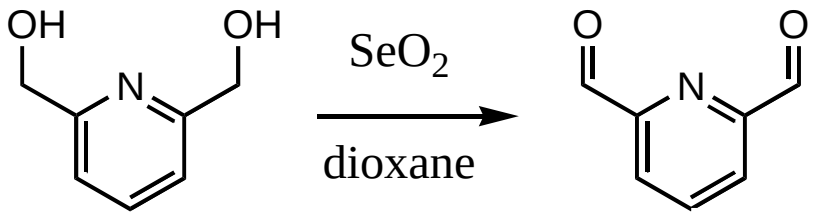

1D

SeO_2 (8.48 g, 76.0 mmol) was suspended in a solution of pyridine dimethanol (5.29 g, 38.0 mmol) in 40 mL dioxane and heated at reflux for 4 hours. The solution turned black after a few minutes. The flask was cooled to room temperature, then 0˚C via an ice bath, and then filtered and solvent was removed from the filtrate to give a yellow solid. The yellow solid was passed through a small plug (SiO_2) using CH_2Cl_2 and solvent was removed under vacuum. The product was recrystallized by layering hexanes on top of a concentrated CH_2Cl_2 solution to give the desired product as a colorless solid (3.86 g, 75 % yield). ^{1}H NMR ($CDCl_3$) δ_H: 10.17 (d, J = 0.8 Hz, 2H, CH(O)), 8.18 (dd, J = 7.8, 0.8 Hz, 2H, Ar-H), 8.08 (m, 1H, Ar-H). ^{1}H NMR data matches literature values. [55]

1E. H_2(Fl-P_2N_3).

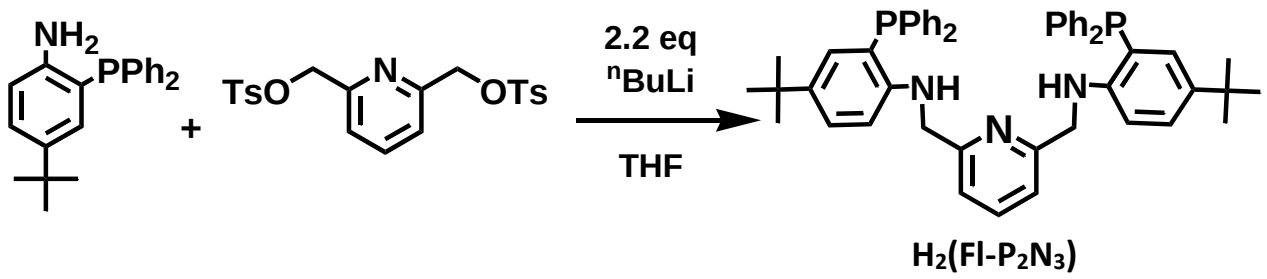

H_2(Fl-P_2N_3)

Argon was bubbled through a solution of **1B** (0.667 g, 2 mmol) in THF (10 mL) for about 10 minutes. After the flask had been cooled to 0°C via an ice bath for 20 minutes, ^{n}BuLi (1.25 mL of a 1.6 M solution in hexanes, 2 mmol) was added dropwise and the contents of the reaction vessel were stirred for about 15 minutes at 0°C. Then a pre-purged (argon) solution of **1C** (0.448 g, 1 mmol) in 10 mL THF was transferred to the cold lithium anilate solution. The reaction was allowed to equilibrate to room temperature overnight while stirring (about 16 hours), then solvent was removed by vacuum distillation. The contents of the flask were poured into 50 mL water in a separatory funnel and were extracted with three 50 mL portions of ethyl acetate. The combined organic layers were dried over $MgSO_4$, filtered, and concentrated *in vacuo*. The remaining yellowish solid is purified on a column of silica gel eluting with dichloromethane to remove the impurities with $R_f > 0.6$ before switching eluents to a mixture of hexane/ethyl acetate (4:1 v/v) to give the desired product in the next band (R_f = 0.59). Removal of solvent gave the desired product as a colorless solid (m = 0.77 g, yield = 57%). ^{1}H NMR ($CDCl_3$) δ_H: 7.35 (m, 20H, PPh), 7.20 (dd, J = 8.7, 2.5 Hz, 2H, Ar-H), 6.88 (d, J = 7.8 Hz, 2H, Ar-H), 6.82 (dd, J = 6.7, 2.5 Hz, 2H, Ar-H), 6.49 (dd, J = 8.5, 5.3 Hz, 2H, Ar-H), 5.37 (m, 2H, NH_2), 4.39 (d, J = 5.7 Hz, 4H, CH_2), 1.08 (s, 18 H, CH_3) ppm. ^{13}C NMR ($CDCl_3$) δ_C: 158.6, 148.2 (d, J = 17.2 Hz), 139.9, 137.3, 135.9 (d, J

= 7.9 Hz), 133.9 (d, J = 19.0 Hz), 131.8 (d, J = 3.9 Hz), 128.9, 128.6 (d, J = 6.9 Hz), 127.5, 119.1, 118.9 (d, J = 8.1 Hz), 110.3 (d, J = 2.6 Hz), 49.6, 34.0, 31.4 ppm. ^{31}P NMR ($CDCl_3$) δ_P: -19.5 ppm.

B. Toward H_2(R-P_2N_3). (2)

2A.

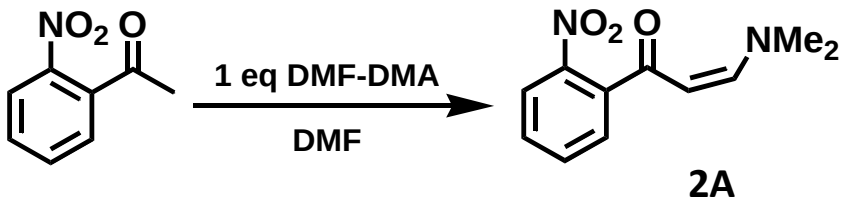

2A

A 100 mL round bottom flask was charged with 2-nitroacetophenone (5.0 g, 30.28 mmol), *N*,*N*-dimethylformamide dimethyl acetal (3.605 g, 30.28 mmol), and 20 mL dimethylformamide before being heated to reflux for 3 hours. The yellow solution turns red upon heating. After cooling to room temperature, the contents of the flask were poured into 50 mL water in a separatory funnel and extracted 3 times with dichloromethane (50 mL each). The combined organic layers were washed with water twice (50 mL each) and a saturated brine solution once (50 mL). The organic layer was dried over $MgSO_4$, filtered, and concentrated *in vacuo*. The product was washed with diethyl ether 3 times (10 mL each) and dried under vacuum to afford a yellow solid (5.91 g, 89% yield). ^{1}H NMR (d6-acetone) δ_H: 7.89 (d, J = 7.6 Hz, 1H, Ar-H), 7.70 (dt, J =

7.5, 1.2 Hz, 1H, Ar-H), 7.61 (m, 2H), 7.48 (br s, 1H, olefin H), 5.35 (d, J = 12.6 Hz, 1H), 3.16 (s, 3H, N-CH_3), 2.92 (s, 3H, N-CH_3). ^{13}C NMR (d6-acetone) δ_C: 220.6, 155.6, 149.3, 139.2, 133.4, 130.5, 129.7, 124.7, 94.8, 45.0, 37.3 ppm.

2B.

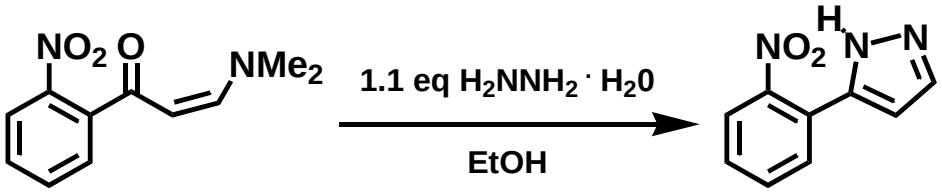

2B

A 100 mL round bottom flask was charged with **2A** (3.63 g, 16.52 mmol), 65% hydrazine monohydrate (1.37 mL, 18.17 mmol), and 20 mL EtOH, then was heated at reflux for 2 hours. The initial yellow solution turned red and then green. EtOH was removed by vacuum distillation and the product mixture was transferred to a separatory funnel using ethyl acetate. 50 mL water was added and the mixture was extracted with three 50 mL portions of ethyl acetate. The combined organic layers were dried over $MgSO_4$, filtered, and concentrated *in vacuo*. The resulting product was loaded onto a column containing silica gel and eluted using a hexane/ethyl acetate (1:1 v/v) solution (R_f = 0.67) to afford a black solid (2.76 g, 88% yield). ^{1}H NMR (acetone-d6) δ_H: 12.35 (br s, 1H, NH), 7.84 (dd, J = 7.8, 1.3 Hz, 1H, benzene H), 7.81 (d, J = 2.3 Hz, 1H, H_3pz), 7.75 (dd, J = 8.0, 1.1 Hz, 1H, Ar-H), 7.68 (dt, J = 7.7, 1.4 Hz, 1H, Ar-H), 7.56 (dt, J = 7.5, 1.4 Hz, 1H, Ar-H), 6.54 (d, J = 2.4 Hz, 1H, H_4pz). ^{13}C NMR (acetone-d6) δ_C: 132.5, 132.3, 131.2, 130.8, 129.3, 129.1, 128.0, 124.2, 104.5 ppm.

2C.

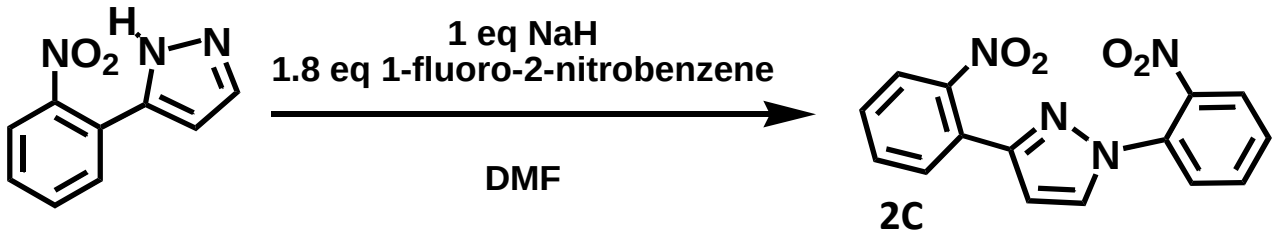

A solution of **2B** (2.706 g, 14.30 mmol) in 10 mL DMF was transferred via canula to a suspension of NaH (0.343 g, 14.30 mmol) in 10 mL DMF. The flask was rinsed twice with DMF (2.5 mL each) to ensure quantitative transfer. The solution was stirred until bubbles (H_2) ceased (about 5 minutes). 1-fluoro-2-nitrobenzene (2.72 mL, 25.7 mmol) was dissolved in DMF (10 mL) was transferred to the reaction mixture and then the mixture was heated at reflux for 24 hours. The reaction progress was monitored by TLC (SiO_2, Hex/EA [4:1 v/v], R_f = 0.39). After cooling to room temperature, the contents of the reaction vessel were poured into 50 mL water in a separatory funnel and were extracted with three 50 mL portions of ethyl acetate. The organic layer was then washed with three 50 mL portions of water to remove DMF. The combined organic layers were dried over $MgSO_4$, filtered, and concentrated *in vacuo*. Excess 1-fluoro-2-nitrobenzene was removed by vacuum distillation to yield the desired product as an orange solid (3.92 g, 88% yield). ^{1}H NMR ($CDCl_3$) δ_H: 7.91 (dd, J = 8.1, 1.3 Hz, 1H, Ar-H), 7.76 (m, 3H), 7.70 (dd, J = 7.4, 1.4 Hz, 1H), 7.63 (m, 2H), 7.54 (m, 1H), 7.49 (m, 1H), 6.63 (d, J = 2.6 Hz, Hpz). ^{13}C NMR ($CDCl_3$) δ_C: 149.8, 149.1, 144.5, 133.3, 133.2, 132.3, 131.3, 131.2, 129.2, 128.8, 126.8, 126.4, 125.3, 123.8, 107.8 ppm.

2D.

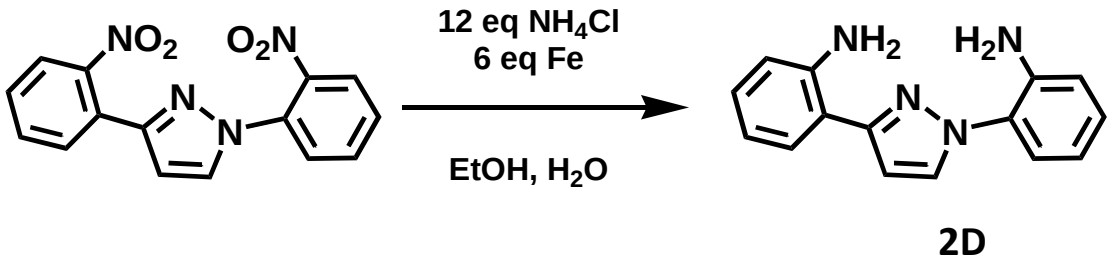

2D

A 250 mL round bottom flask was charged with **2C** (3.74 g, 12.1 mmol), NH_4Cl (7.79 g, 146 mmol), and Fe powder (4.06 g, 72.8 mmol) along with water (50 mL) and EtOH (175 mL), then was heated at reflux for 16 hours. The reaction progress was monitored by TLC (SiO_2, Hex/EA [4:1 v/v], R_f = 0.22). After the mixture had cooled to room temperature, it was filtered to remove Fe_2O_3. The solvent was removed by vacuum distillation and the brownish solid was partitioned between 50 mL each of water and ethyl acetate and the layers were separated. The aqueous layer was extracted twice more with 50 mL ethyl acetate each. The combined organic layers were dried over $MgSO_4$, filtered, and concentrated *in vacuo* to yield the desired product as a light brown solid (2.44 g, 80% yield). ^{1}H NMR ($CDCl_3$) δ_H: 7.73 (m, 1H), 7.60 (d, J = 7.3 Hz, 1H), 7.19 (m, 3H), 6.81 (m, 5H), 4.95 (broad s, 4H). ^{13}C NMR ($CDCl_3$) δ_C: 153.3, 145.0, 141.3, 130.8, 128.9, 128.8, 128.3, 126.7, 124.6, 118.2, 117.4, 117.1, 116.6, 116.0, 104.5 ppm.

2E. H_2(R-P_2N_3)

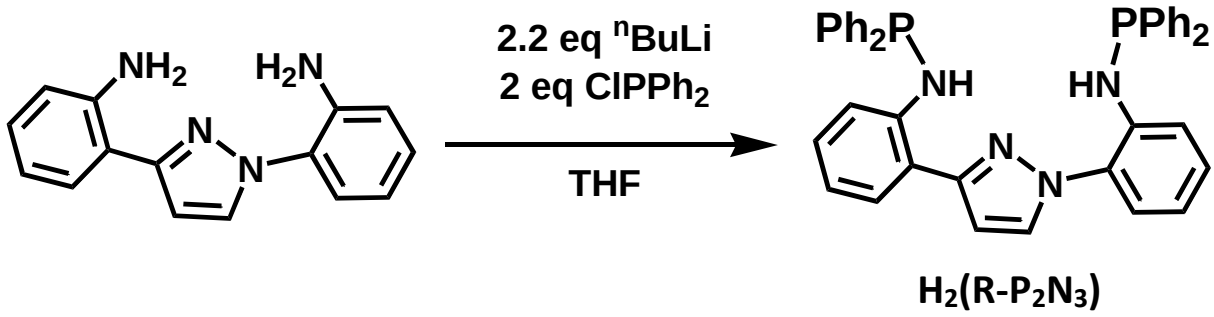

H_2(R-P_2N_3)

^{n}Butyllithium (1.6 M in hexanes, 7.28 mL, 11.64 mmol, 2.2 eq) was slowly added to an argon purged, cold (-78°C) solution of **2D** (1.324 g, 5.29 mmol) in THF (20 mL). After stirring magnetically for 1 hour, it was transferred to a pre-purged (argon) solution of $ClPPh_2$ (2.00 mL, 10.58 mmol) in THF (20 mL). The cold bath was removed. After the reaction mixture had stirred for 15 hours, solvent was removed by vacuum distillation. The contents of the reaction vessel were partitioned between 50 mL water and 50 mL ethyl acetate in a separatory funnel. The aqueous phase was extracted with two more 50 mL portions of ethyl acetate. The combined organic layers were dried over $MgSO_4$, filtered, and concentrated *in vacuo* to yield a yellow oil. The oil was triturated with Et_2O upon which time a white precipitate formed that was collected by filtration and dried under vacuum to yield **H_2(R-P_2N_3)** as a colorless solid (1.77 g, 54% yield). ^{1}H NMR (C_6D_6) δ_H: 8.78 (d, J = 5.6 Hz, 1H), 7.69 (ddd, J = 8.2, 3.9, 0.9 Hz, 1H), 7.55 (m, 6H), 7.29 (m, 4H), 7.10 (dt, J = 7.5, 1.5 Hz, 1H), 6.96 (m, 14H), 6.78 (m, 2H), 6.57 (dt, J = 7.6, 1.3 Hz, 1H), 6.36 (d, J = 2.5 Hz, 1H, H_4pz), 5.98 (d, J = 6.8 Hz, 1H). ^{13}C NMR ($CDCl_3$) δ_C: 154.0, 145.9 (d, J = 16.0 Hz), 142.2 (d, J = 17.9 Hz), 141.4 (d, J = 13.7 Hz), 140.6 (d, J = 12.7 Hz), 131.6, 131.4, 131.4, 131.3, 131.1, 129.6 (d, J = 1.6 Hz), 129.3 (d, J = 1.2 Hz), 129.3, 128.9 (d, J = 1.7 Hz), 128.8, 128.8, 128.7, 125.4, 119.5, 118.7, 117.8 (d, J = 21.3 Hz), 116.5 (d, J = 23.6 Hz), 105.3 ppm. ^{31}P NMR (C_6D_6) δ_P: 31.1, 29.2 ppm.

C. N-confused Scorpionates (3)

3A. [56]

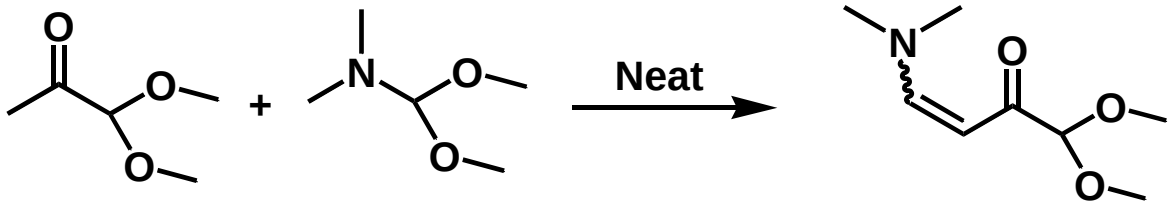

3A

A mixture of methylglyoxal-1,1-dimethylacetal (23.6 g, 24.2 mL, 200 mmol) and N,N-dimethylformamide dimethyl acetal (DMF-DMA)(23.8 g, 26.6 mL, 200 mmol) was heated at 66°C (oil bath) for 30 hours while stirring. The contents of the flask were brought to room temperature and the methanol byproduct was removed by vacuum distillation. The product was then distilled from the crude mixture under vacuum (b.p. = 104°C) to yield the desired product as an orange oil (24.57 g, 71% yield). ^{1}H NMR ($CDCl_3$) δ_H: 7.73 (d, J = 12.6 Hz, 1H, olefin H), 5.33 (d, J = 12.6 Hz, 1H, olefin H), 4.58 (s, 1H, $CHOMe_2$), 3.40 (s, 6H, OCH_3), 3.11 (s, 3H, N-CH_3), 2.86 (s, 3H, N-CH_3) ppm. ^{13}C NMR ($CDCl_3$) δ_C: 190.9, 154.3, 104.2, 54.0, 45.0, 37.1 ppm. NMR data matches literature values.[56]

3B. [44]

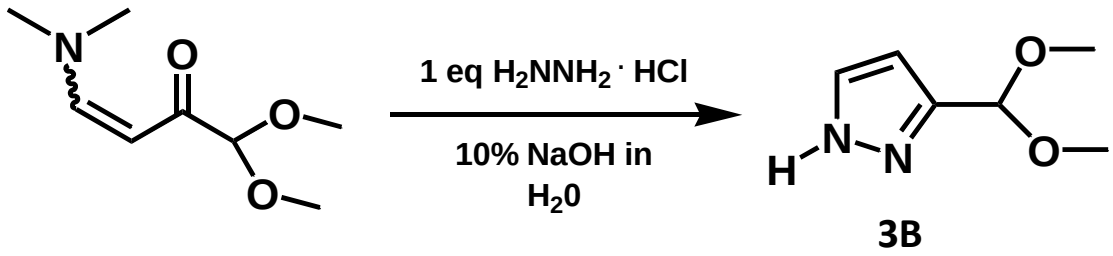

3B

3A (27.37 g, 158.0 mmol) was added to a stirred solution of NaOH (15 g, 375 mmol) and $H_2NNH_2 \cdot HCl$ (10.83 g, 158.0 mmol) in H_2O (150 mL). After the resulting solution had been stirred for 4 hours at room temperature, it was transferred to a separatory funnel and extracted exhaustively with diethyl ether (100 mL, 8x). The combined organic layers were dried over $MgSO_4$, filtered, and concentrated *in vacuo* to yield the desired product as a yellow oil (16.59 g, 116.7 mmol, 74% yield). ^1H NMR ($CDCl_3$) δ_H: 12.83 (br s, 1H, N-H), 7.61 (d, J = 2.2 Hz, 1H, H_5pz), 6.35 (d, J = 2.2 Hz, 1H, H_4pz), 5.62 (s, 1H, $CHOMe_2$), 3.37 (s, 6H, OCH_3). ^{13}C NMR ($CDCl_3$) δ_C: 106.4, 103.5, 98.9, 54.5, 52.5 ppm. NMR data matches literature values.[44]

3C.

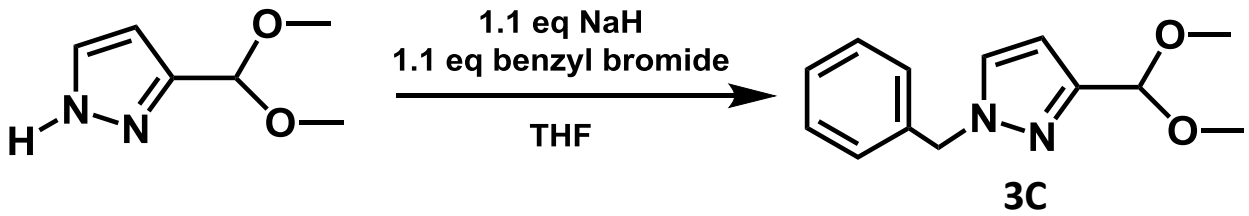

3C

Under argon, **3B** (4.32 g, 30.41 mmol) was added to a suspension of NaH (0.803 g, 33.45 mmol) in THF (100 mL). The solution was allowed to stir at room temperature for 1 hour. Benzyl bromide (3.98 mL, 33.45 mmol) was added via syringe all at once and

the contents were stirred at room temperature overnight. The solvent was removed via vacuum distillation and water (75 mL) and ethyl acetate (75 mL) were used to transfer the contents of the reaction vessel to a separatory funnel. The water layer was extracted with ethyl acetate a total of 3 times (75 mL). The combined organic layers were dried over $MgSO_4$, filtered, and concentrated *in vacuo*. The resulting red oil was loaded onto a column containing silica gel and eluted using a hexane/ethyl acetate (1:1 v/v) solution (R_f = 0.69, stained with I_2, not UV active) to afford the desired product as a yellow oil after solvent had been removed (4.04 g, 17.42 mmol, 57% yield). ^1H NMR ($CDCl_3$) δ_H: 7.31 (m, 4H), 7.19 (m, 2H), 6.33 (d, J = 2.3 Hz, 1H, H_4pz), 5.51 (s, 1H, $CHOMe_2$), 5.32 (s, 2H, CH_2), 3.39 (s, 6H, OCH_3). ^{13}C NMR ($CDCl_3$) δ_C: 150.1, 136.5, 130.1, 128.9, 128.2, 127.8, 104.6, 99.8, 56.1, 53.1 ppm.

3D.

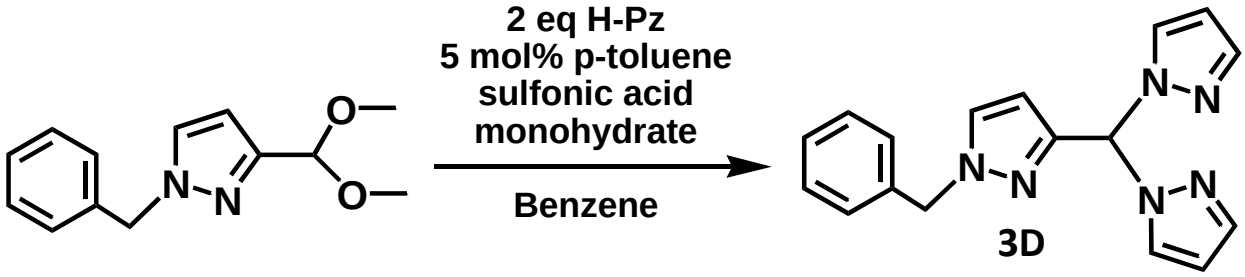

A mixture of **3C** (0.703 g, 3.03 mmol), H-pyrazole (0.412 g, 6.10 mmol), and p-toluenesulfonic acid monohydrate (0.029 g, 0.15 mmol, 5 mol %), and 5 mL C_6H_6 were placed in a round bottom flask with a magnetic stirbar. The flask was connected to a distillation apparatus under argon gas and was heated until most of the volatiles (C_6H_6, MeOH) had distilled, as indicated by a drop in distillate temperature (do no overheat!).

Residual solvent was removed via vacuum distillation at room temperature. Then, water (50 mL) and ethyl acetate (50 mL) were used to transfer the contents of the reaction vessel to a separatory funnel. The water layer was extracted with ethyl acetate a total of 3 times (50 mL each). The combined organic layers were dried over $MgSO_4$, filtered, and solvent was removed *in vacuo*. The crude reaction mixture was loaded onto a column containing silica gel and eluted using a hexane/ethyl acetate (1:1) solution (R_f = 0.56, stained with I_2) to afford a yellow oil that solidified under vacuum. Product was recrystallized from hot Et_2O to yield a colorless solid (0.66 g, 2.39 mmol, 72% yield). ^1H NMR ($CDCl_3$) δ_H: 7.73 (s, 1H, $C_{meth}H$), 7.67 (d, J = 2.3 Hz, 2H, H_3Pz), 7.59 (d, J = 1.8 Hz, 2H, H_5Pz), 7.34 (m, 4H, phenyl H's), 7.21 (m, 2H), 6.36 (d, J = 2.3 Hz, 1H, H_4Pz-NC), 6.29 (dd, J = 1.8, 2.3 Hz, 2H, H_4Pz), 5.31 (s, 2H, CH_2) ppm. ^{13}C NMR ($CDCl_3$) δ_C: 147.1, 140.8, 135.9, 130.7, 129.5, 128.9, 128.3, 127.9, 106.4, 106.3, 73.3, 56.4 ppm.

3E.

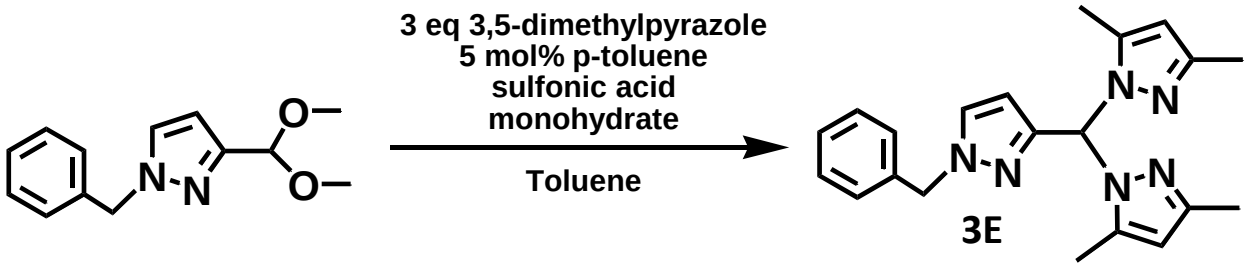

A mixture of **3C** (0.657 g, 2.91 mmol), 3,5-dimethylpyrazole (0.838 g, 8.72 mmol), and p-toluenesulfonic acid monohydrate (0.028 g, 0.15 mmol, 5 mol %), and 5 mL C_6H_6 were placed in a round bottom flask with a magnetic stirbar. The flask was connected to a distillation apparatus under argon gas and was heated until most of the

volatiles (C_6H_6, MeOH) had distilled, as indicated by a drop in distillate temperature (do no overheat!). Residual solvent was removed via vacuum distillation at room temperature. Then, water (50 mL) and ethyl acetate (50 mL) were used to transfer the contents of the reaction vessel to a separatory funnel. The water layer was extracted with ethyl acetate a total of 3 times (50 mL each). The combined organic layers were dried over $MgSO_4$, filtered, and solvent was removed *in vacuo*. The crude reaction mixture was loaded onto a column containing silica gel and eluted using a hexane/ethyl acetate (1:1) solution (R_f = 0.29, stained with I_2) to afford a yellow oil (0.98 g, 2.72 mmol, 94% yield). ^{1}H NMR ($CDCl_3$) δ_H: 7.61 (s, 1H, $C_{meth}H$), 7.31 (m, 4H, phenyl H's), 7.20 (m, 2H), 6.13 (d, J = 1.9 Hz, 1H, H_4Pz-NC), 5.82 (s, 2H, H_5Pz), 5.29 (s, 2H, CH_2), 2.24 (s, 6H, CH_3), 2.20 (s, 6H, CH_3) ppm. ^{13}C NMR ($CDCl_3$) δ_C : 148.2, 148.0, 140.7, 136.4, 130.3, 128.9, 128.2, 127.9, 106.9, 106.7, 70.0, 56.3, 14.0, 11.8 ppm.

3F.

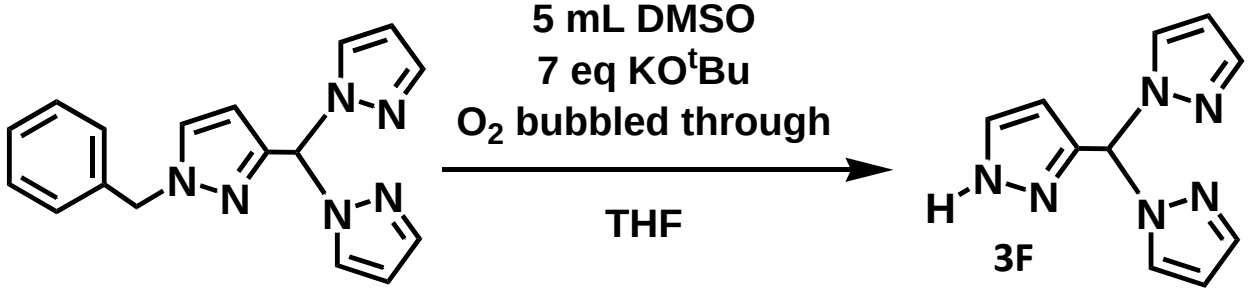

A solution of KO^{t}Bu (0.785 g, 7 mmol) in 7 mL THF was added to a solution of **3D** (0.304 g, 1 mmol) in 5 mL DMSO. Oxygen gas was then bubbled through the solution while stirring for 20 minutes, producing a white precipitate. HCl (3M, 10 mL)

was added to quench and then solid K_2CO_3 was added until the pH had reached 4-5. The contents of the flask were then filtered and the water and THF solvents were removed by vacuum distillation. The solid was extracted with hot acetone and filtered to remove solid KCl. The filtrate was concentrated and the product was recrystallized from Et_2O to yield a colorless solid (0.032 g, 0.15 mmol, 15 % yield). M.P. = 138-140°C. ^{1}H NMR (acetone-d_6) δ_H: 7.86 (dd, J = 2.4, 0.7 Hz, 2H), 7.83 (s, 1H), 7.77 (d, J = 2.2 Hz, 1H), 7.45 (dd, J = 1.8, 0.7 Hz, 2H), 6.46 (d, J = 2.4 Hz, 1H), 6.27 (dd, J = 2.4, 1.8 Hz, 2H) ppm. ^{13}C NMR (acetone-d_6) δ_C: 140.5, 130.7 (br, overlapping signals), 130.2, 106.6, 105.5, 74.0 ppm.

3G.

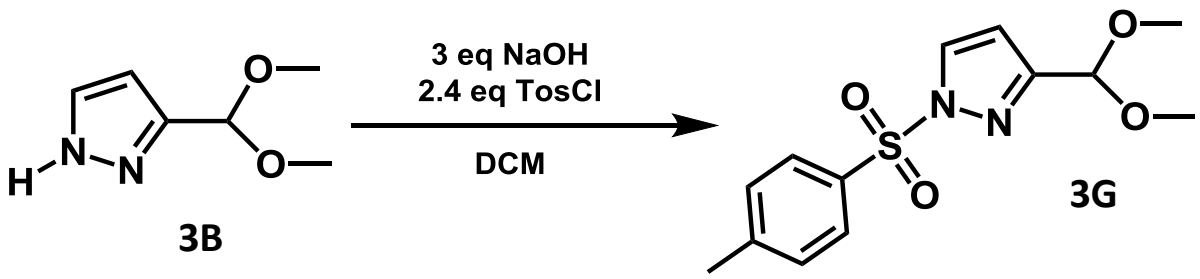

3B (2.30 g, 16.21 mmol) was added to a stirred suspension of NaOH (1.95 g, 48.63 mmol) in DCM (100 mL) and stirred at room temperature for 10 minutes. The reaction vessel was then placed in an ice bath and p-toluenesulfonylchloride (7.42 g, 38.9 mmol) was added slowly over 10 minutes. The reaction was stirred at room temperature for 15 hours. Then, the contents of the reaction vessel were transferred to a separatory funnel. The water layer was extracted with DCM a total of 3 times (100 mL each). The combined organic layers were dried over $MgSO_4$, filtered, and solvent was removed *in*

vacuo. The crude reaction mixture was loaded onto a column containing silica gel and eluted using a hexane/ethyl acetate (3:1) solution to remove excess TosCl (R_f = 0.57) before switching to pure ethyl acetate to elute the desired product as a colorless solid (3.57g, 12.05 mmol, 74% yield). Alternatively, the product can be purified without the use of column chromatography by triturating in diethyl ether and filtering to isolate the desired product. This method allows for larger scale preparation albeit in lower yield (51% yield). M.P. = 84-85°C. ^{1}H NMR ($CDCl_3$) δ_H: 8.05 (d, J = 2.8 Hz, 1H, H_4Pz), 7.88 (d, J = 8.4 Hz, 2H, Ar-H), 7.31 (d, J = 8.4 Hz, Ar-H), 6.47 (d, J = 2.8 Hz, 1H, H_5Pz), 5.35 (s, 1H, $CHOMe_2$), 3.32 (s, 6H, OCH_3), 2.41 (s, 3H, CH_3) ppm. ^{13}C NMR ($CDCl_3$) δ_C: 156.0, 145.9, 134.0, 132.0, 130.0, 128.1, 107.2, 99.3, 53.6, 21.7 ppm.

3H.

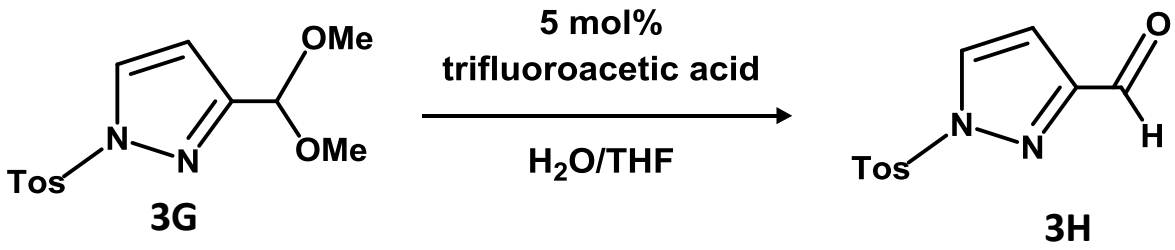

3G (16.34 g, 55.13 mmol), trifluoroacetic acid (0.21 mL, 2.76 mmol), THF (150 mL), and H_2O (50 mL) were combined in a round bottom flask and heated at reflux for 16 hours while stirring. After cooling to room temperature, 100 mL of a concentrated $NaHCO_3$ solution was added to reaction vessel and stirred until bubbles ceased. THF was then removed by vacuum distillation and the contents of the flask were transferred to

a separatory funnel. The water layer was extracted with ethyl acetate a total of 3 times (150 mL each). The combined organic layers were dried over $MgSO_4$, filtered, and solvent was removed by rotary evaporation. The resulting solid was dissolved in minimal boiling heptane, decanted away from red oil, and slowly cooled to -25°C. The solids were then collected by filtration, washed with ice cold hexane, and dried under vacuum to yield a pale yellow solid (10.09 g, 45.4 mmol, 82 % yield). M.P. = 92-94°C. ^{1}H NMR ($CDCl_3$) δ_H: 9.97 (s, 1H, CHO), 8.15 (d, J = 2.8 Hz, 1H, H_5Pz), 7.96 (d, J = 8.4 Hz, 2H, Ar-H), 7.38 (d, J = 8.4 Hz, 2H, Ar-H), 6.84 (d, J = 2.8 Hz, 1H, H_4Pz), 2.45 (s, 3H, CH_3) ppm. ^{13}C NMR ($CDCl_3$) δ_C: 186.0, 154.8, 146.9, 132.9, 132.5, 130.3, 128.5, 106.9, 21.8 ppm.

3I.

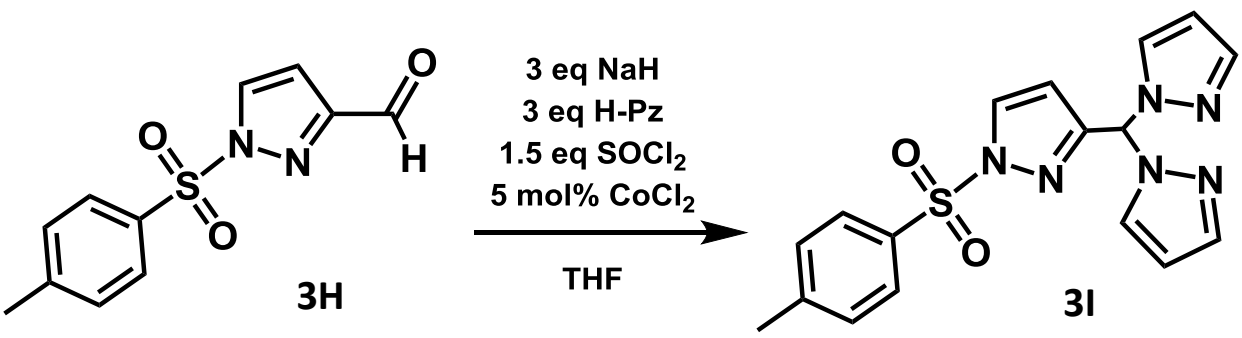

A solution of H-pyrazole (3.12 g, 45.8 mmol) in 25 mL THF was transferred slowly over 5 minutes via canula to a suspension of NaH (1.10 g, 45.8 mmol) in 40 mL THF. The flask was rinsed twice with THF (2.5 mL each) to ensure quantitative transfer. The solution was stirred until bubbles (H_2) ceased (about 5 minutes). $SOCl_2$ (1.67 mL, 22.9 mmol) was added to the reaction mixture through the septum slowly over 5 minutes and then stirred at room temperature for 10 minutes. A solution of **3H** (3.39 g, 15.27

mmol) and $CoCl_2$ (0.1 g, 0.76 mmol) in 25 mL THF was transferred via canula to the reaction mixture. The flask was rinsed twice with THF (2.5 mL each). The reaction mixture was heated at reflux for 15 hours while stirring before being brought to room temperature. The solvent was removed by vacuum distillation and the contents of the reaction vessel were transferred to a separatory funnel with the help of H_2O (100 mL) and ethyl acetate (100 mL). The water layer was extracted with ethyl acetate a total of 3 times (100 mL each). The combined organic layers were dried over $MgSO_4$, filtered, and solvent was removed *in vacuo*. The crude reaction mixture was dry loaded onto a column of silica gel and the impurities with higher R_f's (0.6 and 0.37) were eluted using a hexane/diethyl ether (1:2) solution. Pure ethyl acetate was used to elute the desired product as a colorless solid (4.65 g, 12.6 mmol, 83% yield). Alternatively, the product can be purified without the use of column chromatography by recrystallization from boiling heptane, albeit in lower yield (58% yield). M.P. = 114-116°C. ^{1}H NMR ($CDCl_3$) δ_H: 8.11 (d, J = 2.8 Hz, 1H, H_5Pz-NC), 7.87 (d, J = 8.3 Hz, 2H, Ar-H), 7.66 (s, 1H, $CHPz_2$), 7.56 (m, 4H, H_3Pz and H_5Pz), 7.32 (d, J = 8.3 Hz, 2H, Ar-H), 6.54 (d, J = 2.8 Hz, 1H, H_4Pz-NC), 6.28 (m, 2H, H_3Pz), 2.43 (s, 3H, CH_3) ppm. ^{13}C NMR ($CDCl_3$) δ_C: 152.6, 146.3, 141.0, 133.5, 132.3, 130.1, 129.6, 128.4, 108.8, 106.7, 72.5, 21.8 ppm.

3F. (Alternative Route)

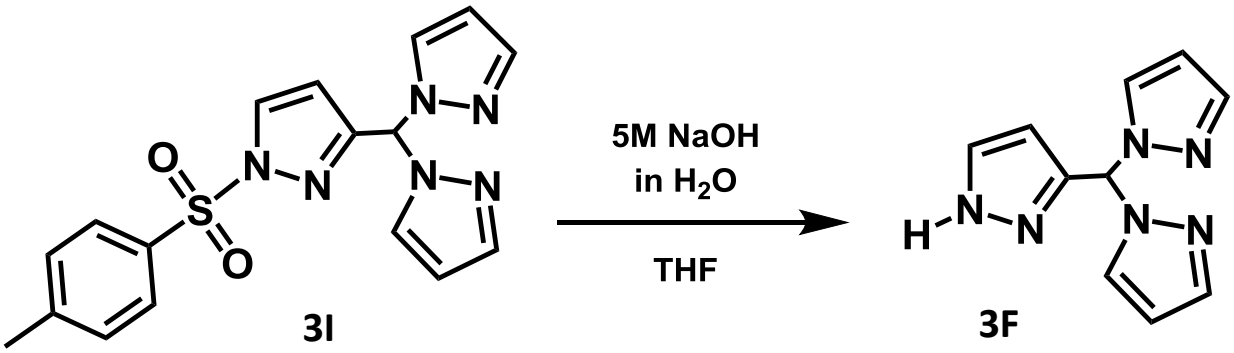

3I (0.392 g, 1.065 mmol) was added to a stirred solution of NaOH (0.60 g, 15 mmol) in H_2O (3 mL) and THF (5mL) and heated at reflux for 10 minutes. THF was then removed by vacuum distillation and the contents of the reaction vessel were transferred to a separatory funnel using DCM (50 mL) and H_20 (30 mL). The water layer was extracted with DCM a total of 4 times (50 mL each) and the combined organic layers were dried over $MgSO_4$, filtered, and solvent was removed *in vacuo*. The product was recrystallized from minimal benzene to afford the desired product as a colorless solid (0.139 g, 0.65 mmol, 61% yield). M.P. = 138-140°C. ^{1}H NMR (acetone-d_6) δ_H: 7.86 (dd, J = 2.4, 0.7 Hz, 2H), 7.83 (s, 1H), 7.77 (d, J = 2.2 Hz, 1H), 7.45 (dd, J = 1.8, 0.7 Hz, 2H), 6.46 (d, J = 2.4 Hz, 1H), 6.27 (dd, J = 2.4, 1.8 Hz, 2H) ppm. M.P. = 138-140 ^{13}C NMR (acetone-d_6) δ_C: 140.5, 130.7 (br, overlapping signals), 130.2, 106.6, 105.5, 74.0 ppm.

5.4 Syntheses of Metal Complexes

A. $H_2(Fl\text{-}P_2N_3)$ Complexes

$[Pt(Cl)\{H_2(Fl\text{-}P_2N_3)\}]Cl$ (2.1)

A solution of $H_2(Fl\text{-}P_2N_3)$ (0.063 g, 0.0814 mmol) and $Pt(EtCN)_2Cl_2$, (0.031 g, 0.0814 mmol) in 2 mL CH_2Cl_2 was stirred under argon at room temperature for 1 hour. Hexane (20 mL) was added to precipitate a yellow solid that was collected by filtration and dried under vacuum. The pale yellow solid was recrystallized by layering pentane on top of a concentrated CH_2Cl_2 solution. X-ray quality crystals were grown by slow evaporation of a CH_2Cl_2 solution. ^{1}H NMR (CD_3CN) δ_H: 8.68 (m, 1H), 7.85 (m, 2H), 7.75 (m, 3H), 7.47 (d, J = 8.9 Hz, 1H), 7.35 (m, 5H), 7.23 (br t, J = 7.5 Hz), 7.15 (m, 4H), 6.86 (m, 2H), 6.76 (m, 5H), 6.61 (dd, J = 11.5, 1.9 Hz, 1H), 6.56 (dd, J = 8.6, 6.8 Hz, 1H), 6.46 (m, 2H), 5.37 (br d, J = 9.3 Hz, 1H), 5.31 (br d, J = 14.0 Hz, 1H), 5.22 (m, 2H), 4.56 (dd, J = 13.7, 7.6 Hz, 1H), 4.43 (dd, J = 17.7, 9.4 Hz, 1H), 2.86 (d, J = 17.8 Hz, 1H), 0.79 (s, 18 H). ^{31}P NMR (CD_3CN) δ_P: 25.0 (d, $J_{P1\text{-}P2}$ = 15.8 Hz), satellite Pt resonances observed: ($J_{P1\text{-}Pt}$ = 1927 Hz), -0.3 (d, $J_{P1\text{-}P2}$ = 15.5 Hz), satellite Pt resonance ($J_{P2\text{-}Pt}$ = 1647 Hz) ppm.

B. $H_2(R\text{-}P_2N_3)$ Complexes

[Pt(Cl){H_2(R-P_2N_3)}]Cl (2.2)

A solution of H_2(Fl-P_2N_3) (0.051 g, 0.083 mmol) and Pt(EtCN)$_2$Cl$_2$, (0.031 g, 0.083 mmol) in 2 mL CH_2Cl_2 was stirred under argon at room temperature for 1 hour. Canula filtration was performed to collect the white precipitate, which was washed with Et_2O and dried under vacuum to afford a colorless solid. X-ray quality crystals were grown by placing the starting materials in a vial along with 1 mL of solvent and not mixing or jostling the reaction vessel. Long colorless needles formed within couple of days (0.03 g, 41 % yield). ^{1}H NMR data was collected but difficult to interpret due to many overlapping signals. ^{31}P NMR (CD_3CN) δ_P: 32.6 (d, J_{P1-P2} = 16.9 Hz), satellite Pt resonances observed: (J_{P1-Pt} = 1936 Hz), 27.3 (d, J_{P1-P2} = 16.9 Hz), satellite Pt resonance (J_{P2-Pt} = 1965 Hz) ppm.

[Ag{H_2(R-P_2N_3)}$_2$](OTf) (2.3)

A solution of Ag(OTf) (0.026 g, 0.1 mmol) and H_2(Fl-P_2N_3) (0.063 g, 0.1 mmol) in 3 mL THF was stirred at room temperature under argon for 12 hours. Solvent was removed under vacuum to give a colorless solid (0.053 g, 35 % yield). X-ray quality crystals were grown by slow vapor diffusion of Et_2O onto a concentrated $ClCH_2CH_2Cl$ solution.

Zr(NMe_2)$_2$(R-P_2N_3) (2.4)

A solution of H_2(Fl-P_2N_3) (0.0155 g, 0.025 mmol) and $Zr(NMe_2)_4$ (0.0067 g, 0.025 mmol) in 1 mL CD_2Cl_2 in a vial under argon was shaken vigorously for 1 minute. The solution turned bright yellow instantly. NMR data were acquired using the crude reaction mixture. X-ray quality crystals slowly precipitated out of solution. ^{1}H NMR (C_6D_6) δ_H: 7.85 (m, 3H), 7.77 (m, 5H), 7.61 (m, 2H), 7.28 (br s, 1H), 7.21 (m, 4H), 7.14 (m, 9H), 6.99 (m, 1H), 6.87 (m, 2H), 6.78 (dd, J = 7.9, 1.6 Hz, 1H), 6.63 (m, 2H) ppm. ^{31}P NMR (C_6D_6) δ_P: 34.67 (br s), 4.80 (br s) ppm.

C. N-confused Scorpionate Complexes

[Fe(BN-NC-TPM)$_2$](BF$_4$)$_2$ (3.1) (BF$_4$)$_2$

Under argon, a solution of **3D** (0.66 g, 2.17 mmol) in 10 mL THF was added to a solution of Fe(BF_4) · 6 H_2O (0.366 g, 1.084 mmol) in 10 mL THF. The former flask was washed with 5 mL THF that was transferred to the reaction solution. A white solid precipitated almost instantly. The suspension was stirred for 1 hour and then was cannula filtered. The solid was washed with two 2mL portions of THF, 2 mL Et_2O, and was dried under vacuum to give 0.678 g (68% yield) **5** as a colorless solid. X-Ray quality crystals were grown by slow vapor diffusion of Et_2O into a concentrated acetonitrile solution of the complex and contain 2 solvent molecules (CH_3CN). Crystal structures were solved at 100 and 240K. ^{1}H NMR (CD_3CN) δ_H: 50.9 (br s), 45.9 (br s), 41.3 (br s), 14.2 (br s), 11.0 (br s), 10.7 (br s), 10.4 (br s), 7.3 (br s), 3.5 (br s), 2.2 (br s) ppm. Elemental Anal.

Calc. (found) for $C_{34}H_{32}N_{12}B_2F_8Fe$: %C 48.72 (48.73), %H 3.85 (3.67), %N 20.05 (19.85).

[Fe(BN-NC-TPM)$_2$](OTf)$_2$ (3.1) (OTf)$_2$

Under argon, a solution of **3D** (0.304 g, 1 mmol) in 5 mL THF was added to a solution of $Fe(OTf)_2$ (0.177 g, 0.5 mmol) in 5 mL THF. The former flask was washed with 2 mL THF that was transferred to the reaction solution. A white solid precipitated after a few minutes. The suspension was stirred for 1 hour and then was canula filtered. The solid was washed with two 2mL portions of THF, 2 mL Et_2O, and was dried under vacuum to give 0.43 g (89% yield) **6** as a colorless solid. X-Ray quality crystals were grown by slow vapor diffusion of Et_2O into a concentrated acetonitrile solution of the complex. ^{1}H NMR (CD_3CN) δ_H: 50.8 (br s), 45.9 (br s), 41.2 (br s), 14.1 (br s), 10.9 (br s), 10.6 (br s), 10.3 (br s), 7.1 (br s), 3.4 (br s), 2.2 (br s). Elemental Anal. Calc. (found): %C 44.92 (44.58), %H 3.35 (3.40), %N 17.46 (16.85).

[Fe(BN-NC-TPM*)$_2$(BF$_4$)$_2$ (3.1*) (BF$_4$)$_2$

This complex was prepared in a similar manner to the complex **3.1 (BF$_4$)$_2$** except that **3E** ligand (0.136 g, 0.377 mmol) was used instead of **3D** along with the $Fe(BF_4) \cdot 6$ H_2O (0.064 g, 0.189 mmol). The reaction was stirred at room temperature for 16 hours and then was cannula filtered. The solid was washed with two 2mL portions of THF, 2 mL Et_2O, and was dried under vacuum to give 0.04 g (21% yield) **7** as a colorless solid.

X-ray quality crystals were grown by slow vapor diffusion of Et_2O into a concentrated acetonitrile solution of the complex.

[Fe(BN-NC -TPM*)$_2$(OTf)$_2$ (3.1*) (OTf)$_2$

This complex was prepared in a similar manner to the complex **(3.1) (OTf)$_2$** except that **3E** ligand (0.189 g, 0.524 mmol) was used instead of **3D** along with Fe(OTf) (0.093 g, 0.262 mmol). The reaction was stirred at room temperature for 16 hours and then was cannula filtered. The solid was washed with two 2mL portions of THF, 2 mL Et_2O, and was dried under vacuum to give 0.1 g (36% yield) **8** as a colorless solid. X-ray quality crystals were grown by slow vapor diffusion of Et_2O into a concentrated acetonitrile solution of the complex.

[Fe(H-NC-TPM)$_2$](BF$_4$)$_2$ (3.2) (BF$_4$)$_2$

An acetone solution (5 mL) of **3F** (0.264 g, 1.23 mmol) was cannula transferred to an acetone solution (5 mL) of $Fe(BF_4) \cdot 6\ H_2O$ (0.122 g, 0.362 mmol) and was stirred at room temperature for 15 hours. The solution turned pink immediately and pink solids formed. The solution was cannula filtered and the pink solid was washed with acetone 2 times (3 mL each), Et_2O (3 mL), and dried under vacuum to afford complex **9** as a pink solid (0.385 g, 0.59 mmol, 95% yield). Attempts to grow x-ray quality crystals of **(3.2) (BF$_4$)$_2$** proved to be unsuccessful as the crystals were too small and disordered for single crystal x-ray diffraction. The disordered crystals were deep pink. This complex was then

pushed forward in a reaction to swap out the counter ion (BF_4) for tetraphenylborate (BPh_4) in hopes that crystallization of this complex would be more successful. Elemental Anal. Calc. (found) for $C_{20}H_{20}N_{12}B_2F_8Fe$: %C 36.51 (36.72), %H 3.06 (3.05), %N 25.55 (25.54). M.P. = 250$^+$. ^{1}H NMR (CD_3CN) δ_H: 24.6 (v. br. s), 18.6 (v. br. s), 18.4 (v. br. s), 17.8 (v. br. s), 17.1 (v. br. s), 16.3 (v. br. s), 15.9 (v. v. br. s), 10.5 (v. br. s), 10.1 (v. br. s), 7.6 (v. br. s), 7.4 (v. br. s), 2.16 (s), 2.09 (s), -4.8 (v. br s) ppm.

[Fe(H-NC-TPM)$_2$](BPh$_4$)$_2$·2 CH$_3$CN (3.2) (BPh$_4$)$_2$·2 CH$_3$CN

Excess $NaBPh_4$ (0.18 g, 0.53 mmol) was added to a solution of **(3.2)(BF$_4$)$_2$** (0.10 g, 0.15 mmol) in 5 mL water and stirred at room temperature for 16 hours. A milky white suspension formed almost immediately. Solvent was removed by vacuum distillation and the remaining solid was washed with minimal cold water to give 0.026 g (4 % yield) of **10** as an off white solid. X-ray quality crystals were grown by slow vapor diffusion of Et_2O into a filtered acetonitrile solution of the complex. It was noted that the off white solid yielded an orange solution when dissolved in acetonitrile and that once filtered, the solution was pink. ^{1}H NMR (CD_3CN) δ_H: 7.27 (br m, 20H), 6.99 (br m, 20H), 6.84 (br m, 10 H).

[Fe(Tos-NC-TPM)$_2$](BF$_4$)$_2$ (3.3) (BF$_4$)$_2$

This complex was prepared in a similar manner to the complex **(3.1)(BF$_4$)$_2$** except that the **3I** ligand (0.195 g, 0.53 mmol) was used instead of **3D** along with the Fe(BF_4) · 6

H_2O (0.089 g, 0.265 mmol). The reaction was stirred at room temperature for 16 hours and then was cannula filtered. The solid was washed with two 2 mL portions of THF, 2 mL Et_2O, and was dried under vacuum to give 0.22 g (86% yield) **11** as a colorless solid. M.P. > 250°C. X-ray quality crystals were grown by slow vapor diffusion of Et_2O into a concentrated acetonitrile solution of the complex. ^1H NMR (CD_3CN) δ_H: 49.8 (v. br. s), 8.11 (v. br. s), 3.65 (br. s), 3.25 (v. br. s), 1.81, 1.25 (v. br. s) ppm.

[Fe(Tos-NC-TPM)$_2$](OTf)$_2$ (3.3) (OTf)$_2$

This complex was prepared in a similar manner to the complex **(3.1) (OTf)$_2$** except that the **3I** ligand (0.195 g, 0.529 mmol) was used instead of **3D** along with $Fe(OTf)_2$ (0.093 g, 0.263 mmol). The reaction was stirred at room temperature for 16 hours and then was canula filtered. The solid was washed with two 2mL portions of THF, 2 mL Et_2O, and was dried under vacuum to give 0.204 g (71% yield) **12** as a colorless solid. M.P. Decomposition was observed over 201°C. ^1H NMR (CD_3CN) δ_H: 48.9 (v. br. s), 8.0 (v. br. s), 3.65 (br. s), 3.1 (v. br. s), 1.81 (br. s), 1.26 (v. br. s) ppm.

Bibliography

1. Appel, A. M.; Bercaw, J. E.; Bocarsly, A. B.; Dobbek, H.; DuBois, D. L.; Dupuis, M.; Ferry, J. G.; Fujita, E.; Hille, R.; Kenis, P. A. J.; Kerfeld, C. A.; Morris, R. H.; Peden, C. H. F.; Portis, A. R.; Ragsdale, S. W.; Rauchfuss, T. B.; Reek, J. N. H.; Seefeldt, L. C.; Thauer, R. K.; Waldrop, G. L. *Chem. Rev*. **2013**, *113*, 6621-6658.

2. Doney, S. C.; Fabry, V. J.; Feely, R. A.; Kleypas, J. A. *Annu. Rev. Mar. Sci*. **2009**, *1*, 169-192.

3. Frese, K. W. Jr.; In *Electrochemical and Electrocatalytic Reactions of Carbon Dioxide*; Sullivan, B. P.; Krist, K.; Guard, H. E. Eds.; Elsevier: New York, 1993; Chapter 6.

4. Rosen, B. A.; Salehi-Khojin, A.; Thorson, M. R.; Zhu, W.; Whipple, D. T.; Kenis, P. J. A.; Masel, R. I. *Science*. **2011**, *334*, 643-644.

5. Jeoung, J. H.; Dobbek, H. *Science.* **2007**, *318*, 1461-1464.

6. Miyazaki, S.; Koga, Y.; Matsumoto, T.; Matsubara, K. *Chem. Commun*. **2010**, *46*, 1932-1934.

7. Seravalli, J.; Ragsdale, S. W. *Biochem.* **2008**, *47*, 6770-6781.

8. Romanov, V.; Soong, Y.; Carney, C.; Rush, G. E.; Nielsen, B.; O'Connor, W. *ChemBioEng Rev.* **2015**. 2, 231-256.

9. Schloegl, R. *Angew. Chem. Int. Ed*. **2015**. 54, 3465-3520.

10. Zeng, X.; Hatakeyama, M.; Ogata, K.; Liu, J.; Wang, Y.; Gao, Q.; Fujii, K.; Fujihira, M.; Jin, F.; Nakamura, S. *Chem. Phys*. **2014**, 16, 19836-19840.

11. Menard, G.; Stephan, D. W. *J. Am. Chem. Soc*. **2010**, *132*, 1796-1797.

12. Stephan, D. W. *Dalton Trans.* **2009**, 3129-3136.

13. Welch, G. C.; San Juan, R. R.; Masuda, J. D.; Stephan, D. W. *Science.* **2006**, *314*, 1124-1126.

14. Dureen, M. A.; Lough, A.; Gilbert, T. M.; Stephan, D. W. *Chem. Comm.* **2008**, 4303-4305.

15. Chase, P. A.; Stephan, D. W. *Angew. Chem., Int. Ed.* **2008**, *47*, 7433-7437.

16. Gusev, D.G. *Angew. Chem. Int. Ed.* **2012**, *51*, 2772-2775.

17. Grützmacher, H. *Angew. Chem. Int. Ed.* **2009**, *48*, 559-563.

18. Baranger, A. M.; Hollander, F. J.; Bergman, R. G. *J. Am. Chem. Soc.* **1993**, *115*, 7890-7891.

19. Greenwood, B. P.; Forman, S. I.; Rowe, G. T.; Chen, C.; Foxman, B. M.; Thomas, C. M. *Inorg. Chem*. **2009**, *48*, 6251-6260.

20. Konrad, M.; Wuthe, S.; Meyer, F.; Kaifer, E. *Eur. J. Inorg. Chem*. **2001**, 2233-2240.

21. Doyle, G.; Eriksen, K. A.; Van Engen, D. *J. Am. Chem. Soc*. **1986**, *108*, 445-451.

22. Banerjee, S.; Karanananda, M. K.; Sean R. Parmelee, S. R.; Jayarathne, U.; Mankad. N. P. *Inorg. Chem.* **2014**, 53, 11307-11315.

23. King, R. B. *Acc. Chem. Res*. **1970**, 3, 417-427.

24. Hartwig J. F. *Chem. Rev*. **2010**, *110*, 890-931.

25. Harvey, J. D.; Ziegler, C. J. *Coord. Chem. Rev*. **2003**, *247*, 1 – 19.

26. Hoyt, J. M.; Schmidt, V. A.; Tondreau, A. M.; Chirik, P. J. *Science*. **2015**, 349, 6251, 960-963.

27. Brookhart, M.; Small, B. L. *J. Am. Chem. Soc.* **1998**, *120*, 28, 7143–7144.

28. Anderson, N. H.; Odoh, S. O.; Yao, Y.; Williams, U. J.; Schaefer, B. A.; Kiernicki, J. J.; Lewis, A. J.; Goshert, M. D.; Fanwick, P. E.; Schelter, E. J.; Walensky, J. R.; Gagliardi, L.; Bart, S. C. *Nat. Chem*. **2014**, 6, 919-926.

29. Kiernicki, J. J.; Fanwick, P. E.; Bart, S. C. *Chem. Commun*. **2014**, 50, 8189-8192.

30. Niall T. Coogan, N. T.; Michael A. Chimes, M. A.; Raftery, J.; Mocilac, P.; Denecke, M. A. *J. Org. Chem*. **2015**, 80, 8684−8693.

31. Ozer, H; Kocakaya, S. O.; Akgun, A.; Hosgoeren, H.; Togrul, M. *Tetrahedron: Asymmetry*. **2009**, 20, 1541-1546.

32. Ansell, C. W. G.; Cooper, M. K.; Dancey, K. P.; Duckworth, P. A.; Henrick, K.; McParlin, M.; Organ, G.; Tasker, P. *J. Chem. Soc. Chem. Comm.* **1985**, *8*, 437 – 439.

33. Banti, C.N.; Giannoulis, A.D.; Kourkoumelis, N.; Owczarzak, A. M.; Kubicki, M.; Hadjikakou, S. K. *J. Inorg. Biochem*. **2015**, 142, 132–144.

34. Nagashima, H.; Sunada, Y.; Sue, T. *Eur. J. Inorg. Chem.* **2007**, 2897 – 2908.

35. Reger, D. L.; Little, C. A.; Rheingold, A. L.; Lam, M.; Liable-Sand, L. M.; Rhagitan, B.; Concolino, T.; Mohan, A.; Long, G. J.; Briois, V.; Grandjean, F. *Inorg. Chem.* **2001**, *40*, 1508-1520.

36. Oliver, J. D.; Mullica, D. F.; Hutchinson, B. B.; Milligan, W. O. *Inorg. Chem.* **1980**, 19, 165-169.

37. Brooker, Sally; *Chem. Soc. Rev.* **2015**, 44, 2880-3348.

38. Evans, D. F. *J. Chem. Soc*., **1959**, 2003–2005.

39. Gütlich, P. *Z. Anorg. Allg. Chem*., **2012**, 638, 15–43.

40. Feltham, H. L. C.; Johnson, C.; Elliot, A. B. S.; Gordon, K. C.; Albrecht, M.; Brooker, S. *Inorg. Chem*. **2015**, *54*, 2902–2909.

41. Gandolfi, C.; Moitzi, C.; Schurtenberger, P.; Morgan, G. G.; Albrecht, M. *J. Am. Chem. Soc*. **2008**, *130*, 14434–14435.

42. Sorai, M.; Nakazawa, Y.; Nakano, M.; Miyazaki, Y. *Chem. Rev*. **2013**, 113, 41–122.

43. Halcrow, M. A. *Chem. Soc. Rev*., **2011**, *40*, 4119–4142.

44. Allin, S. M.; Barton, W. R. S.; Bowman, W. R.; Bridge, E.; Elsegood, M. R. J.; McInally, T.; McKee, V. *Tetrahedron*. **2008**, 64, 7745-7758.

45. Moubaraki, B.; Leita, B. A.; Halder, G. J.; Batten, S. R.; Jensen, P.; Smith, J. P.; Cashion, J. D.; Kepert, C. J.; Letard, J.-F.; Murray, K. S. *Dalton Trans*. **2007**, 39, 4413-4426.

46. Goodman, M. A.; Nazarenko, A. Y.; Casavant, B. J.; Li, Z.; Brennessel, W. W.; DeMarco, M. J.; Long, G.; Goodman, M. S. *Inorg. Chem*. **2012**, 51, 1084-1093.

47. Laitar, D. S.; Müller, P.; Sadighi, J. P. *J. Am. Chem. Soc*. **2005**, 127, 17196-17197.

48. Zeng, X.; Hatakeyama, M.; Ogata, K.; Liu, J.; Wang, Y.; Gao, Q.; Fujii, K.; Fujihira, M.; Jin, F.; Nakamura, S. *Phys. Chem. Chem. Phys*, **2014**, 16, 19836—19840.

49. Stephanie G. N. Roundhill, S. G. N.; Roundhill, D. M.; Bloomquist, D. R.; Landee, C.; Willett, R. D.; Dooley, D. M.; Gray, H. B. *Inorg Chem*. **1979**, 18, 831-835.

50. Trofimenko, S.; Calabrese, J. C.; Thompson, J. S.; *Inorg. Chem*. **1987**, 26, 1507-1514.

51. Young, M. B.; Barrow, J. C.; Glass, K. L.; Lundell, G. F.; Newton, C. L.; Pellicore, J. M.; † Kenneth E. Rittle, K. E.; Selnick, H. G.; Stauffer, K. J.; Vacca, J. P.; Williams, P. D.; Bohn, D.; Clayton, F. C.; Cook, J. J.; Krueger, J. A.; Kuo, L. C.; Lewis, S. D.; Lucas, B. J.; McMasters, D. R.; Miller-Stein C.; Pietrak, B. L.; Wallace, A. A.; White, R. B.; Wong, B.; Yan, Y.; Nantermet, P. G.; *J. Med. Chem*. **2004,** 47, 2995-3008.

52. Trapp, I.; González-Gallardo, S.; Hohnstein, S.; Garnier, D.; Oña-Burgos, P.; Breher, F. *Dalton Trans*. **2014**, 43, 4313–4319.

53. Silvia, J. S.; Cummins, C. C. *J. Am. Chem. Soc*. **2010**, 132, 2169–2171.

54. Coulson; D. R. *Inorg. Synth*. **1990**, *28*, 107-109.

55. Peng, Y.; Li, Z.; Zeng, Y.; Xie, X.; Wang, H.; Li, L.; Liu, X. *Microchim Acta*. **2010**, 170, 17–26.

56. Martins, M. A. P.; Frizzo, C. P.; Moreira, D. N.; Rosa, F. A.; Marzari, M. R. B.; Zanatta, N.; Bonacorso, H. G. *Catal. Commun*. **2008**, 9, 1375-1378.